Department of Precision and Microsystems Engineering

The constant inertia mechanism and its use in a high-speed 2-DoF inherently dynamically balanced parallel manipulator

D. Boere

Report no	:	2022.053
Coach	:	Dr. Ir. V van der Wijk
Professor	:	Prof. Dr. Ir J.L. Herder
Specialisation	:	Mechatronic System Design
Type of report	:	MSc Thesis
Date	:	27 September 2022

TU Delft Delft University of Technology

Challenge the future

The constant inertia mechanism

and its use in a high-speed 2-DoF inherently dynamically balanced parallel manipulator

by

D. Boere

to obtain the degree of Master of Science
at the Delft University of Technology,
to be defended publicly on Tuesday September 27, 2022 at 3:00 PM.

Student number:	4955587	
Project duration:	February 1, 2021 – September 27, 2022	
Thesis committee:	Dr. ir. V. van der Wijk	TU Delft, supervisor
	Prof. dr. ir. J.L. Herder,	TU Delft
	Dr. ir. J.P. Meijaard,	TU Delft

An electronic version of this thesis is available at http://repository.tudelft.nl/.

TU Delft

Contents

1

Introduction

Parallel manipulators have received more attention in the industry. Their appealing ability of high-speed, high stiffness to weight ratio, and therefore the increase of agility, accuracy and higher payload capacities are very desirable [1]. However, these advantages come at the cost of singularity introductions, smaller workspace and lower dexterity. These robotic manipulators are desired to move faster and with more accuracy. When the cycle time can be lowered, more operations can be done in a certain amount of time. When a robotic arm is actuated with more torque, its rise time will be shorter. Although travelling at a higher speed can induce more vibrations to the base. So the desired destination is achieved faster, but vibrations are still present. The robot must wait until the vibrations are degraded to be within the desired boundaries of the precise location, also called settling time. These vibrations also induce wear and fatigue in the robot. So, moving faster does not always mean the cycle time will decrease. A way to attenuate these vibrations is to dynamically balance the manipulator. Dynamically balancing means that the change of linear and angular momentum is equal to zero. Also called shaking force and shaking moment balanced, respectively.

Dynamic balancing will heavily increase the movable mass and inertia [2], and if not taken into account in the design process, it can do more harm than good with regard to controllability [3]. Most examples of dynamically balanced parallel manipulators in literature are theoretical examples of structures that can be balanced. The manipulators that are built and experimentally verified are scarce.

To dynamic balance, a single rotatable link, gears or belts are often used on a force balanced link to obtain a counter-rotation. A literature study that recently describes them can be found in Ref. [4]. Gears and belts can reduce the dynamic performance of high-speed manipulators if not enough care is taken for the backlash [5]. Another technique is to copy a structure, so a movement is done in the opposite direction with the same mass and inertia [2]. Gosselin et al. established three reactionless four-bars that balance themself by distributing the mass over the links [6]. These examples are inherently balanced, meaning they balance themself in their workspace and do not need to be actively balanced. Active balancing means a (force balanced) link is combined with active controlled elements, e.g. flywheels, to obtain a counter-movement. This solution is heavily dependent on optimized control [7]. Active balancing is easier for multi-DoF structures, but inherently balanced structures are favourable regarding controllability for a single link.

To obtain multi-DoF balanced structures, a balanced link can be pasted onto another link, as it acts as a point mass, the whole system can be balanced together [2]. Also associated with link-by-link balancing. This necessitates placing actuators on distal links, which is primarily not wanted due to the added movable mass. All the aforementioned balancing techniques can be used on an arbitrary link to obtain full balancing for 2-DoF links in series. Some examples with belts and gears can be found in Ref. [8] and [9]. Parallelogram structures can be force balanced by placing counter-masses near the rotatable pivot point. This ensured that no mass is needed to be added to the distal links. In Ref. [10] a copied mechanism with belts is suggested. In Ref [11], a 2-DoF copied mechanism is proposed, which is only dynamical balanced along two perpendicular paths. The reactionless four-bars can also be combined to obtain multi-DoF parallel structures [12]. However, using multiple reactionless four-bars in series does heavily increase the complexity. With active counter-rotations, the following examples can be found in Ref. [13] [14].

Three notable examples of fabricated balanced parallel manipulators are known in the literature. The Hummingbird, presented in 1992, is a 2-DoF manipulator consisting of a parallelogram and has counter-masses near the origin to force balance the manipulator. It uses an active flywheel that induces a counter-rotation to cancel the angular momentum [15]. This manipulator was designed for the chip industry and could reach up to 50 G of accelerations in a workspace of 13 by 13 mm. Because this solution depends on active controlling of the flywheel, it is necessary to have optimal control otherwise, fully balancing will not be obtained. The reduced reaction forces resulted in a 90% reduction in reaction moments due to non-ideal actuators and friction. The Besi Robot [16] uses the same structure as the Hummingbird. It was designed for a bigger workspace around 25 cm, this came at the cost of the maximum peak accelerations reduced to 10 G. No experimental values are known that imply the reduced reaction forces. The DUAL-V is a redundant 4-RRR planar parallel manipulator [17]. It accomplishes dynamic balancing by copying a force balanced mechanism around the end-effector. The copied mechanism ensures dynamic balancing for an orthogonal trajectory through the middle of the workspace. It has a workspace of around 17 cm and could reach up to 20 G of peak accelerations. It has 97% lower shaking forces and up to a 96% lower shaking moment for the balanced trajectories in its workspace. For motion throughout the workspace, it showed 93% lower shaking forces and 16% lower shaking moment.

In Ref. [18], a study was done on the controllability of dynamic balancing techniques applicable to a single rotatable link. This study showed that the inverted four-bar is an appropriate building block for high dynamic performances. It obtains moment balance by distributing masses close to pivot points, and no additional counter-rotations are needed. This was also experimentally verified in Ref. [19]. Also, some 2-DoF structures are suggested that make use of the inverted four-bar, but most of them are not fully balanced in their workspace because of their inconsistent angular momentum. The research that takes balancing into account, as well as controllability for multi-DoF structures, is scarce, and no multi-DoF manipulator exists that is inherently dynamically balanced and is applicable for higher accelerations.

1.1. Research goals

This thesis focuses on combining controllability and dynamic balancing to develop a 2-DoF inherently dynamically balanced manipulator, so it is applicable for high accelerations. Three papers are written, and all can be read individually. All the papers contribute knowledge to obtain the primary goal. The research goal of every paper is as follows:

- **Obtain the design choices that have the most influence on stiffness in multi-DoF high-speed parallel manipulators**

- **To develop 2-DoF fully inherently dynamically balanced structures that are applicable for higher accelerations using a constant inertia mechanism**

- **Design and experimentally verify a 2-DoF inherently dynamically balanced structure with a constant inertia mechanism**

1.2. Thesis outline

In Chapter 2, a literature study is performed on high-speed parallel manipulators and what design choices influence the stiffness in any direction. This can be seen as an intro to high-speed parallel manipulators. For IBinv4B, a prototype of the dynamically balanced reactionless four-bar, the out-of-plane stiffness was insufficient for the high forces, therefore reducing the eigenfrequency [19]. For high-speed manipulators, stiffness in any direction is essential, as every mode can be activated. Even the out-of-plane frequencies for a planar manipulator [1]. The literature study aims to obtain design guidelines for high-speed parallel manipulators that can be applied so they can be implemented in a later design. Chapter 3 investigates why the solution in Ref. [19] is not fully balanced in its complete workspace and what is needed to obtain this. A constant inertia mechanism (CIM) is presented, and design solutions that use the CIM for inherently dynamical balancing. In Chapter 4, a design solution of Chapter 3 is designed and optimized on eigenfrequency, as well as experimentally validation on

dynamic balancing. The focus was on manufacturing and realizing the design to prove that controllability and balancing can be combined. Chapter 5 gives an evaluation of the design and what could be interesting for further research so higher accelerations or spatial balancing can be obtained. In the last chapter, a conclusion is given on the work of this thesis.

2

The most influential design choices on stiffness in multi-degree of freedom high-speed parallel manipulators

The most influential design choices on stiffness in multi-degree of freedom high-speed parallel manipulators

D. Boere, V. van der Wijk

***Abstract*—Using parallel manipulators at high speed for pick-and-place operations has recently received more attention. Moving at higher speeds means that the cycle time of a pick-and-place operation can be decreased. Although, moving with high accelerations will induce high forces and thus vibrations to a manipulator. Even for planar manipulators, the out-of-plane vibration modes can be executed. So having a manipulator that is stiff in every direction is essential for reaching high speeds. Many components influence the stiffness of a manipulator. Even if the base and the movable platform, which are almost always modeled as infinite stiff, are not rigid enough, they can have a negative influence on the stiffness. Thus infinite stiff structures must be ensured to be rigid. Many design choices can influence the total stiffness in any direction. This paper investigates the choices made in the literature for multi-DoF high-speed parallel manipulators that have influence. Adding stiffness almost always comes hand in hand with added mass, which has negative effects on controllability. So solely adding stiffness does not always mean that the manipulator will perform better. Adding more active redundant chains from the base to the end-effector can significantly increase the stiffness and dynamic performance of a parallel manipulator, thus being a good option for obtaining high speeds. Components that are in series must be stiff in every direction. This paper also presents design guidelines for obtaining sufficient stiffness for a high-speed parallel manipulator.**

I. Introduction

The use of parallel manipulators has become more popular in industries. Especially with their appealing ability of high-speed, high stiffness to weight ratio, and thus increased agility, accuracy and higher payload capacities. These abilities have given them more appeal compared with serial manipulators [1], [2], which have almost reached their limit [3], [4]. However, these advantages come at the cost of singularity introductions, smaller workspace and lower dexterity.

Many parallel manipulators have been invented and built, designed specifically for their use in the high-speed industry. A notable manipulator is Clavel's Delta robot, invented around 1980, which has three degrees of freedom (DoF) and can reach up to 10 G of acceleration. This manipulator was specially designed for the pick-and-place industry. The movable mass was significantly reduced because of the smart design. This made it an optimal manipulator for low mass, and high speeds [5]. Since then many high-speed parallel manipulators have been invented and build [6]–[27]

For the pick-and-place industry, high-speed and high precision (dynamic performance) is the key to a good manipulator. Because of the properties of the parallel manipulator, it is believed that they will supply the increasing demand for faster and more precise manipulators. Stiffness is one of the essential properties of a manipulator. It determines the external forces it can handle and is an important factor for the natural frequencies. The performance of a manipulator is often limited by its first natural frequency [28]. This can be in the movable direction but also in the constrained direction [1]. Working close to those frequencies will trigger vibrations and decrease the dynamic performance. The natural frequencies can be obtained using equation (1). One can see that if the stiffness matrix increases, the natural frequencies also increase. Hence the stiffer the mechanism and the lower the mass, the higher the natural frequencies. This will lead to more controllable bandwidth and thus higher precision it can have on high speeds [29].

$$\omega = \sqrt{\frac{K}{M}} \tag{1}$$

For higher speeds, the stiffness in every direction must be sufficient to obtain high performance. For example, if a planar manipulator's stiffness is low in the out-of-plane direction, this vibration mode can still be triggered. Although, increasing the stiffness will most likely lead to increased material and thus more mass, leading to poorer performance. So for the optimal design, an optimum must be found that balances the mass and the stiffness. One can increase the stiffness in a parallel manipulator in smart ways to increase the dynamic performance, but one can also decrease the needed stiffness by reducing the mass.

This literature paper will investigate what design choices influence the stiffness in every direction for multi-DoF high-speed macro parallel manipulators and derive the design guidelines for obtaining sufficient stiffness.

Parallel manipulators have different appearances, although they all have similar properties that link them together. In Fig. 1, a standardisation of a parallel manipulator is visible. Every manipulator exists of a base that is primarily rigid and is connected to the world. From the base, multiple chains are connected to the end-effector. A chain can consist of the following: joints, either passive or active and links. Active joints are also referred to as actuators. If two or more chains exist from the end-effector to the base, the manipulator will be parallel. If it is only one chain, then it is a series manipulator.

This paper will follow the structure of a parallel manipulator. In chapter II, general knowledge of the stiffness and the parallel manipulators will be given. In chapter III, the components that are placed in series of a chain will be analysed. In chapter IV, the chains that are in parallel with each other will be reviewed. Chapter V studies the base and the end-effector. Chapter VI will discuss the whole mechanism mechanically and control-wise, and in chapter VII, a conclusion will be given to the research goal.

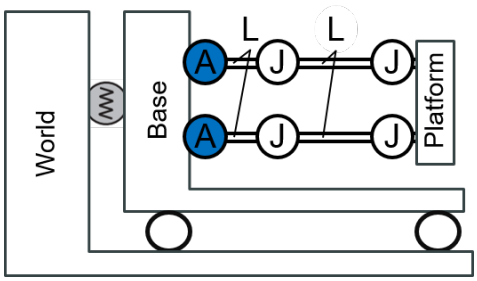

Figure 1. Standard design of a parallel manipulator, with chains consisting of actuators, links and joints that connect the base to the platform. Based on Ref. [3]

II. General

Stiffness is the ability to resist deformations caused by externally applied forces, or in basic formula form $\mathbf{K} = \mathbf{F}.\delta\mathbf{x}^{-1}$ [30]. In parallel manipulators, the stiffness matrix that has to be obtained is the Cartesian stiffness matrix of the end-effector. This point endures external forces by pick-and-place operations or needs to be tracked with the most precision. This matrix, also revered to $\mathbf{K}$ or $\mathbf{K}_c$, tells what kind of force in what direction the end-effector can endure. This is a six-by-six matrix where one diagonal term corresponds with a direction in Cartesian space. The inverse of a stiffness matrix is called a compliance matrix or $\mathbf{k}$. There are two types of stiffnesses. The dynamic stiffness $\mathbf{D}s = \mathbf{K} - \omega^2 * \mathbf{M}$ where the manipulator is in movement, and the rate of this movement decreases its dynamic stiffness [31]. While the other is static stiffness $\mathbf{S}s = \mathbf{k}$ where the end-effector does not move, so $\omega = 0$. The Static stiffness is used to determent the stiffness of a manipulator in its entire workspace, giving an overview of where this manipulator is stiff and where it is compliant. Components used in manipulators can either be placed in parallel or in series. While looking at figure 1 it can be seen that most chain components are in series except if a loop is added to a chain. The stiffness of components in series can be calculated by the use of equation (2). So a chain is as weak or strong as its weakest component. The chains connecting the base with the end-effector are placed in parallel. Hence placing multiple chains will increase the stiffness (see equation (3)).

$$\frac{1}{\mathbf{k}_{eqSeries}} = \frac{1}{\mathbf{k}_{Actuator}} + \frac{1}{\mathbf{k}_{Joints}} + \frac{1}{\mathbf{k}_{Links}} \tag{2}$$

$$\mathbf{k}_{eqParallel} = \mathbf{k}_{Chain\#1} + \mathbf{k}_{Chain\#n} \tag{3}$$

Design guideline Optimizing the weakest component first in a chain has the most significant influence on the total chain stiffness. Adding multiple chains will increase the total stiffness.

A. Obtaining the stiffness

In literature, there are three main ways to thoroughly compute the stiffness matrix for a parallel manipulator [3]. The Finite Element Analysis (FEA), Matrix Structural Analysis (MSA) and the Virtual Joint Analysis (VJA). The FEA has the most computational time but is the most reliable. Its accuracy is dependent on its computational time. Here joints and links are modelled with their true dimensions. This method is mostly used to validate the final design.MSA incorporates the main ideas of FEA but uses larger flexible elements like beams. Divining each beam into elements with two nodes gives it a 12 by 12 stiffness matrix derived from the Euler-Bernoulli presentation. This method gives a reasonable trade-off between computational time and accuracy [32]. The VJM, uses virtual joints to be modelled as springs and other structures as rigid [33]. This method takes the least amount of computational time, but because of the lumped models, it can deviate from the physical values. To increase the accuracy, a beam can be divided into smaller beams giving it more computational time but also increase the accuracy [34]. For high-speed manipulators, it is important to know where the first natural frequency will arise so it can be accounted for or stiffened if needed [28]. In Ref. [1], for a planar parallel mechanism, the first natural frequency was calculated, giving seven times higher with a simple Jacobian method, which did not account for the elasticity of the links, compared to the VJM method.

Design guideline: Using a proper method to compute the stiffness accurately in all directions so that no hidden eigenfrequency will be created while still having a low computational time.

B. Singularities

Singularities are important points in the workspace of a manipulator and can lead to bad behaviour of the end-effector. These can be points where the end-effector gains an extra DoF or an infinite actuation velocity that leads to no output velocity. So these are points where the kinetostatic behaviour of a mechanism suddenly changes [35]. Many papers have been written about this topic, and a summary can be found in Ref. [29].

A common way to obtain the singularities is by using Gosselin and Angele's way of using the input-output velocities. They defined three types of singularities [36]. The first two types are the most commonly occurring. The third type is a combination of the first and second ones. Zlatanov noted some more "hidden" singularities can occur for some particular manipulators [37]. Input-output velocities can not obtain this type (redundant passive motion). The input-output formula is given as follows

$$\mathbf{J}_q\dot{\mathbf{q}} = \mathbf{J}_x\dot{\mathbf{x}} \tag{4}$$

Where $\dot{\mathbf{q}}$ are the velocities of the actuators or input velocities and $\dot{\mathbf{x}}$ are the velocities of the end-effector or the output velocities.

Type I: Occurs when $Det(\mathbf{J}_q) = 0$. Also known as redundant input singularities or serial singularities [36]. These singularities occur when a chain either reaches a boundary of its workspace or an internal boundary limiting different sub-regions of the workspace. This will correspond that an actuator can have a velocity without it having to produce motion onto the end-effector ($\dot{\mathbf{q}} \neq 0$). An example can be seen in the left picture in Fig 2.

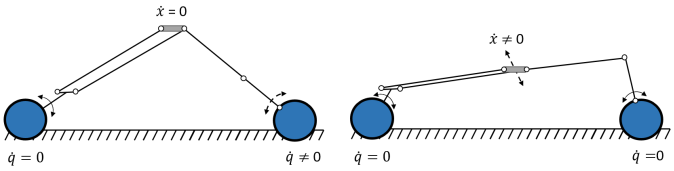

Figure 2. Singularities example for the 2-RRR manipulator of type I (serial) and type II (parallel) based on Ref. [18]

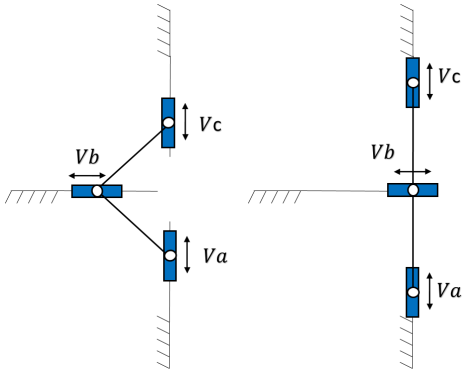

Figure 3. Singularity example for redundant passive motion singularities

Type II: Occurs when $Det(J_x) = 0$. Also known as over-mobilities or parallel singularities [36]. Unlike type I, these singularities lay within the chain's workspace. It corresponds to the end-effector having poor stiffness in a certain direction and is locally movable even when all the actuators are locked ($\dot{v} \neq 0$). An example can be seen in the right picture in Fig 2.

Type III: A combination of Type I and II. Both $Det(\mathbf{J}_q) = 0$ and $Det(\mathbf{J}_x) = 0$. The actuators may move while the end-effector is locked, and vice versa.

Redundant passive motion singularities: Also called internal singularities [38]. This is a special kind of singularity that can only occur for some mechanism with special parameters and can not directly be distracted from $Det(\mathbf{J}_q)$ or $Det(\mathbf{J}_x)$ [18]. An example can be an uncontrollable joint when the actuator and end-effector are both locked. Although these will probably not occur in a 'simple' parallel manipulator, for higher DoF, this can be a problem [37]. An example can be seen in Fig 3. Having V_a as input velocity and V_c as output one can see that the singularity in the right picture using equation (4) will not be discovered. Meanwhile, V_b can have a velocity without having an input or output velocity.

Design guideline: Make a complete kinematic model of the manipulator to obtain all the singularities in the workspace.

C. Design

For parallel manipulators, although many variations are present [39], two groups can be distinguished, planar and spatial ones. These two can again be divided into three common types [40], the RRR, RPR, and PRR, where R stands for a rotational joint and P for a prismatic joint. The underscore means that this joint is an active joint. There are other types of joint configurations, but they are not mentioned here because they are almost not used for high-speed macro manipulators.

One of the reasons parallel mechanisms can reach higher dynamic performance over series is that every actuator can be placed statically on the base [41]. Although this is not mandatory, placing the actuator statically means that it does not have to move for any motion, so the movable mass and inertia are significantly reduced [6].

Design guideline: Having the actuator at the base reduces the movable mass and inertia. Hence, making it more attractive for high-speed.

In table I, three basic types are given, for a planar configuration, with their common properties. Note that these three manipulators are divided because of how they are actuated and where this actuator is placed. Adding an extra DoF by adding extra chains, or by altering the platform, or altering the active joints will still count as the same group.

The RRR group uses a rotational actuator. Hence needing, it to have two links on both sides to create a planar 2-DoF movement. Having two links gives it a higher reachable workspace than the other groups, but comes the cost of the axial stiffness and available output force [7]. The rotational actuators can have direct drivers without transmissions. This type is often used in pick-and-place units that carry objects with small masses [11].

The RPR group is often referred to as a motion platform. This design has prismatic actuated joints within a chain. This gives it a small workspace but a high axial stiffness because the links will mostly be placed perpendicular to the end-effector. Here the actuators are not placed on the base so this will increase the movable mass.

The PRR group uses prismatic joints and has specs that are in-between the other two groups. This group can have high axial stiffness while maintaining a higher reachable workspace. This type is commonly used for milling operations [42], but also for pick and place operations that are needed to carry more mass [20].

For multi-DoF manipulators, to get a more accessible and homogeneous insight on the stiffness, placing the actuators symmetric around an axis is wanted for the distribution of force and moments along the kinematic chains [19]. This will also give a better insight into the Type II singularities [43] as well as a symmetrical workspace and easier controllable manipulators [44].

Design guideline Having a symmetric design will obtain a more homogeneous insight of the stiffness.

It is task-specific on how many DoF a manipulator needs. Pick-and-place manipulators can vary from 2T, 3T and 3T1R being the most common. The latter is called a Schöenfield motion. While haptic devices and motion bases commonly need 6-DoF. Increasing the DoF will also increase the complexity of the manipulator, making it harder to keep the actuators at the base or to maintain a symmetric design. So keeping the DoF as low as possible for the specific task will be less complex.

III. Individual components of a chain

The total stiffness in series is taken by the sum of every component's inverse stiffness (eq 3). Hence, marginally smaller stiffness has a huge impact on the average stiffness of

2 DoF parallel manipulator			
Type	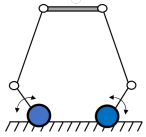	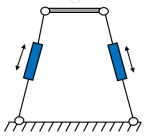	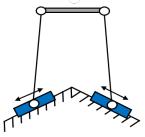
Structure	2-$\underline{R}$RR	2-R$\underline{P}$R	2-$\underline{P}$RR
Output force	Small	Large	Large
Actuator location	Base	Moving	Base
Moving mass	Low	Large	Low
Speed	Very fast	Dependent	Fast
Rigid	Poor	Good	Good
Workspace	Large	Small	Large

Table I
THE THREE BASIC TYPES OF PARALLEL MANIPULATORS FOR A PLANAR 2-DOF, BASED ON REF. [40]. NOTE THAT THE PLATFORM MUST BE CONSTRAINED HORIZONTALLY

this chain. So to improve the stiffness of a chain, the stiffness of every component needs to be analyzed and optimized, and it is best to improve the weakest component first.

A. Active joints and passive joints

Actuators or active joints give the manipulator the ability to move in specific directions. They also add virtual stiffness to the system. A more robust actuator means more virtual stiffness can be applied [3]. Actuation can either be linear or rotational. It is design and objective are dependent on which actuator is more suitable. The most used joints in parallel manipulators are revolute, prismatic, universal and ball-and-socket joints [29].

1) Drive: Transmissions like belts and gears can be used to convert speed to torque or vice versa. Transmissions will most likely implement extra backlash and wear that can reduce the stiffness [14]. Using them on oscillating links can create noise [45]. They are also highly non-linear to model and expensive to make precise [46]. Although some high-speed manipulators have been produced with gears, they had to use expensive anti-backlash gears to counter the negative effects [10], [14]. For high-speed manipulators, direct drivers are preferred [6]. Electric motors already have the full torque available upon starting.Although they have some good applications, they suffer from torque ripples. This is a periodic decrease or increase in the output torque and is a result of the magnetic fields that are switched. These torque ripples can induce vibrations in the system or lead to a loss of stiffness in the movable direction [47].

Design guideline: If the force of an actuator is sufficient, do not use transmissions and use direct drives, this will result in a higher performance.

2) Actuation redundancy: If a manipulator has more actuators than DoF, then this manipulator has actuation redundancy. This actuator can be placed in two places to create different redundancy's: 1) on a joint that is in an already existing chain *in-branch redundancy* and 2) on the base creating another chain to the end-effector *additional actuated branches* [20] [6]. The latter obtained more attention because the actuator can be placed stationary on the base, while by the first, the actuator has to move as well, adding extra movable mass and inertia to the system. Although this can be solved using a parallelogram so two actuators can be stationary and in the same chain [48]. Both can avoid type II in workspace singularities and thus increase the stiffness in these points [49]. Using multiple actuators also increases the available force that will be implemented in the system. Hence the complexity of the mechanism and control will increase. Attention must be paid to force redundancy, and the effects of internal forces [7].

Design guideline: Use actuation redundancy to counter the type II singularities in the workspace.

3) Stiffness in joints: Joints are often modelled as frictionless, and perfectly movable [50]. Although, in real life, a joint always has play, friction and backlash. Simple joints with lesser DoF can generally be made more precise and have less play, and backlash [51]. Pre-loading a joint will impose a force in the movable direction, and it can counter the effect of backlash [34]. The elasticity of a joint can become critical in high-speed manipulators. So these effects must be accounted for when designing. Compliant joints get their movement through elastic deformation by a slender structure [52]. The integration of compliant joints can counter the harmful effects of normal joints. Compared to normal joints, these joints are mostly less stiff in the out-of-plane direction. Although it is highly dependent on its design, optimizing can increase its stiffness. However, they have limited motion in their elastic range to ensure linear behaviour and forces are needed for deformations. These can decrease the actuation load capacity [53]. Because of the limited motion, compliant joints are often used in motion stages that can reach high precision in a plane. Some parallel manipulators exist that have a bigger workspace with compliant joints [54] [55]. Although, they are not widely used yet. In Ref. [56] Pashkevich et al. used the effects of preloaded joints to increase the stiffness near singularities and eliminate undesired buckling effects. The negative effects are the increased control difficulty and the harder stiffness mapping. In Ref. [57], springs were used in parallel with the actuators to decrease the energy consumption by 68%, but this is only suitable for specific loading and specific trajectories.

Design guideline: The use of preloaded joints can decrease the backlash in the joints and if used well have positive effects on the stiffness and the actuation torque.

Variable Stiffness Springs (VSS) can be used in series with an actuator to create Variable Stiffness Actuators (VSA). Its stiffness can be controlled and altered during motion. There are many types of VSAs most of them are explained in Ref. [58]. the common uses of VSAs are: shock absorption, stiffness variation with a constant load, stiffness variation at a constant position, cyclic movements, and explosive movements [59]. The use of variable stiffness can make it safer for robotics to operate or interact with or around humans. They are also used to decrease energy consumption in parallel manipulators. Although using them at high speeds, VSAs will lead to uncontrolled robot deflections [60]. In the same paper, they propose to use the VSS in a parallel arrangement to the actuators. By doing this, it is possible to reduce the energy by up to 48% while still being able to move at high speeds. Although, the active stiffness changes create harder control.

B. Links

Links are often rigid bodies that can withstand forces and vibrations. Although, the elasticity of the links can become critical for high speeds. So this must be accounted for [1]. In general, to increase the stiffness of a link is to optimize the material or to optimize the link geometry. In equation (5), the components of the six-by-six compliance matrix are visible for a cantilever beam. This matrix is the inverse of the stiffness matrix and gives an index on how much a link deforms with a given force. This is a symmetric matrix with the non-diagonal terms being the coupling terms.

$$\begin{aligned} &k_{11} = \tfrac{L}{EA};\ k_{22} = \tfrac{L^3}{3EI_z};\ k_{33} = \tfrac{L^3}{3EI_y};\ k_{44} = \tfrac{L}{GJ};\\ &k_{55} = \tfrac{L}{EI_y};\ k_{66} = \tfrac{L}{EI_z};\ k_{35} = \tfrac{-L^2}{2EI_y};\ k_{26} = \tfrac{L^2}{2EI_z}; \end{aligned} \tag{5}$$

were:
E is Young's modulus of a link. G is the Coulombs modulus of a link. A is the area of the link. L is the length of a link. J is the polar moment of inertia. I_i is the second moment of inertia of a link.

1) The geometry of a link: The stiffness of a link depends heavily on its geometry. Optimizing the geometry of a link can increase its stiffness in the desired direction. Altering the links' length will also significantly affect the reachable workspace. Design-specific manipulators can have smaller link lengths and thus obtain higher stiffness.

Design guideline Use design optimal workspace so no stiffness will be lost due to increased link lengths.

Topology optimization is used to get a design-specific optimization of a link. It divides the link into small elements that are optimized using mathematical algorithms. It is based on adding or removing material in these elements. While a stiff structure has much material in this direction, optimizing solely on stiffness will result in unfeasible designs with no material removed. To obtain a feasible design, constraint equations that counter the stiffness have to be added, like maximum volume. Another way is to change the objective function to optimize the mass or natural frequency. Works have proven that by optimizing a design, the natural frequency can be increased by 500% [46] This technique can have high computational time while optimizing. The structure that is created for the link is often difficult to manufacture. Attention must be paid to the optimization method because some methods will only give an optimum for a given point in a workspace, not the global workspace [61].

Buckling is a non-linear phenomenon when a slender structure endures compressing loading, exceeding a critical value. Although buckling effects are mostly unreachable in robotics [62], when minimizing the cross-section links can become critical. Loading the slender structures in traction will not endure these effects.

Design guideline: Having a design that the external forces load a link as much as possible in traction, so buckling and bending will not be a problem.

2) Material of a link: The materials that are widely used in parallel manipulators are aluminium and steel. While the former is lighter and cheaper, the latter is stronger. Using the right type of material for a manipulator can increase the stiffness and so accuracy. Recently composites are more often used for manipulators. They have many advantages over metals, they are mostly lighter, have a good Young's modulus to density ratio and are not prone to corrosion. But their raw material costs are expensive and labour intensive to produce [63]. Because of the lesser material that can be used, composites can become more prone to buckling/bending effects if no attention is paid to those phenomena [64]. In manipulators, heavier and stiffer materials are used near the base on proximal links because these links are more prone to bending. Lighter materials are used near the end-effector because far away links induce more inertia. This is commonly used on the distal links in delta-like robots [65].

Design guideline: Use stiffer material on the links near the base to counter bending moments.

Design guideline: Composite materials can best be used on distal links to decrease movable mass while still being stiff enough. Although making them slender can introduce the buckling effect if not accounted for.

3) Extra parallel links: Extra links can be added to the system to constrain the platform in a specific direction. This is most commonly done by using parallelograms in spatial delta-like robots to constrain the rotational movement of the platform, but it can still move translationally while staying horizontally. Instead of one distal link, these manipulators have four bars that compose a parallelogram. Because two or more parallelograms are used that are not in the same plane, it will be constrained. If rotational or spherical joints are used, then they also implement a motion. See Fig 4. Examples are delta-like robots as the $Par4$ [19], or the $X4$ [15]. In planar configurations, the parallel distal links still allow a rotation of the platform because they are in the same plane. To constrain the rotational movement of the platform, inner distal links must be added. For PRR and RPR configurations, these links can be directly connected to the movable component, as can be seen in the many examples given in Ref. [51]. For the RRR configuration, a passive proximal link connected to the inner distal link has to be added to obtain the right constraint. Adding such a constraint can be done for one side, but adding it on both sides increases the stiffness, keeps a symmetric behaviour and can eliminate clearance in the joints. Although the structure complexity increases. Planar manipulators that use these inner distal links are the $Diamond$ [27] and the $IRSBOT-2$ [21]. Using parallelograms can help to withstand higher rotational loads. Although, it will be more prone to bending effects [66]. Using a parallelogram will impose a more complex structure with redundant constraints, and the fabrication accuracy should be high enough otherwise, the accumulation of errors will be induced. For parallelograms this will not be a critical point as typically, only 1-DoF joints are needed [51]. In-between links can be added to increase the stiffness even further so the parallelogram is less prone to bending. This way, damping and preloading can also be introduced [49]. Although, adding extra links can over-constrain the mechanism, which in itself can induce internal

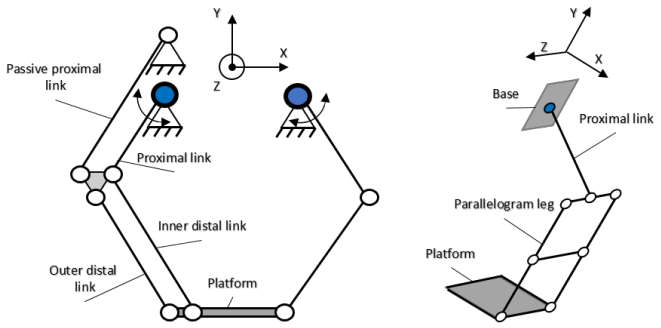

Figure 4. Constraining the platform for the rotational movements for a planar 2-RRR manipulator (left). A parallelogram leg can constrain the platform horizontally if multiple parallelograms are used that are not in the same plane for spatial manipulators (right)

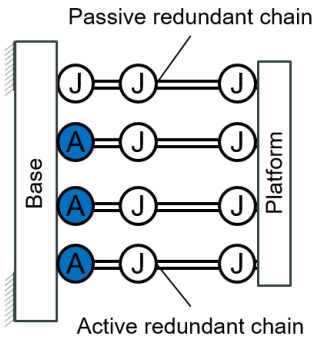

Figure 5. Visualization of an active and passive redundant chain for a 2-DoF parallel manipulator. Except for type II singularity areas, removing a redundant chain does not decrease the workspace. Note that the base is rigid connected to the world in this drawing

stresses.

Parallelogram links are mostly used in manipulators that apply axial forces to them. The cartesian axis $Ortoglide$ also uses these links for every axis point [8]. Here the stiffness was obtained with and without the use of parallelograms. Using them, a decrease in buckling and transverse stiffness was perceived, and an increase in rotational stiffness [66].

For planar mechanisms where the force of the end-effector is applied perpendicular to the plane of the manipulator (Z-direction in Fig. 4). This structure will probably do more wrong than good because of the perpendicular force applied to the end-effector and, thus, to the parallelograms. It is used in the wall-mounted parallel manipulator in Ref. [17] to create a vertical motion (Z-direction). Although this could also be solved using an external actuator [16]. If this is more favourable is questionable.

Design guideline: Use parallelogram links to implement a constraint to the platform or to increase a spatial DoF. This will increase rotational stiffness at the cost of transverse stiffness.

IV. Chains in parallel

When adding joints and links together, a chain is made. These chains connect the end-effector with the base. When a chain is actuated, it is called an active chain; when it has no actuation, it is called a passive chain. Redundant chains are extra chains that do not add motion to the manipulator. These redundant chains can be discarded, and the manipulator still has the same workspace and motion (except for type II singularities). Redundant chains can be added to the system to increase stiffness in its particular direction. Hence adding redundant chains can best be done in the direction where the manipulator is weakest.

A. Active redundant chains

Active chains have multiple advantages when they are added to a manipulator. Adding them will increase the stiffness (as can be seen in equation (3)), and the available actuation force will increase because of the added actuator in the chain [67]–[69]. Adding multiple chains is common for milling machines as the $ARROW$, which needs increased stiffness to withstand the external forces for milling operations [42].

The LIRMM group thinks that actuation redundancy is a key to obtaining high speeds for parallel manipulators. The LIRMM group has experimented with adding active redundant chains creating the $R4$ and $R6$ delta-like manipulators [6]. Because of the redundant actuators that can deliver more torque and the increased stiffness, these manipulators can obtain accelerations up to 80 G [70]. Although adding more chains can over-constrain the system, which can negatively affect the system, especially at high speeds, creating vibrations. In Ref. [68], Wu et al. tested the improvement of a second redundant chain, and while this increased the stiffness a little, it negatively affected the first natural frequency because of the added mass. So adding an active redundant chain does not always have a positive impact when also natural frequency or other design principles are considered. Another use of redundant actuators is the counteract the type II singularities inside the workspace of the manipulator [71].

Design guideline: Adding active chains increases the stiffness. They also positively affect type II singularities and the available actuation forces that can be delivered. Although one must consider the placement of the chain because of the added mass, it can decrease the natural frequency. Attention must be paid to over-constraining the mechanism and the increased control difficulties.

B. Passive redundant chains

Passive chains in a manipulator will move along with the end-effector but are not actuated by themself. This means that they can increase the stiffness in a constrained direction, but will not add any actuation force to the system. As mentioned before, to sustain high accelerations, a manipulator should be stiff enough in all directions [1]. So passive chains should be used to increase the stiffness where it is the weakest, mainly in a perpendicular direction to the end-effector relative to another chain for planar mechanisms. Some theoretical examples are given in Ref. [24], which in the end led to the $Par2$ manipulator. The $Par2$ has ten times more stiffness and even lighter parts in each chain than its predecessor $\underline{R}RRR\underline{R}$ without the passive chains. Although the numerical results were quite promising, experiments gave insight into poor

accuracy because of the uncontrolled parasitic effects added by a metal strip that coupled the passive chains. In Ref. [21] the $Par2$ was redesigned to the $IRSBot-2$. Here the passive chains were removed. To keep the out-of-plane stiffness, the parallelogram legs were set under an angle making a more triangular shape. This change decreased the complexity and increased the workspace while still being stiff enough for high speeds.

Design guideline: Adding passive redundant chains can increase the stiffness if placed well. Although, it is better to use active redundant chains to also increase actuation forces.

V. Rigid Structures

The chains connect the base and the platform. Those two components are mostly modelled as rigid structures because they are very stiff compared to other components and thus have minor effects on the precision [50].

Design guideline: If a component is modelled as infinite stiff, it must be ensured that it is rigid enough to not have an influence on the performance.

A. Base

The base is a rigid structure that is the beginning of a parallel manipulator where all the chains "grow" from. It is mostly a thick rigid plate or a structure composed of rigid beams. For rigid plates, the most vulnerable stiffness is the one perpendicular to the plane [72]. To obtain higher out-of-plane stiffness to counter moment forces, the plate's thickness must increase. Increasing the thickness will have a cubic term influence on the out-of-plane stiffness. Making a structure thicker also means more material. A sandwich structure (outer layers stiff inner layer weak but with low mass) is an option lower mass is obtained while still having high stiffness [73].

B. End-effector

The point of interest of a manipulator is called an end-effector. This is the point that will be controlled and has to track motions. A gripper can be applied to this point for pick and place operations. In some cases, a manipulator connects all chains at one point, but in most cases, a mobile platform is added, which can include an extra DoF (rotational). Just like the base, the platform is mainly modelled as rigid to make it less complex. The platform moves with the most speed compared to the rest of the manipulator. So optimizing the mass can reduce the applied torque. In Ref. [19], a reduction of 30% was obtained.

For pick-and-place manipulators, a Schöenflies motion (3T1R) is mostly desired [49]. Increasing the DoF means more actuators and more complex designs. A way to implement an extra rotation or translation is to add an actuator on the movable platform. This will, however, implement extra movable mass. The Delta manipulator solved this by adding an extra leg from the base to the end-effector. Although, this needed a slender prismatic joint with a low lifetime on higher speeds. It is also possible to implement joints into the platform creating a movable platform to increase a rotational DoF. Attention must be paid to not using prismatic joints because of their low service life on high speeds, and the possible internal singularities [19]. Manipulators that use this kind of platform are described in Ref. [15], [17]. Using this platform gives the ability to actuate the rotation DoF from the base with an extra chain. However, no full rotations are possible with this concept.

Design guideline: If a rotating end-effector is wanted, use a rotating platform instead of an extra actuator to reduce mass. Attention needs to be paid to increased joint count and limited reachable angle.

VI. Whole mechanism

When every part is added together, a parallel mechanism is created. When a manipulator moves at high speed, it will create vibrations to the base because of the accelerated mass and inertia. These vibrations can increase wear, noise and fatigue. These vibrations can be attenuated by balancing the structure mechanically or by altering the control.

A. Mechanical

1) Dynamic balancing: Dynamic balancing is a way to minimize the exerted forces to the base. Dynamically balancing means that the manipulator is shaking force balanced and shaking moment balanced. Shaking force means that the linear momentum stays constant or equal to zero for every movement. This happens when the CoM stays on the same point for every trajectory. Shaking moment is when the angular momentum stays constant or equal to zero for every trajectory in the workspace [45]. If a manipulator is fully dynamically balanced, no vibrations will be exerted onto the base. This means that the base does not need to be rightly connected to the world, and the settling time can be improved. The primary way of balancing is to add counter-masses and counter-inertias to the manipulator. This will heavily increase the movable mass, increase the needed actuation force and decrease the natural frequencies [74]. The increase of mass can be around 500% [75]. Although other techniques are known to shaking force or dynamically balance a structure, that is mostly explained in Ref. [45]. The DUAL-V manipulator force balanced the structure using a parallelogram and mirrored it around an axis, gaining dynamical balance for multiple trajectories. This manipulator could reach accelerations up to 20 G [76]. Another high-speed dynamically balanced manipulator is the hummingbird, which is fully shaking force balanced and uses an active counter rotation to be dynamically balanced. It can reach up to 50 G of acceleration. Although, it has a small workspace of 13 by 13 mm [25].

Design guideline: Making a manipulator dynamically balanced allows it to not exert vibrations onto the base, so the base does not need to be rigidly connected to the world. This comes at the cost of an increase in mass and inertia.

2) Internal stresses: Parallel manipulators have closed loops that can create internal forces in the system. Internal force elements balance each other out and do not perform any effective work [2]. However, they have effects on the total stiffness of the manipulator. Basically, adding an internal

tensile force to a structure increases the stiffness, while adding an internal compressive force will decrease its stiffness [77]. It has low relevance on manipulators that are mainly designed to be stiff. Although, for the balanced inverted four-bar linkage, a planar 1-DoF manipulator has one actuation point and one support point, connecting the manipulator to the base. The out-of-plane stiffness was quite important because of the high accelerations and, thus, high tensile loading that is exerted on the link between the two connection points. This led to an execution of the out-of-plane vibrations [78]. Although, this is a series manipulator, this can also happen to parallel manipulators. Internal stresses can also have a negative impact on the lifetime of actuators and joints [2]. On slender structures, internal forces have even more impact on the stiffness [79]. Wire manipulators use this effectively to increase the stiffness and decrease the vibrations [80]. Because of the low mass of the wires, these manipulators can obtain very high speeds. Up to 43 G was obtained by the Falcon wire robot [81].

B. Control

Control is a huge topic, and here only the very basics that are most talked about for high-speed manipulators are covered. Control of a manipulator is mostly about how actuation is planned for a trajectory. Although control can not increase stiffness, it can attenuate vibrations so that the needed stiffness for some motions decreases.

1) Motion profile: A motion profile generates velocities and accelerations for a given trajectory. Optimising the motion profile can degenerate the vibration that is induced. It will be a trade-off between rapidity and cancellation of undesirable vibrations [82]. A common motion profile is trapezoidal, although the sudden jerk difference creates vibrations. Making the corners smoother by using an "S" curve to reduce jerk can degenerate the vibrations [83]. Higher-order polynomials usually create less jerk. However, they are harder to implement. The "Bang bang" motion profiles are based on keeping the acceleration as low as possible for the whole path [84]. Input shaping is another motion profile that can cancel its vibrations by creating an impulse at the right time. These input shapers can reduce the vibrations up to 80%, although motion time increases [85].

2) Trajectory Generation: The trajectory that the end-effector makes from A to B can be done in infinite possible ways. For pick and place objectives, only points A and B are determined and require high precision. For constrained motion, the whole path that the end-effector makes is critical [86]. The easiest path-for-pick and place operations will be a straight line from A to B. However, this will not always be the path with the least amount of vibrations attenuated. By controlling the trajectories for specific paths, one can minimise the vibrations exerted onto the base. This can best be explained by the dynamic stiffness, $\mathbf{D}s = \mathbf{k} - \omega^2 * \mathbf{M}$. If the dynamic stiffness becomes close to zero, vibrations will occur [87]. This will not be a problem at low speeds, but vibrations will occur when high speeds are obtained. For standard pick and place operations, a trajectory has mostly some 90°edges somewhere in the travelled path. In Fig. 6 the standard Adept cycle is visible. Going From A vertically up then horizontally to aligning with B and then vertically down to B. These 90°edges create discontinuities in acceleration. To overcome these discontinuously, the actuators must generate extreme torques, which can lead to unwanted vibrations. To overcome this, the path's corners can be smooth so that the vibrations will be flattened out [88]. Design-specific trajectories are based on having high stiffness in points A and B and between a much lower stiffness. However, this is only suited for design-specific manipulators and not manipulators that are built for general cases. To decrease the vibrations, a path can be based on the highest stiffness, so the static stiffness will be maximised [89]. In Ref. [31], they proved that dynamic stiffness could be increased if a singularity of type II occurs in the planned path. So while at this specific point, the static stiffness is zero, the dynamic stiffness can be used to cross this point and increase the workspace [90]. Another path planning is based on minimising the movable mass for a trajectory. Instead of tracking the end-effector, it plans the CoM to have the shortest path from point A to B, giving it a "Bang-Bang" motion profile. This will reduce the maximal acceleration value of the CoM. It will not completely reduce the shaking forces, but it can have a reduction of up to 70% [91], [92]. Although many paths are possible, no clear solution has yet been given for the minimal vibration trajectory for high-speed manipulators [84].

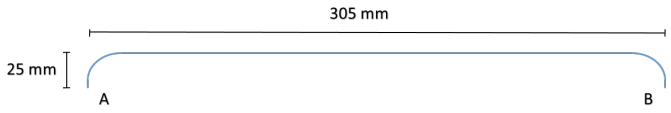

Figure 6. A visualisation of the standard Adept cycle that is used for manipulators

Design guideline: Control can minimise the vibrations that are induced. It is task and design specific, which path and motion profile is more advantageous. So a full model must be made to obtain the optimised control.

VII. Conclusion

Stiffness is one of the most important properties of a parallel manipulator that indicates dynamic performance. For high speeds, stiff structures are needed not to be impaired by vibrations. Although, increasing the stiffness will also likely increase the mass, which decreases the dynamic performance. So designing a manipulator solely on stiffness will not automatically mean that it will have good dynamic properties. This literature study was carried out to determent what design choices are used in parallel manipulators that influence the stiffness, with the scope of high speeds and the derivation of the design goals for obtaining sufficient stiffness.

Obtaining a sufficient model is advised to map the stiffness and know where the singularities will be. Although this is an obvious way of thinking, there are examples of manipulators that optimize the stiffness in one direction but "forget" it in another. This will lead to a low first natural frequency hidden in the model, thus creating poor dynamic performance. Having a sufficient model will also give an insight into where the

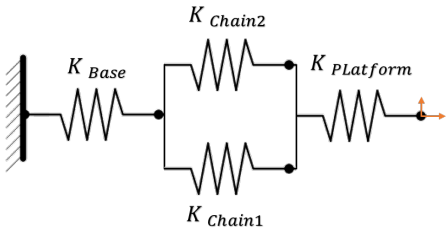

Figure 7. A visualization of a standard simplified parallel manipulator (that can also be seen in Fig 1) converted to a spring model

stiffness can best be optimized if needed. The stiffness of a manipulator depends on every component's stiffness in all directions. So if one models a component as rigid, it must be ensured it is, so it will not become critical. For planar manipulators, the out-of-plane direction can also become critical. So when designing a high-speed manipulator, it must be stiff in every direction. An example of a simplified manipulator that is converted to a spring model can be seen in Fig. 7 The total stiffness of the manipulator can be written down into equation (6). Note that every component is a six-by-six stiffness matrix.

$$\frac{1}{\mathbf{K}_{Manipulator}} = \frac{1}{\mathbf{K}_{Base}} + \frac{1}{\mathbf{K}_{Chain1} + \mathbf{K}_{Chain2}} + \frac{1}{\mathbf{K}_{Platform}} \tag{6}$$

In this equation, it is well visible that many components have an influence on the total stiffness. The base and the platform are mostly modelled as infinite stiff, so they must be ensured to be rigid enough not to influence the performance. If this is the case, then increasing the stiffness of the end-effector can best be done in either two ways: 1) Adding parallel redundant chains to the system increases the stiffness the most to where they are applied. These redundant chains can either be active or passive. Passive chains will theoretically increase the stiffness, although, in practice, they can introduce vibrations to the system. Making a redundant chain active can solve this problem and add extra actuation forces to the system. Making it a very good option for obtaining high speeds and improving the stiffness. Actuation redundancy will also have positive effects on type II singularities. Although, control difficulties will be increased, and attention needs to be paid to increased internal forces. A redundant chain will also add mass to the system, which, in itself, can have negative effects on the dynamic performance. A chain can best be placed in the direction where the Cartesian stiffness of the end-effector is the lowest. So attention needs to be paid to where a chain is placed. Planar manipulators that can not rely on extra spatial chains, and that need extra out-of-pane stiffness can make use of extra parallel links that are placed under an angle. 2) Optimize the average stiffness of a chain by improving the stiffness of the weakest component. The most common ways are by altering the material of the components in a chain or by altering the geometry of the links, giving it high stiffness and low mass while still being stiff enough not to endure bending or buckling phenomena. The elasticity of the joints can also be a critical point for manipulators. The most common materials that are used are aluminium and steel, but composites can be used to increase stiffness and decrease mass. Although, attention needs to be paid to making links slender while loading them in a compressing way because buckling effects can occur. Other things that can be done that have an influence on the stiffness for better dynamic performance are: placing the actuators symmetrically around the base and using similar chains to give a homogeneous distribution of the stiffness and the singularities. Loading the end-effector can best be done in traction way of the links. Some transmissions can induce vibrations, bad stiffness and backlash, so it is better to use direct drives if the actuation force is sufficient. Dynamically balancing a manipulator can eliminate the vibrations on the base, so the base does not have to be rigidly connected to the world. However, this will increase the movable mass and inertia. Altering the control does not need changes in the manipulator's design but only digitally. So it can always be altered after a manipulator has been designed. It does not increase the stiffness by itself but accomplices that fewer vibrations will be exposed, so some components are still sufficient if they are less stiff. Control can consist of the path's geometry, and the motion profile one follows. Abrupt direction changes will create vibrations, so smooth paths must be generated. No general optimal path is found for this problem, although using the "bang-bang" profile while generating the shortest path for the CoM can reduce the shaking force significantly. However, this limits the trajectory options. Every manipulator has its advantages and disadvantages. So not one particular solution will be the most promising. Although, these design guidelines will give a good indication of sufficient stiffness for high-speed parallel manipulators.

REFERENCES

[1] S. Briot, A. Pashkevich, and D. Chablat, "On the optimal design of parallel robots taking into account their deformations and natural frequencies," *Proceedings of the ASME Design Engineering Technical Conference*, vol. 7, no. PARTS A AND B, pp. 367–376, 2009.

[2] M. Luces, J. K. Mills, and B. Benhabib, "A Review of Redundant Parallel Kinematic Mechanisms," *Journal of Intelligent and Robotic Systems: Theory and Applications*, vol. 86, no. 2, pp. 175–198, 2017.

[3] A. Pashkevich, D. Chablat, and P. Wenger, "Stiffness analysis of 3-d.o.f. overconstrained translational parallel manipulators," *Proceedings - IEEE International Conference on Robotics and Automation*, no. June, pp. 1562–1567, 2008.

[4] Y. Chouaibi, A. H. Chebbi, Z. Affi, and L. Romdhane, "Analytical modeling and analysis of the clearance induced orientation error of the RAF translational parallel manipulator," *Robotica*, vol. 34, no. 8, pp. 1898–1921, 2016.

[5] F. Pierrot, C. Reynaud, and A. Fournier, "Delta: A simple and efficient parallel robot," *Robotica*, vol. 8, no. 2, pp. 105–109, 1990.

[6] D. Corbel, M. Gouttefarde, O. Company, and F. Pierrot, "Actuation redundancy as a way to improve the acceleration capabilities of 3T and 3T1R pick-and-place parallel manipulators," *Journal of Mechanisms and Robotics*, vol. 2, no. 4, 2010.

[7] K. Nagai and Z. Liu, "Re-design of force redundant parallel mechanisms by introducing kinematical redundancy," *2009 IEEE/RSJ International Conference on Intelligent Robots and Systems, IROS 2009*, pp. 5898–5904, 2009.

[8] P. Wenger and D. Chablat, "Design of a 3 Axis Parallel Machine Tool for High Speed Machining : The Orthoglide DESIGN OF A 3 AXIS PARALLEL MACHINE TOOL FOR HIGH SPEED MACHINING : THE ORTHOGLIDE Félix Majou Key Words : Parallel Machine tool Design , Isotropic Design , Singularity axi," no. June, 2007.

[9] B. van der Zon, "Besi zoekt snelheidslimiet pakken en plaatsen op," Sep 2007. [Online]. Available: https://mechatronicamachinebouw.nl/artikel/besi-zoekt-snelheidslimiet-pakken-en-plaatsen-op/

[10] S. Kock and W. Schumacher, "A mixed elastic and rigid-body dynamic model of an actuation redundant parallel robot with high-reduction gears," *Robotics and Automation, 2000. Proceedings. ICRA '00. IEEE International Conference on*, vol. 2, no. April, pp. 1918–1923 vol.2, 2000.

[11] F. Pierrot, C. Reynaud, and A. Fournier, "Delta: A simple and efficient parallel robot," *Robotica*, vol. 8, no. 2, pp. 105–109, 1990.

[12] F. Pierrot and O. Company, "H4: A new family of 4-dof parallel robots," *IEEE/ASME International Conference on Advanced Intelligent Mechatronics, AIM*, pp. 508–513, 1999.

[13] H. Otah, "14: A New Parallel Mechanism for Scara Motions," 2003.

[14] E. Uzunoğlu, M. Özkahya, E. Paksoy, B. Taner, M. I. Can Dede, and G. Kiper, "Conceptual Design of a 2-DoF Planar High-Speed Industrial Parallel Manipulator," *Mechanisms and Machine Science*, vol. 79, pp. 344–353, 2020.

[15] S. Staicu, Z. Shao, Z. Zhang, X. Tang, and L. Wang, "Kinematic analysis of the X4 translational–rotational parallel robot," *International Journal of Advanced Robotic Systems*, vol. 15, no. 5, pp. 1–12, 2018.

[16] L. Campos, F. Bourbonnais, I. A. Bonev, and P. Bigras, "Development of a five-bar parallel robot with large workspace," *Proceedings of the ASME Design Engineering Technical Conference*, vol. 2, no. PARTS A AND B, pp. 917–922, 2010.

[17] G. Wu, "Kinematic Analysis and Optimal Design of a Wall-mounted Four-limb Parallel Schönflies-motion Robot for Pick-and-place Operations," *Journal of Intelligent and Robotic Systems: Theory and Applications*, vol. 85, no. 3-4, pp. 663–677, 2017.

[18] V. Nabat, M. De La O Rodriguez, O. Company, S. Krut, and F. Pierrot, "Par4: Very high speed parallel robot for pick-and-place," *2005 IEEE/RSJ International Conference on Intelligent Robots and Systems, IROS*, pp. 553–558, 2005.

[19] F. Pierrot, V. Nabat, O. Company, S. Krut, and P. Poignet, "Optimal design of a 4-DOF parallel manipulator: From academia to industry," *IEEE Transactions on Robotics*, vol. 25, no. 2, pp. 213–224, 2009.

[20] L. Xu, X. Chai, Q. Li, L. Zhang, and W. Ye, "Design and Experimental Investigation of a New 2R1T Overconstrained Parallel Kinematic Machine with Actuation Redundancy," *Journal of Mechanisms and Robotics*, vol. 11, no. 3, pp. 1–10, 2019.

[21] C. Germain, S. Briot, V. Glazunov, S. Caro, C. Germain, S. Briot, V. Glazunov, S. Caro, and P. W. I. A, "IRSBOT-2 : A Novel Two-Dof Parallel Robot for High-Speed Operations To cite this version : HAL Id : hal-00590082," 2019.

[22] V. Van der Wijk, *Methodology for analysis and synthesis of inherently force and moment-balanced mechanisms - theory and applications*, 2014. [Online]. Available: https://doi.org/10.3990/1.9789036536301

[23] L. R. Douat, I. Queinnec, G. Garcia, M. Michelin, F. Pierrot, and S. Tarbouriech, "Identification and vibration attenuation for the parallel robot par2," *IEEE Transactions on Control Systems Technology*, vol. 22, no. 1, pp. 190–200, 2014.

[24] O. Company, F. Pierrot, S. Krut, C. Baradat, and V. Nabat, "Par2: A spatial mechanism for fast planar two-degree-of-freedom pick-and-place applications," *Meccanica*, vol. 46, no. 1, pp. 239–248, 2011.

[25] J. P. Karidis, G. Mcvicker, J. P. Pawletko, L. C. Zai, M. Goldowsky, R. E. Brown, and R. R. Comulada, "The Hummingbird Minipositioner-Providing Three-Axis Motion At 50 G's With Low Reactions," Tech. Rep.

[26] F. Marquet, S. Krut, and O. Company, "With Unlimited Rotation Capacities."

[27] T. Huang, Z. Li, M. Li, D. G. Chetwynd, and C. M. Gosselin, "Conceptual design and dimensional synthesis of a novel 2-DOF translational parallel robot for pick-and-place operations," *Journal of Mechanical Design, Transactions of the ASME*, vol. 126, no. 3, pp. 449–455, 2004.

[28] A. G. Hoevenaars, S. Krut, and J. L. Herder, "Jacobian-based natural frequency analysis of parallel manipulators," *Mechanism and Machine Theory*, vol. 148, 2020.

[29] Y. Jin, H. Chanal, and F. Paccot, *Parallel robots*, 2015.

[30] Y. Chouaibi, A. H. Chebbi, Z. Affi, and L. Romdhane, "Analytical modeling and analysis of the clearance induced orientation error of the RAF translational parallel manipulator," *Robotica*, vol. 34, no. 8, pp. 1898–1921, 2016.

[31] J. Prades, F. Jourdan, O. Company, S. Krut, and F. Pierrot, "Dynamics effects on natural frequencies in modal analysis of PKMs," *2015 20th International Conference on Methods and Models in Automation and Robotics, MMAR 2015*, pp. 300–305, 2015.

[32] A. Klimchik, A. Pashkevich, and D. Chablat, "Fundamentals of manipulator stiffness modeling using matrix structural analysis," *Mechanism and Machine Theory*, vol. 133, pp. 365–394, 2019. [Online]. Available: https://doi.org/10.1016/j.mechmachtheory.2018.11.023

[33] A. Pashkevich, A. Klimchik, D. Chablat, A. Pashkevich, A. Klimchik, D. Chablat, A. Pashkevich, A. Klimchik, and D. Chablat, "Enhanced stiffness modeling of manipulators with passive joints To cite this version : HAL Id : hal-00583167 Enhanced stiffness modeling of manipulators with passive joints," 2011.

[34] A. Klimchik, D. Chablat, and A. Pashkevich, "Stiffness modeling for perfect and non-perfect parallel manipulators under internal and external loadings," *Mechanism and Machine Theory*, vol. 79, pp. 1–28, 2014. [Online]. Available: http://dx.doi.org/10.1016/j.mechmachtheory.2014.04.002

[35] M. Conconi and M. Carricato, "Kinematic chains," *Mechanisms and Machine Science*, vol. 40, no. 4, pp. 1–20, 2016.

[36] C. Gosselin and J. Angeles, "Singularity Analysis of Closed-Loop Kinematic Chains," *IEEE Transactions on Robotics and Automation*, vol. 6, no. 3, pp. 281–290, 1990.

[37] A. Müller, *Singular Configurations of Mechanisms*, 2014, no. September.

[38] N. Tsagarakis, M. Laffranchi, B. Vanderborght, and D. Caldwell, "A compact soft actuator unit for small scale human friendly robots," pp. 4356–4362, 2009.

[39] R. L. Williams and B. H. Shelley, "Inverse kinematics for planar parallel manipulators," *Proceedings of the ASME Design Engineering Technical Conference*, vol. 2, pp. 1–6, 1997.

[40] Y. Koseki, T. Arai, K. Sugimoto, T. Takatuji, and M. Goto, "Design and accuracy evaluation of high-speed and high precision parallel mechanism," *Proceedings - IEEE International Conference on Robotics and Automation*, vol. 2, no. May, pp. 1340–1345, 1998.

[41] U. D. Sophia-antipolis, "Manipulator L I," *Design*, no. April, pp. 3738–3743, 1996.

[42] S. A. Shayya, S. Krut, O. Company, C. Baradat, S. A. Shayya, S. Krut, O. Company, C. Baradat, and F. P. A. Novel, "A Novel 4 DoFs (3T-1R) Parallel Manipulator with Actuation Redundancy - Workspace Analysis François Pierrot To cite this version : HAL Id : lirmm-00906202 A Novel 4 DoFs (3T-1R) Parallel Manipulator with Actuation Redundancy – Workspace Analysis," 2013.

[43] J. C. Fauroux, "A method for modeling analytical stiffness of a lower mobility parallel manipulator," *Proceedings - IEEE International Conference on Robotics and Automation*, vol. 2005, no. May 2014, pp. 3232–3237, 2005.

[44] S. Sun, J. W. Cheung, and Y. Lou, "A study on five-bar manipulators for semiconductor packaging applications," *Proceedings of the 2007 IEEE International Conference on Mechatronics and Automation, ICMA 2007*, pp. 1811–1816, 2007.

[45] V. Arakelian, "Inertia forces and moments balancing in robot manipulators: a review," *Advanced Robotics*, vol. 31, no. 14, pp. 717–726, jul 2017.

[46] S. Briot, A. Goldsztejn, S. Briot, A. Goldsztejn, T. Optimization, and R. Application, "Topology Optimization of Industrial Robots : Application to a Five-bar Mechanism To cite this version : HAL Id : hal-01587979 Topology Optimization of Industrial Robots : Application to a Five-bar Mechanism," 2019.

[47] A. B. Asaf Ali and D. Casado-Valdes, "Symbiosis between Torque Ripple and Vibrations of Large Electrically Excited Synchronous Motor," *Proceedings - 2018 23rd International Conference on Electrical Machines, ICEM 2018*, pp. 419–426, 2018.

[48] K. Nagait, "Development of Parallel Manipulator " NINJA " with Ult ra-High- Accelerat ion 1 Introduction Trade-off in mechanism design and," pp. 3678–3685, 2003.

[49] X.-J. Liu and J. Wang, *Parallel Kinematics: Type, Kinematics, and Optimal Design*, 2014.

[50] T. Huang, X. Zhao, and D. J. Whitehouse, "Stiffness estimation of a tripod-based parallel kinematic machine," *IEEE Transactions on Robotics and Automation*, vol. 18, no. 1, pp. 50–58, 2002.

[51] X. J. Liu and J. Wang, "Some new parallel mechanisms containing the planar four-bar parallelogram," *International Journal of Robotics Research*, vol. 22, no. 9, pp. 717–732, 2003.

[52] L. L. Howell, *Compliant Mechanisms*. Dordrecht: Springer Netherlands, 2016, pp. 604–611. [Online]. Available: https://doi.org/10.1007/978-94-017-9780-1_302

[53] J. Sun, *Open Aircraft Performance Modeling Based on an Analysis of Aircraft Surveillance Data*, 2019.

[54] A. G. Hoevenaars, P. Lambert, and J. L. Herder, "Jacobian-based stiffness analysis method for parallel manipulators with non-redundant legs," *Proceedings of the Institution of Mechanical Engineers, Part C: Journal of Mechanical Engineering Science*, vol. 230, no. 3, pp. 341–352, 2016.

[55] R. Cornelissen, A. Müller, and R. Aarts, "A compliant and redundantly actuated 2-dof 3rrr pkm: Best of both worlds?" pp. 163–171, 2020.

[56] A. Pashkevich, A. Klimchik, and D. Chablat, "Stiffness Analysis of Parallel Manipulators with Preloaded Passive Joints," *Advances in Robot Kinematics: Motion in Man and Machine*, pp. 465–474, 2010.

[57] L. Scalera, G. Carabin, R. Vidoni, and T. Wongratanaphisan, "Energy efficiency in a 4-dof parallel robot featuring compliant elements," *International Journal of Mechanics and Control*, vol. 20, no. 2, pp. 1–9, 2019.

[58] B. Vanderborght, A. Albu-Schaeffer, A. Bicchi, E. Burdet, D. G. Caldwell, R. Carloni, M. Catalano, O. Eiberger, W. Friedl, G. Ganesh, M. Garabini, M. Grebenstein, G. Grioli, S. Haddadin, H. Hoppner, A. Jafari, M. Laffranchi, D. Lefeber, F. Petit, S. Stramigioli, N. Tsagarakis, M. Van Damme, R. Van Ham, L. C. Visser, and S. Wolf, "Variable impedance actuators: A review," *Robotics and Autonomous Systems*, vol. 61, no. 12, pp. 1601–1614, 2013. [Online]. Available: http://dx.doi.org/10.1016/j.robot.2013.06.009

[59] S. Wolf, G. Grioli, O. Eiberger, W. Friedl, M. Grebenstein, H. Hoppner, E. Burdet, D. G. Caldwell, R. Carloni, M. G. Catalano, D. Lefeber, S. Stramigioli, N. Tsagarakis, M. Van Damme, R. Van Ham, B. Vanderborght, L. C. Visser, A. Bicchi, and A. Albu-Schaffer, "Variable Stiffness Actuators: Review on Design and Components," *IEEE/ASME Transactions on Mechatronics*, vol. 21, no. 5, pp. 2418–2430, 2016.

[60] R. B. Hill, S. Briot, A. Chriette, and P. Martinet, "Increasing energy efficiency of high-speed parallel robots by using variable stiffness springs and optimal motion generation," *Proceedings of the ASME Design Engineering Technical Conference*, vol. 5B-2018, 2018.

[61] S. Briot and A. Goldsztejn, "Topology optimization of industrial robots: Application to a five-bar mechanism," *Mechanism and Machine Theory*, vol. 120, pp. 30–56, 2018.

[62] A. Klimchik, "Enhanced stiffness modeling of serial and parallel manipulators for robotic-based processing of high performance materials To cite this version : HAL Id : tel-00711978," 2012.

[63] C. Lester and S. Nutt, "Composite Materials: Advantages and Cost Factors," pp. 1–5, 2018. [Online]. Available: http://www.elevatedmaterials.com/wp-content/uploads/2018/04/White-Paper-1-CFRP-Advantages-Cost-Factors.pdf

[64] G. Szuladziński, "Performance of composites versus metals under extreme loading," *International Journal of Protective Structures*, vol. 8, no. 1, pp. 86–108, 2017.

[65] M. Opl, M. Holub, J. Pavlík, F. Bradáč, P. Blecha, J. Kozubík, and J. Coufal, "DELTA - Robot with parallel kinematics," *Mechatronics: Recent Technological and Scientific Advances*, no. January 2012, pp. 445–452, 2011.

[66] A. Pashkevich, A. Klimchik, and D. Chablat, "Enhanced stiffness modeling of manipulators with passive joints," *Mechanism and Machine Theory*, vol. 46, no. 5, pp. 662–679, 2011. [Online]. Available: http://dx.doi.org/10.1016/j.mechmachtheory.2010.12.008

[67] C. Gosselin, "Stiffness Mapping for Parallel Manipulators," *IEEE Transactions on Robotics and Automation*, vol. 6, no. 3, pp. 377–382, 1990.

[68] L. Wang, G. Yu, and J. Wu, "A comparison study on the stiffness and natural frequency of a redundant parallel conveyor and its nonredundant counterpart," *Advances in Mechanical Engineering*, vol. 9, no. 11, pp. 1–11, 2017.

[69] G. Grioli, S. Wolf, M. Garabini, M. Catalano, E. Burdet, D. Caldwell, R. Carloni, W. Friedl, M. Grebenstein, M. Laffranchi, D. Lefeber, S. Stramigioli, N. Tsagarakis, M. Van Damme, B. Vanderborght, A. Albu-Schaeffer, and A. Bicchi, "Variable stiffness actuators: The user's point of view," *International Journal of Robotics Research*, vol. 34, no. 6, pp. 727–743, 2015.

[70] G. S. Natal, A. Chemori, and F. Pierrot, "Dual-space control of extremely fast parallel manipulators: Payload changes and the 100G experiment," *IEEE Transactions on Control Systems Technology*, vol. 23, no. 4, pp. 1520–1535, 2015.

[71] P. Buttolo and B. Hannaford, "Advantages of actuation redundancy for the design of haptic displays," *American Society of Mechanical Engineers, Dynamic Systems and Control Division (Publication) DSC*, vol. 57-2, no. September, pp. 623–630, 1995.

[72] E. Oñate, *Structural Analysis with the Finite Element Method Linear Statics Volume 2. Beams, Plates and Shells*, 2013, vol. First Edit. [Online]. Available: http://medcontent.metapress.com/index/A65RM03P4874243N.pdf

[73] X. Li, G. Li, and C. H. Wang, "Optimisation of composite sandwich structures subjected to combined torsion and bending stiffness requirements," *Applied Composite Materials*, vol. 19, no. 3-4, pp. 689–704, 2012.

[74] V. Van der Wijk, B. Demeulenaere, C. Gosselin, and J. L. Herder, "Comparative Analysis for Low-Mass and Low-Inertia Dynamic Balancing of Mechanisms," *Journal of Mechanisms and Robotics*, vol. 4, no. 3, jun 2012.

[75] B. Jennett, "Balancing benefits." *The Health service journal*, vol. 96, no. 5005, pp. 40–44, 1986.

[76] T. Laliberté and C. Gosselin, "Synthesis, optimization and experimental validation of reactionless two-DOF parallel mechanisms using counter-mechanisms," *Meccanica*, vol. 51, no. 12, pp. 3211–3225, dec 2016.

[77] M. A. ADLI, K. NAGAI, K. MIYATA, and H. HANAFUSA, "Analysis of Internal Force Effect in Parallel Manipulators," *Transactions of the Society of Instrument and Control Engineers*, vol. 27, no. 11, pp. 1266–1273, 1991.

[78] M. Zomerdijk, V. Van der Wijk, "Reducing settling time in high acceleration applications of macro scale robotic manipulators with dynamic balancing," 2020.

[79] J. Prades, "Dynamique linéarisée totale : Application aux robots parallèles To cite this version : HAL Id : tel-02155174 DE L ' UNIVERSITÉ DE M ONTPELLIER Dynamique linéarisée totale : Application aux robots parallèles Présentée par Julien PRADES," 2019.

[80] , " falcon," vol. 15, no. 1, pp. 82–89, 1997. [Online]. Available: http://rraj.rsj-web.org/back_wp/wp-content/uploads/15e61e20d5c3f53d5130a2597b755e17.pdf

[81] S. Behzadipour, "Ultra-High-Speed Cable-Based Robots," 2005.

[82] J.-Y. Dieulot, I. Thimoumi, F. Colas, and R. Béarée, "Numerical Aspects and Performances of Trajectory Planning Methods of Flexible Axes," *International Journal of Computers Communications Control*, vol. 1, no. 4, p. 35, 2006.

[83] R. M. Schmidt, G. Schitter, and A. Rankers, *The design of high performance mechatronics-: high-Tech functionality by multidisciplinary system integration*. Ios Press, 2020.

[84] C. J. Barnard, S. Briot, and S. Caro, "Trajectory generation for high speed pick and place robots," *ASME 2012 11th Biennial Conference on Engineering Systems Design and Analysis, ESDA 2012*, vol. 3, no. July, pp. 165–174, 2012.

[85] Q. C. Nguyen and H. Q. T. Ngo, "Input Shaping Control To Reduce Residual Vibration of a Flexible Beam," *Journal of Computer Science and Cybernetics*, vol. 32, no. 1, pp. 75–90, 2016.

[86] A. Olabi, R. Bearee, E. Nyiri, and O. Gibaru, "Enhanced trajectory planning for machining with industrial six-axis robots," *Proceedings of the IEEE International Conference on Industrial Technology*, no. November, pp. 500–506, 2010.

[87] S. Sabin, "Understanding and using dynamic stiffness-A Tutorial," *Orbit. Second Quarter*, vol. 2, pp. 44–54, 2000. [Online]. Available: http://scholar.google.com/scholar?cluster=3255990986989098504&hl=en&as_sdt=0,22

[88] J. F. Gauthier, J. Angeles, and S. Nokleby, *Optimization of a Test Trajectory for SCARA Systems*. Dordrecht: Springer Netherlands, 2008, pp. 225–234. [Online]. Available: https://doi.org/10.1007/978-1-4020-8600-7_24

[89] J. Aginaga, I. Zabalza, O. Altuzarra, and J. Nájera, "Improving static stiffness of the 6 - R US parallel manipulator using inverse singularities," *Robotics and Computer-Integrated Manufacturing*, vol. 28, no. 4, pp. 458–471, 2012.

[90] G. Pagis, N. Bouton, S. Briot, P. Martinet, G. Pagis, N. Bouton, S. Briot, P. Martinet, and E. Parallel, "Enlarging Parallel Robot Workspace through Type-2 Singularity Crossing To cite this version : HAL Id : hal-01114340 Enlarging Parallel Robot Workspace through Type 2 Singularity Crossing : Controller Design and Benchmarking," 2019.

[91] Y. L. Wu, X. Z. Wu, and S. Y. Li, "PD control of redundant parallel manipulators," *Guofang Keji Daxue Xuebao/Journal of National University of Defense Technology*, vol. 23, no. 3, pp. 111–114, 2001.

[92] S. Briot, V. Arakelian, and J. P. Le Baron, "Shaking force minimization of high-speed robots via centre of mass acceleration control," *Mechanism and Machine Theory*, vol. 57, pp. 1–12, nov 2012.

3

Design solutions to inherently dynamically balance a 2-DoF parallelogram with a constant inertia mechanism

Design solutions to inherently dynamically balance a 2-DoF parallelogram with a constant inertia mechanism

D. Boere, V. van der Wijk

***Abstract*—Robotic manipulators are desired to move faster and faster. Moving with high acceleration often means that more vibrations will occur. One of the reasons for this fact is the forces that are induced on the base by the movable mass. A way to attenuate these vibrations is to dynamically balance the mechanism. Fully dynamically balanced means that the change of angular and linear momentum is zero for every movement in the workspace. This paper investigates using a counter-parallelogram to obtain fully inherently dynamically balanced mechanisms for 2-DoF. The counter-parallelogram coupled to the parallelogram is an interesting idea because it keeps the inertia around the origin constant, making a constant inertia mechanism. Variations of this mechanism are presented by changing the coupled angle or the properties of the links. This will make it suitable to be balanced by reactionless four-bars or counter-rotatable mechanisms. The counter-parallelogram does not add mass to distal links, making it suitable for better dynamic performance than balancing the distal links. Seven new design solutions will be presented that are inherently dynamically balanced, where one design solution is numerically elaborated and confirmed to be fully dynamically balanced.**

***Index Terms*—** Parallel manipulators, Constant inertia, Shaking force balanced, Shaking moment balanced, Inherently dynamically balanced

I. Introduction

Parallel manipulators are excellent candidates for good dynamic performance because of their low moving inertia, high dexterity, compact size, and high power-to-weight ratio [1]. However, moving at high speed exerts high forces on the base, which can lead to fatigue, noise and vibrations [2]. Shaking force and shaking moment balanced structures heavily reduce the vibrations exerted on the base. Obtaining fully balanced structures often increases mass, and inertia greatly increases [3]. Increased mass and inertia decrease the rise time for manipulators. However, the dynamic balancing helps eliminate the waiting time for vibrations to die out, obtaining a lower cycle time in general [4].

Some multi-DoF (degrees of freedom) fully dynamically balanced parallel structures exist. Most of them rely on making the structure force balanced and adding an active counter-rotation to make it dynamically balanced [4]–[7]. Although active counter-rotations need control and drives, which increases complexity and cost [8]. Also, active balancing often does not entirely reduce the reaction forces because of limited control.

Some structures rely on balancing links individually, as in Ref. [9]–[12]. Although this means that masses or actuators need to be placed on distal links, which decreases the dynamic performance significantly [13]. Another possibility is copying a structure so the copied links will move in the opposite direction, and therefore the angular momentum is cancelled, making it fully balanced [14]. The disadvantage of this solution is that these structures are overhanging and, therefore, hard to use over a conveyor belt or something likewise for the industry. Another way to dynamically balance a 2-DoF structure is using a force-balanced structure and using the same or another force-balanced structure connected with belts or gears so that the angular momentum is cancelled for every trajectory in the workspace [15].

So far, to the author's knowledge, no 2-DoF structure exists that does not balance distal links, depend on adding actuators on movable links, or uses an active counter-rotation to obtain a fully inherently dynamic balanced mechanism. The goal of this paper is to find a 2-DoF mechanism that complies with the named characteristics. In Ref. [3], Zomerdijk proposed a structure that satisfies all the named properties. However, this structure is not yet fully dynamically balanced because of the inconstant angular momentum in the workspace.

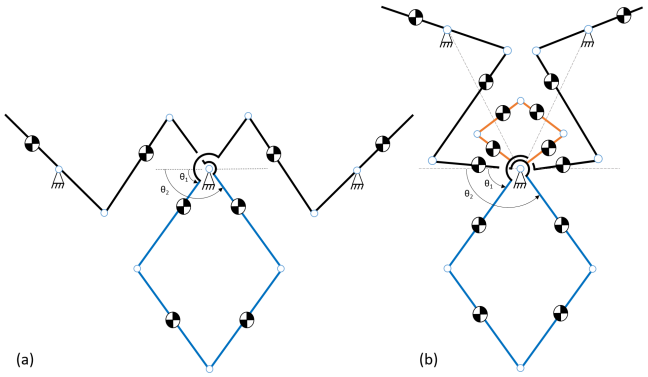

Figure 1. (a), Zomerdijk's proposed dynamically balanced degenerated five-bar linkage based on a pantograph [3]. Note that this mechanism is not dynamically balanced. (b), the proposed design solution for a fully inherently dynamically balanced mechanism.

In chapter II the structure of Zomerdijk is analysed and explained why it is not feasible to be fully balanced and what is needed to obtain this. In chapter III counter-inertias are used to obtain a constant inertia mechanism (CIM), with constant inertia around the origin, making it a building block to be dynamically balanced. Chapter IV describes seven design solutions to fully inherently dynamically balance a 2-DoF parallelogram, with the use of the CIM. One design solution is numerically evaluated. In the chapter V, the design solutions are discussed. In the last chapter a conclusion is given.

II. Investigation of the dynamically balanced degenerated five-bar linkage

This chapter gives more background knowledge on dynamic balancing and how to obtain this for a parallelogram. In Fig. 1, the proposed mechanism of Zomerdijk is visible. In his master thesis, he compared different balancing methods for controllability (high eigenfrequency) to dynamically balance a single rotatable link [3]. The inverted four-bar, which is a reactionless four-bar, became the most optimal as regards controllability if not a full rotation is desired. Combining two inverted four-bars (displayed in black), together with a parallelogram (displayed in blue) was proposed by Zomerdijk. The parallelogram can move in 2D planar space, and the added inverted four-bars make the mechanism reactionless. Although this mechanism is not dynamically balanced for every trajectory because of the variable inertia for different input angles for the parallelogram.

A. Balancing conditions

To fully balance a mechanism, the change of linear momentum and angular momentum should both be zero. A structure with constant linear momentum is called shaking force balanced. As is shown in the following equation

$$\bar{P} = \sum \dot{\bar{r}}_i m_i = 0 \tag{1}$$

With i being the element, $\bar{r}_i$ being the position vector to the center of mass (CoM) of an element, and m_i being the mass of this element. If a mechanism is shaking force balanced, the CoM will be stationary for every movement. When the mechanism has constant angular momentum see equation (2), it is called shaking moment balanced [16].

$$\frac{d\bar{H}}{dt} = \sum \bar{r}_i \times (\ddot{\bar{r}}_i m_i) + I_i \ddot{\bar{\theta}}_i = 0 \tag{2}$$

With I_i, the mass moment of inertia (will be referred to as inertia) and $\ddot{\bar{\theta}}_i$, the angular accelerations of the element. When a mechanism satisfies both equations, the mechanism is dynamically balanced and will not exert reaction forces on the base.

B. Balancing a single rotatable link

A structure can balance a single rotatable link to keep the CoM in the exact location and induce a counter-rotation so the sum of angular momentum will be zero. Shaking force balance can be done by adding a counter-mass to the rotatable link, which relocates the CoM to the origin. A counter-rotation is often realized with belts or gears that rotate a flywheel in the opposite direction [17]. Gosselin et al. established three Cases to inherently dynamically balance four-bar linkages [9]. Inherently balanced means they do not need any added counter-rotations or other structures to be fully balanced, so the mechanism balances itself. These three Cases can also dynamically balance a single rotatable link. So if a mechanism, like a single link, contains the same position for the CoM, the same inertia and angular momentum around its rotation point, it will be able to be made reactionless by one of the three Cases.

C. Original parallelogram

A parallelogram is a frequently used structure to obtain a 2-DoF mechanism. A parallelogram has the property that the CoM stays on the same length as the rotation point for both local frames. This makes it an applicable structure for shaking force balancing as all the counter-masses can be added near the base (fisher's method) [18]. Which is far better for the dynamic performance compared to balancing far away links [13]. Multiple parallelograms can be added together for obtaining shaking force balance [19]. As the inertia and the distance to the CoM should be constant, the angular momentum should also be constant for every movement in the workspace. In this paper, when constant angular momentum is mentioned, a constant velocity input for $\dot{\theta}_i$ is used. In formula form, this will be:

$$\bar{H} = \sum \bar{r}_i \times (\dot{\bar{r}}_i m_i) + I_i \dot{\bar{\theta}}_i \tag{3}$$

The angular momentum of a system can be calculated around the CoM, or a fixed point of a system [20]. The angular momentum for both DoF around the origin of a parallelogram for every beam will be as followed

$$\bar{H}_{O1} = \begin{bmatrix} I_1 + m_1(p_1^2 + q_1^2) \\ 0 \end{bmatrix} \cdot \begin{bmatrix} \dot{\theta}_1 \\ \dot{\theta}_2 \end{bmatrix} \tag{4}$$

$$\bar{H}_{O2} = \begin{bmatrix} 0 \\ I_2 + m_2(p_2^2 + q_2^2) \end{bmatrix} \cdot \begin{bmatrix} \dot{\theta}_1 \\ \dot{\theta}_2 \end{bmatrix} \tag{5}$$

$$\bar{H}_{O3} = \begin{bmatrix} L_1 m_3 (p_3 c(\theta_1 - \theta_2) + q_3 s(\theta_1 - \theta_2)) \\ L_1 m_3 (p_3 c(\theta_1 - \theta_2) + q_3 s(\theta_1 - \theta_2)) \end{bmatrix} \cdot \begin{bmatrix} \dot{\theta}_1 \\ \dot{\theta}_2 \end{bmatrix} + \begin{bmatrix} m_3 L_1^2 \\ I_3 + m_3(p_3^2 + q_3^2) \end{bmatrix} \cdot \begin{bmatrix} \dot{\theta}_1 \\ \dot{\theta}_2 \end{bmatrix} \tag{6}$$

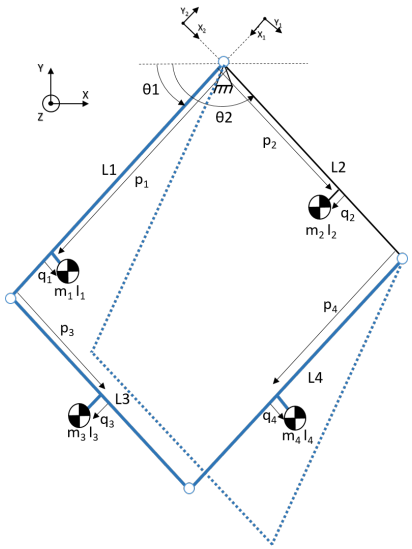

Figure 2. A visualization of the movement of a parallelogram when one DoF is actuated.

$$\bar{H}_{O4} = \begin{bmatrix} L_2 m_4 (p_4 c(\theta_1 - \theta_2) - q_4 s(\theta_1 - \theta_2)) \\ L_2 m_4 (p_4 c(\theta_1 - \theta_2) - q_4 s(\theta_1 - \theta_2)) \end{bmatrix} \cdot \begin{bmatrix} \dot{\theta}_1 \\ \dot{\theta}_2 \end{bmatrix} + \begin{bmatrix} I_4 + m_4(p_4^2 + q_4^2) \\ m_4 L_2^2 \end{bmatrix} \cdot \begin{bmatrix} \dot{\theta}_1 \\ \dot{\theta}_2 \end{bmatrix} \tag{7}$$

With s() and c() as shorthand for sin() and cos(), respectively. L_i is the length of a beam. p_i and q_i are the positions of the CoM. One can see that the angular momentum of beam 1 and 2 are constant for any input θ_1 or θ_2. On the other hand, beam 3 and 4 depend on these input angles and will not be constant in the whole workspace. For this particular reason, a single parallelogram DoF will not act as a rotatable beam and will, therefore, not be able to be fully balanced by a constant counter-rotatable structure.

III. Obtaining constant angular momentum for a 2-DoF parallelogram

This chapter presents a solution for obtaining constant angular momentum for a 2-DoF parallelogram. First, the equations will be derived for a parallelogram and what is needed to obtain this. Later a solution will be presented as well as the formulas for obtaining constant angular momentum.

A. Mathematically obtaining constant angular momentum for a single parallelogram

For obtaining the equations for constant angular momentum, one can balance the two DoF separately, so balance firstly θ_1 and afterwards θ_2 or vice versa. One can also take the DoF together, creating two subsets of velocities that, together, can create every movement. Doing this will better visualise what is needed to obtain constant angular momentum in a 2-DoF workspace. The two sets are as follows

$$\begin{bmatrix} \dot{\theta}_1 \\ \dot{\theta}_2 \end{bmatrix} or \begin{bmatrix} -\dot{\theta}_1 \\ \dot{\theta}_2 \end{bmatrix} \tag{8}$$

When using the same arbitrary values for the first set, the end-effector will create a rotation around the origin (as can be seen in the first figure in Fig. 14 in appendix -A). With the second set, the end-effector will create a vertical ellipsoidal movement from or to the origin (second figure in Fig. 14). If this movement's link lengths are the same, it will be a vertical line.

In both cases, the mass of beam 1 and 2 will always be at a constant distance to the origin and so do not have any effect on

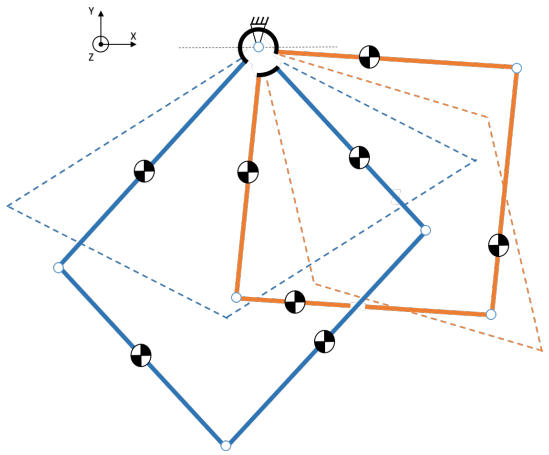

Figure 3. A visualisation of the movement of the two parallelograms that make a constant inertia mechanism (CIM) around the origin

the change of the angular momentum. The second movement set ($[-\dot{\theta}_1, \dot{\theta}_2]^T$) does not have any effect on the change of angular momentum for a parallelogram (see appendix -B for elaboration), so only the first movement set ($[\dot{\theta}_1, \dot{\theta}_2]^T$) needs to be made constant. The first movement set is a rotation around the origin. This means that the inertia around the origin should be constant for obtaining constant angular momentum for the whole workspace. Taking this movement set and using it for adding the angular momentum of beam 3 and 4 together and discarding the constant terms that are not a function of θ_1 or θ_2. This will give the following

$$\begin{aligned} eq_1(\theta_1, \theta_2) = \\ &(L_1 m_3 p_3 + L_2 m_4 p_4) cos(\theta_1 - \theta_2) + \\ &(-L_1 m_3 q_3 - L_2 m_4 q_4) sin(\theta_1 - \theta_2) \\ &= constant \quad \forall \quad (\theta_1, \theta_2) \end{aligned} \tag{9}$$

One can see that for a solution, the equation should be constant for every input angle. This will result in the terms before the cos, and sin should be zero. This will lead to $p3 = -p4$ and $q3 = -q4$. This can be achieved by adding counter-masses to the distal links, but this is generally not wanted due to a decay in eigenfrequency [13].

B. Obtaining constant inertia with a counter-inertia

To obtain constant inertia around the origin a counter-inertia has to be added to the parallelogram that contracts when the parallelogram expands and vice versa. A solution is to add another parallelogram that is constrained in a way that this motion happens, as is depicted in Fig. 3. This counter-inertia structure with the properties of a parallelogram (which will now be referred to as a counter-parallelogram) will keep the inertia and, therefore, the angular momentum constant if the mass distribution is right. The counter-parallelogram can be rotated around the origin with an angle (γ) and keep the inertia constant. This is depicted in Fig. 4. By adding a counter-parallelogram, the general solution for obtaining constant inertia can be obtained by adding beams 3, 4, 3^* and 4^* together and discarding the constant terms that are not a function of θ_1 or θ_2. This will give the following equation

$$\begin{aligned} eq_2(\theta_1, \theta_2) = \\ &(L_1 m_3 p_3 + L_2 m_4 p_4 - L_1^* m_3^* p_3^* - L_2^* m_4^* p_4^*) c(\theta_1 - \theta_2) + \\ &(-L_1 m_3 q_3 - L_2 m_4 q_4 + L_1^* m_3^* q_3^* + L_2^* m_4^* q_4^*) s(\theta_1 - \theta_2) \\ &= constant \quad \forall \quad (\theta_1, \theta_2) \end{aligned} \tag{10}$$

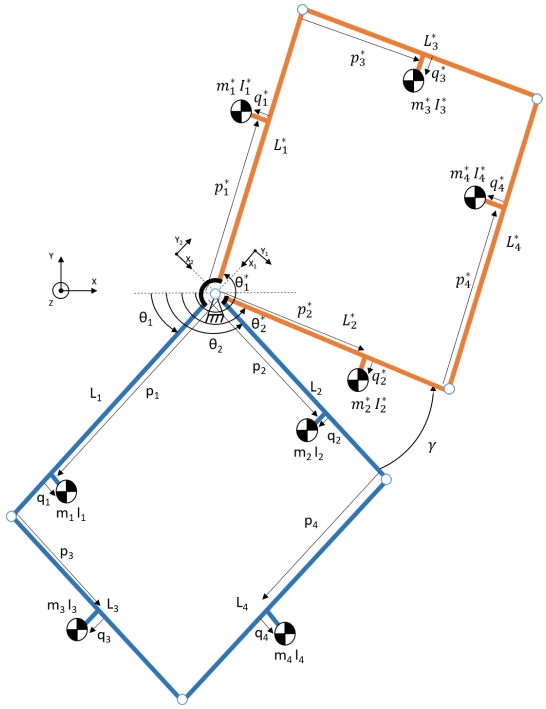

Figure 4. A general solution to mirror an arbitrary parallelogram around a link to obtain constant angular momentum.

Again, for a solution, the equation should be constant for every input angle. This will lead to two balancing conditions, as can be seen in equations (11) and (12). In equations (13) and (14) the constraints are given for the counter-parallelogram to be properly constrained. The four balancing conditions can lead to infinitely many solutions for an arbitrary parallelogram.

$$L_1 m_3 p_3 + L_2 m_4 p_4 - L_1^* m_3^* p_3^* - L_2^* m_4^* p_4^* = 0 \tag{11}$$

$$- L_1 m_3 q_3 - L_2 m_4 q_4 + L_1^* m_3^* q_3^* + L_2^* m_4^* q_4^* = 0 \tag{12}$$

$$\theta_1^* = \theta_1 + \gamma + pi \tag{13}$$

$$\theta_2^* = \theta_2 + \gamma \tag{14}$$

The position of the CoM for both DoF are important points for balancing as a mass has to be in collinear to this point to obtain force balancing. The CoM moves in the workspace but their distance to the origin will stay the same. Their place can be written in a vector notation $[x, y]^T$ in their local frame as

$$\bar{r}_{\theta 1} = \begin{bmatrix} \frac{(p_1 m_1 + q_2 m_2 + p_4 m_4 + (L_1 + q_3) m_3)}{(m_1 + m_2 + m_3 + m_4)} \\ 0 \end{bmatrix} - \bar{R} \begin{bmatrix} \frac{(p_1^* m_1^* - q_2^* m_2^* + p_4^* m_4^* + (L_1^* - q_3^*) m_3^*)}{(m_1^* + m_2^* + m_3^* + m_4^*)} \\ 0 \end{bmatrix} \tag{15}$$

$$\bar{r}_{\theta 2} = \begin{bmatrix} \frac{(p_2 m_2 + q_1 m_1 + p_3 m_3 + (L_2 + q_4) m_4)}{(m_1 + m_2 + m_3 + m_4)} \\ 0 \end{bmatrix} + \bar{R} \begin{bmatrix} \frac{(p_2^* m_2^* - q_1^* m_1^* + p_3^* m_3^* + (L_2^* - q_4^*) m_4^*)}{(m_1^* + m_2^* + m_3^* + m_4^*)} \\ 0 \end{bmatrix} \tag{16}$$

Where $\bar{R}$ is the rotation matrix around the z-axis with angle (γ). The reduced inertia per input angles around the origin can be obtained from the kinetic energy as

$$T_{O\theta_1} = \frac{1}{2} I_{\theta 1}^{red} \dot{\theta}_1^2 \tag{17}$$

$$T_{O\theta_2} = \frac{1}{2} I_{\theta 2}^{red} \dot{\theta}_2^2 \tag{18}$$

Because of a parallelogram structure, some beams only translate without rotating, if one DoF is actuated, in the global frame. Giving the following equations for the inertia as

$$\begin{aligned} I_{\theta 1}^{red} = I_1 + m_1(p_1^2 + q_1^2) + I_1^* + m_1^*(p_1^{*2} + q_1^{*2}) + \\ m_3(L_1 + q_3)^2 + m_3^*(L_1^* - q_3^*)^2 + \\ I_4 + m_4(p_4^2 + q_4^2) + I_4^* + m_4^*(p_4^{*2} + q_4^{*2}) \end{aligned} \tag{19}$$

$$\begin{aligned} I_{\theta 2}^{red} = I_2 + m_2(p_2^2 + q_2^2) + I_2^* + m_2^*(p_2^{*2} + q_2^{*2}) + \\ m_4(L_2 + q_4)^2 + m_4^*(L_2^* - q_4^*)^2 + \\ I_3 + m_3(p_3^2 + q_3^2) + I_3^* + m_3^*(p_3^{*2} + q_3^{*2}) \end{aligned} \tag{20}$$

C. Obtaining a specific case to always obtain constant angular momentum

Two solutions that always give a structure the same angular momentum for constant input velocity in its workspace. The first is, mirroring the original parallelogram across beam 1 or 2 and rotating it further with an arbitrary angle (γ). See Fig. 4. The second is to copy the original parallelogram and rotate it around an arbitrary angle (γ). (See Fig. 15). For both cases, the mass of every beam should be kept the same, and the position of these masses (q_i) should be negative for the copied structure. Both must also comply with equations (13) and (14).

IV. 2-DoF inherently dynamically balanced design solutions

In Fig. 4, a general 2-DoF structure is presented with constant CoM, inertia and angular momentum around its origin for every local DoF for the whole workspace. In this chapter, seven different 2-DoF inherently dynamically balanced Design solutions are displayed, as well as the numerical confirmation of the dynamic balancing of one Design solution.

A. Seven different Design solutions

In Fig. 9 till 11 the Design solutions are shown. For every solution, only one balancing DoF (θ_1) is drawn to make the figures clearer. Angle (γ) is drawn at 90° but can be chosen arbitrarily. Every original parallelogram (always drawn in blue) and counter-parallelogram (always drawn in orange) that is given in the examples must comply with the balancing equations (11) till (14). The links of L_1 and L_1^* are constrained to each other as are L_2 and L_2^*. The links that are in black are the counter-rotations. For Fig. 5 till 10 these are the added reactionless four-bar linkages taken from [21]. In Fig. 11 it is the counter-rotation. To comply with the balancing conditions, the perpendicular distance (q_i) of every added reactionless four-bar must be zero. Note that the given solutions are not perfectly drawn to scale.

B. Numerical confirmation of Design solution 4 that it is inherently dynamically balanced

An inherently dynamically balanced 2-DoF structure based on Ds4 is presented in Fig. 12. The CoM is in the middle of every link except for the links $L_{2\theta_k}$ and $L_{3\theta_k}$. k means that it is applicable for both inverted four-bars. This structure uses a counter-parallelogram and two inverted four-bars with the following balancing equations (11) till (14), and $CaseII$ in appendix -D. In Spacar [22], this structure

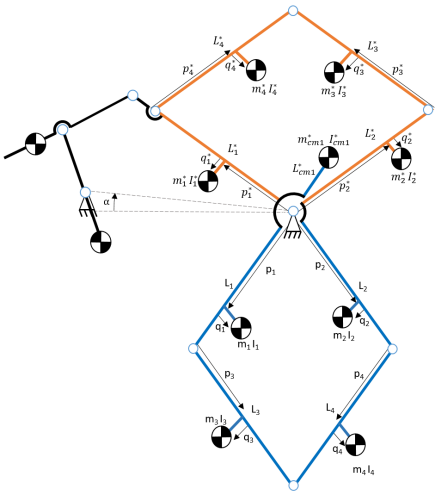

Figure 5. Ds1, this solution uses a Case I reactionless four-bar to be balanced. A counter-mass is used to move the CoM in line with the first link of the parallelogram

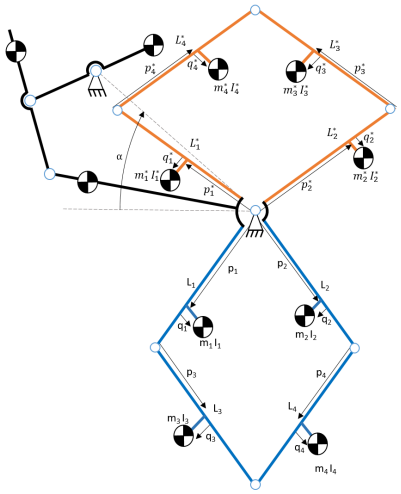

Figure 6. Ds2, a parallelogram dynamically balanced by a Case I reactionless four-bar

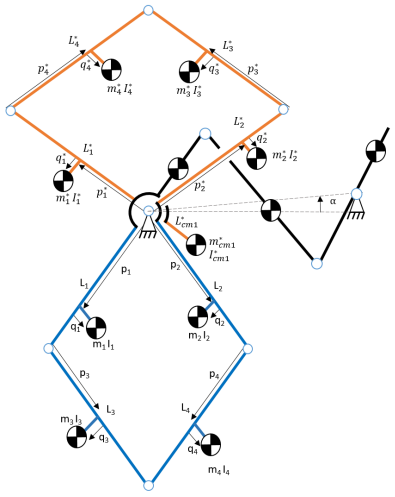

Figure 7. Ds3, this solution uses a Case II reactionless four-bar to be balanced. A counter-mass is used to move the CoM in line with the first link of the parallelogram.

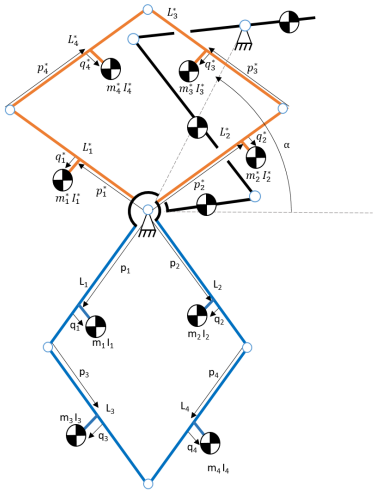

Figure 8. Ds4, a parallelogram dynamically balanced by a Case II reactionless four-bar

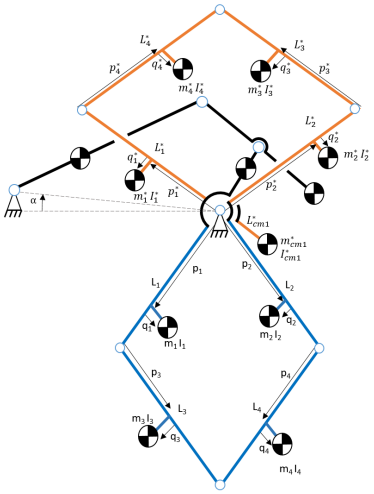

Figure 9. Ds5, this solution uses a Case III reactionless four-bar. A counter-mass is used to move the CoM in line with the first link of the parallelogram.

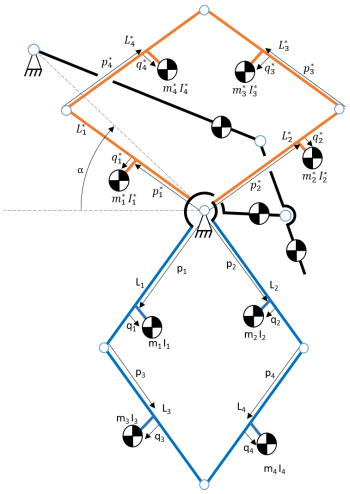

Figure 10. Ds6, a parallelogram dynamically balanced by a Case III reactionless four-bar

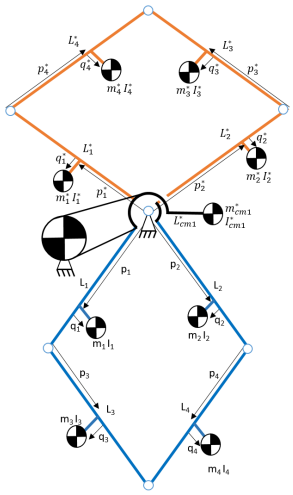

Figure 11. Ds7, a parallelogram force balanced by a counter-mass and dynamically balanced by a counter-rotation connected with belts or gears

is simulated and validated to be completely balanced. In table I, all the lengths, masses, CoM and moment of inertia are listed that are used for every beam. Note that every CoM is in the middle of that particular beam, meaning that q is zero. In Fig. 13, the results are plotted for an arbitrary movement.

Table I
PARAMETERS OF AN INHERENTLY BALANCED STRUCTURE BASED ON DS4, VISUALIZED IN FIG. 12

(mm)	(mm)	(kg)	(kgm^2)
$L_1 = 200$	$p_1 = 100$	$m_1 = 0.3900$	$I_1 = 0.001300000$
$L_2 = 100$	$p_2 = 50$	$m_2 = 0.1950$	$I_2 = 0.000162500$
$L_3 = 100$	$p_3 = 50$	$m_3 = 0.1950$	$I_3 = 0.000162500$
$L_4 = 200$	$p_4 = 100$	$m_4 = 0.3900$	$I_4 = 0.001300000$
$L_1^* = 50$	$p_1^* = 25$	$m_1^* = 0.0975$	$I_1^* = 0.000020312$
$L_2^* = 80$	$p_2^* = 40$	$m_2^* = 0.1560$	$I_2^* = 0.000083200$
$L_3^* = 80$	$p_3^* = 40$	$m_3^* = 2.8275$	$I_3^* = 0.000083200$
$L_4^* = 50$	$p_4^* = 25$	$m_4^* = 0.0975$	$I_4^* = 0.000020312$
$L_{1\theta_k} = 70$	$p_{1\theta_k} = 35$	$m_{1\theta_k} = 0.1365$	$I_{1\theta_k} = 0.000055737$
$L_{2\theta_k} = 230$	$p_{2\theta_k} = 115$	$m_{2\theta_k} = 0.8970$	$I_{2\theta_k} = 0.003954275$
$L_{3\theta_k} = 70$	$p_{3\theta_k} = 35$	$m_{3\theta_k} = 0.1365$	$I_{3\theta_k} = 0.000055737$
$L_{4\theta_k} = 230$			
$L_{3r\theta_k} = 2L_{3\theta_k}$			
	$p^*_{2\theta_1} = 150$	$m^*_{2\theta_1} = 6.2066$	$I^*_{2\theta_1} = 0.043958399$
	$p^*_{3\theta_1} = 10$	$m^*_{3\theta_1} = 30.9965$	$I^*_{3\theta_1} = 0.013075564$
	$p^*_{2\theta_2} = 150$	$m^*_{2\theta_2} = 4.2624$	$I^*_{2\theta_2} = 0.038608256$
	$p^*_{3\theta_2} = 5$	$m^*_{3\theta_2} = 44.2411$	$I^*_{3\theta_2} = 0.003301417$

V. DISCUSSION

This paper presents some new design solutions for inherently balancing a 2-DoF parallelogram by using a counter-parallelogram. The counter-parallelogram is an interesting idea because while using constant speed, it keeps the angular momentum constant for both DoF in its whole workspace. As this technique already exists, but only if distal links are balanced. The counter-parallelogram uses masses near a pivot point, which is more advantageous for better controllability. Using a parallelogram with a counter-parallelogram makes both DoF act as a single rotatable beam (constant CoM, inertia, angular momentum). Therefore making the structure optimal for a new building block that can be used to be dynamically balanced by reactionless four-bars or counter-rotatable masses.

Two general solutions are given that always give constant inertia for a parallelogram. It is proven that any parallelogram can be made that it has constant inertia and thus constant angular momentum with

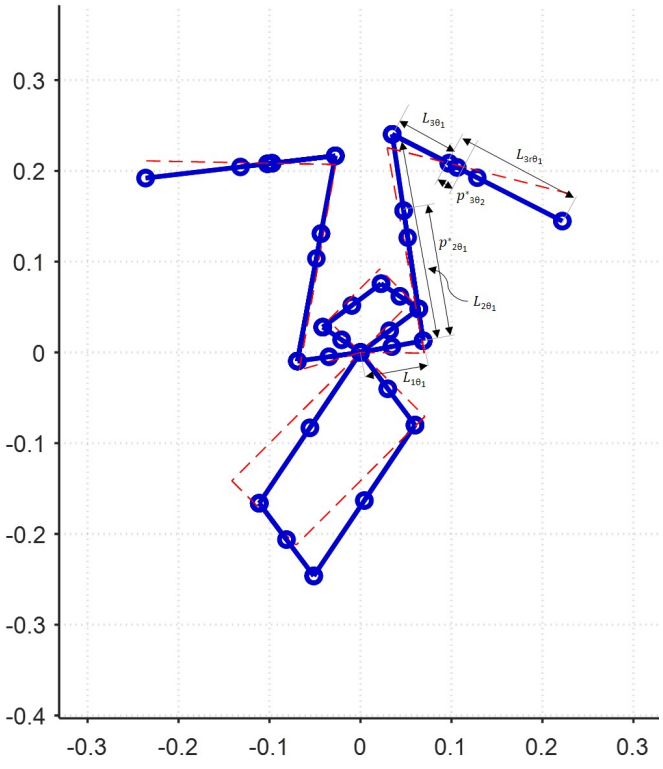

Figure 12. A visualization of the movement of an inherently dynamically balanced 2-DoF structure based on Ds4

an infinite amount of counter-parallelograms. Using such a counter-parallelogram will increase the mass and inertia by approximately a factor of two compared to the original parallelogram because of the copied structure. Beam lengths and places of the mass can be altered to increase or decrease this factor while maintaining balance conditions.

Seven inherently dynamically balanced design solutions are given that are all dynamically balanced. Case I till III of the reactionless four-bars are used. Case I and III have small workspaces that can become close to singular fast. The interference of their links can lead to an even smaller workspace. Case II, on the other hand, has a bigger workspace and will therefore be more appropriate to use for a manipulator. The first link of Case II and III must lay on the opposite side of the revolute joint to the local DoF CoM to fulfil the balancing conditions. The first link of Case I CoM can lay on itself, and therefore it can be in the extension of the DoF CoM itself. This can accomplish that the mechanism has no collision (except for its origin) for the whole workspace. Counter-masses can be used to relocate the local DoF CoM so the first link of the four-bar can also be relocated to a more convenient position, which is done for Ds1-3-5. However, this will heavily increase the movable mass.

All reactionless four-bars in the Ds can be mirrored around their first link to create a slightly different orientated solution that is still valid. All fixed points of the reactionless four-bars can also be rotated around an angle α with respect to the origin. This can relocate the four-bars' singularity positions and shift, increase, or decrease the workspace. This can also lower or increase the inertia and eigenfrequency ratio of that position [3].

Ds7 uses a counter-mass to make the mechanism force balanced. A counter-rotatable mass makes the mechanism dynamically balanced. It can be attached by gears or belts, with most of the solutions on a single rotatable link described in Ref. [23]. An example in the literature that looks like this Ds is the invention in Ref. [11]. This manipulator can be made more optimal for controllability to shift the counter-masses on the distal links to the base on a counter-parallelogram. Using a counter-rotatable mass is estimated to be less sufficient for higher acceleration because of the lower eigenfrequency ratios that can be obtained [3]. Using belts or gears can also induce backlash and wear, which can reduce the balancing conditions [24]. The parallelogram and the counter-parallelogram can also be actively balanced by a counter-rotatable drive if the counter-parallelogram makes the control easier because the angular momentum is not a function of position anymore, and only input velocity can be investigated.

All Ds can also be made with a six-bar linkage, but a solution is harder to obtain (see appendix -E). By doing this, the actuators can be closer to the Origin of that DoF, or less interference of the links can be achieved. Alternatively, even actuation redundancy can be used [25]. Using a six-bar will impose an extra DoF (rotation of the added link) which is not wanted. This can be mechanically constrained as in Ref. [26]. If the six-bar linkage can be made to have constant inertia with a counter-six-bar linkage and still be optimal for controllability can be interesting research.

Ds3 and Ds4 are tested in Spacar and numerically confirmed to be completely dynamically balanced. The results of Ds4 can be seen in this paper. In Fig. 1 (b), a proposed design is visible that implements the inverted four-bars as a building block, with the consideration of controllability, but adds a counter-parallelogram to obtain a CIM and therefore obtain a fully inherently dynamically balanced mechanism sufficient for high acceleration applications.

VI. Conclusion

In this paper, a constant inertia mechanism (CIM) is proposed, consisting of a parallelogram and counter-parallelogram, which obtain constant inertia around their pivot point in their workspace. Variations of this mechanism are presented by changing the coupled angle or the properties of the links. Seven design solutions combine the CIM with balancing techniques for a single rotatable link to obtain 2-DoF structures that are inherently dynamically balanced in their entire workspace, with no active counter-rotations. One design solution is elaborated, and the results confirm that it is completely dynamically balanced. A suggestion is made for an inherently dynamically balanced 2-DoF parallel manipulator consisting of a CIM and two inverted four-bars sufficient for higher acceleration applications.

References

[1] S. Briot, A. Pashkevich, and D. Chablat, "On the optimal design of parallel robots taking into account their deformations and natural frequencies," *Proceedings of the ASME Design Engineering Technical Conference*, vol. 7, no. PARTS A AND B, pp. 367–376, 2009.

[2] G. Lowen and R. Berkof, "Survey of investigations into the balancing of linkages," *Journal of mechanisms*, vol. 3, no. 4, pp. 221–231, 1968.

[3] M. V. d. W. Zomerdijk, "Reducing settling time in high acceleration applications of macro scale robotic manipulators with dynamic balancing," Dec 2020. [Online]. Available: http://resolver.tudelft.nl/uuid:5cadc48b-098a-4a82-adfa-c68500d8764f

[4] B. van der Zon, "Besi zoekt snelheidslimiet pakken en plaatsen op," Sep 2007. [Online]. Available: https://mechatronicamachinebouw.nl/artikel/besi-zoekt-snelheidslimiet-pakken-en-plaatsen-op/

[5] J. P. Karidis, G. Mcvicker, J. P. Pawletko, L. C. Zai, M. Goldowsky, R. E. Brown, and R. R. Comulada, "The Hummingbird Minipositioner-Providing Three-Axis Motion At 50 G's With Low Reactions," Tech. Rep.

[6] J.-F. Collard and C. Gosselin, "Optimal synthesis of a planar reactionless three-degree-of-freedom parallel mechanism," 2011.

[7] V. H. Arakelian and M. R. Smith, "Design of planar 3-DOF 3-RRR reactionless parallel manipulators," *Mechatronics*, vol. 18, no. 10, pp. 601–606, 2008. [Online]. Available: http://dx.doi.org/10.1016/j.mechatronics.2008.05.002

[8] V. Van der Wijk and J. Herder, "Dynamic balancing of mechanisms by using an actively driven counter-rotary counter-mass for low mass and low inertia," in *Proceedings of the Second International Workshop on Fundamental Issues and Future Research Directions for Parallel Mechanisms and Manipulators, Montpellier*, 2008, pp. 241–251.

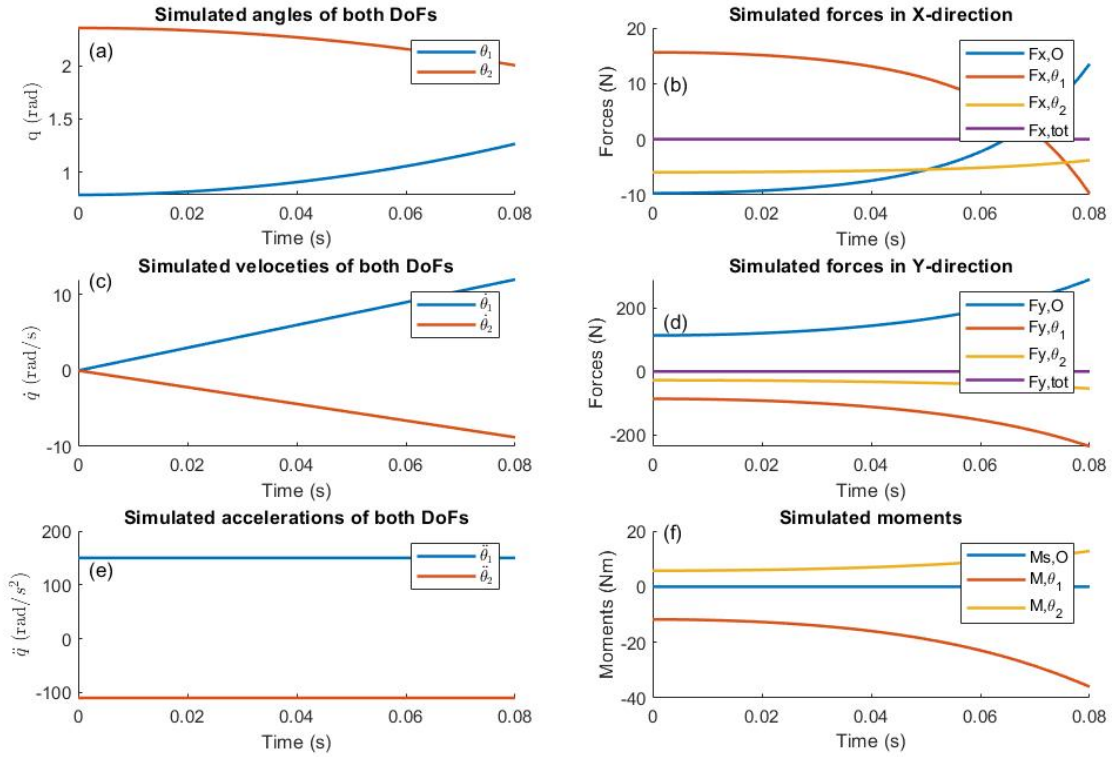

Figure 13. The figure shows the output angles (a), output velocities (c), output accelerations (e), shaking forces in x- and y-direction, (b) and (c), respectively and the shaking moment (d). The total forces (F, tot) or shaking force balance are the sums of the reaction forces in the origin and both actuator points. The shaking moment (Ms, O) is the sum of all angular moments around the origin. This is displayed together with the motor torques (Ms,θ_1 Ms,θ_2). Note that the order of the shaking force and moment balance is in 1e-13, which is the tolerance of the objective function.

[9] Y. Wu and C. M. Gosselin, "Synthesis of reactionless spatial 3-DoF and 6-DoF mechanisms without separate counter-rotations," *International Journal of Robotics Research*, vol. 23, no. 6, pp. 625–642, jun 2004.

[10] V. Van der Wijk and J. L. Herder, "Double pendulum balanced by counter-rotary counter-masses as useful element for synthesis of dynamically balanced mechanisms," in *International Design Engineering Technical Conferences and Computers and Information in Engineering Conference*, vol. 43260, 2008, pp. 453–463.

[11] J. Herder, A. Ariens, B. Bakker, and H. Menschaar, "Wo2006080846 - five-bar mechanism with dynamic balancing means and method for dynamically balancing a five-bar mechanism," Patent, 2006.

[12] V. Van Der Wijk and J. L. Herder, "Synthesis of dynamically balanced mechanisms by using counter-rotary countermass balanced double pendula," *Journal of Mechanical Design, Transactions of the ASME*, vol. 131, no. 11, pp. 1 110 031–1 110 038, 2009.

[13] J. J. De Jong, B. E. Schaars, and D. M. Brouwer, "The influence of flexibility on the force balance quality: A frequency domain approach," in *European Society for Precision Engineering and Nanotechnology, Conference Proceedings - 19th International Conference and Exhibition, EUSPEN 2019*, 2019.

[14] V. van der Wijk, S. Krut, F. Pierrot, and J. L. Herder, "Design and experimental evaluation of a dynamically balanced redundant planar 4-RRR parallel manipulator," *The International Journal of Robotics Research*, vol. 32, no. 6, pp. 744–759, may 2013.

[15] T. Laliberté and C. Gosselin, "Synthesis, optimization and experimental validation of reactionless two-DOF parallel mechanisms using counter-mechanisms," *Meccanica*, vol. 51, no. 12, pp. 3211–3225, dec 2016.

[16] V. Arakelian, "Inertia forces and moments balancing in robot manipulators: a review," *Advanced Robotics*, vol. 31, no. 14, pp. 717–726, jul 2017.

[17] V. Van der Wijk, B. Demeulenaere, C. Gosselin, and J. L. Herder, "Comparative Analysis for Low-Mass and Low-Inertia Dynamic Balancing of Mechanisms," *Journal of Mechanisms and Robotics*, vol. 4, no. 3, jun 2012.

[18] V. v. d. Wijk and J. L. Herder, "The work of otto fischer and the historical development of his method of principal vectors for mechanism and machine science," in *Explorations in the History of Machines and Mechanisms*. Springer, 2012, pp. 521–534.

[19] V. Van der Wijk, *Methodology for analysis and synthesis of inherently force and moment-balanced mechanisms - theory and applications*, 2014. [Online]. Available: https://doi.org/10.3990/1.9789036536301

[20] H. Vallery and A. L. Schwab, *Advanced Dynamics*. Delft University of Technology, 2017.

[21] C. Gosselin, R. Ricard, and C. M. Gosselin, "On the development of reactionless parallel manipulators Cable-driven robotics, dynamic trajectory planning View project Master in Robotics View project ON THE DEVELOPMENT OF REACTIONLESS PARALLEL MANIPULATORS," Tech. Rep. [Online]. Available: https://www.researchgate.net/publication/247035201

[22] J. B. Jonker and J. P. Meijaard, "Spacar — computer program for dynamic analysis of flexible spatial mechanisms and manipulators," Berlin, Heidelberg, pp. 123–143, 1990.

[23] V. Van der Wijk, B. Demeulenaere, C. Gosselin, and J. L. Herder, "Comparative analysis for low-mass and low-inertia dynamic balancing of mechanisms," 2012.

[24] E. Uzunoğlu, M. Özkahya, E. Paksoy, B. Taner, M. I. Can Dede, and G. Kiper, "Conceptual Design of a 2-DoF Planar High-Speed Industrial Parallel Manipulator," *Mechanisms and Machine Science*, vol. 79, pp. 344–353, 2020.

[25] K. Nagai and Z. Liu, "Re-design of force redundant parallel mechanisms by introducing kinematical redundancy," *2009 IEEE/RSJ International Conference on Intelligent Robots and Systems, IROS 2009*, pp. 5898–5904, 2009.

[26] C. Germain, S. Briot, V. Glazunov, S. Caro, C. Germain, S. Briot, V. Glazunov, S. Caro, and P. W. I. A, "IRSBOT-2 : A Novel Two-Dof Parallel Robot for High-Speed Operations To cite this version : HAL Id : hal-00590082," 2019.

VII. Appendices

A. Movements of a parallelogram

Here the two movement sets that a parallelogram can make are visualised in Fig. 14. With the first being ($[\dot{\theta}_1, \dot{\theta}_2]^T$) and the second being ($[\dot{\theta}_1, -\dot{\theta}_2]^T$). Together a parallelogram can make every trajectory.

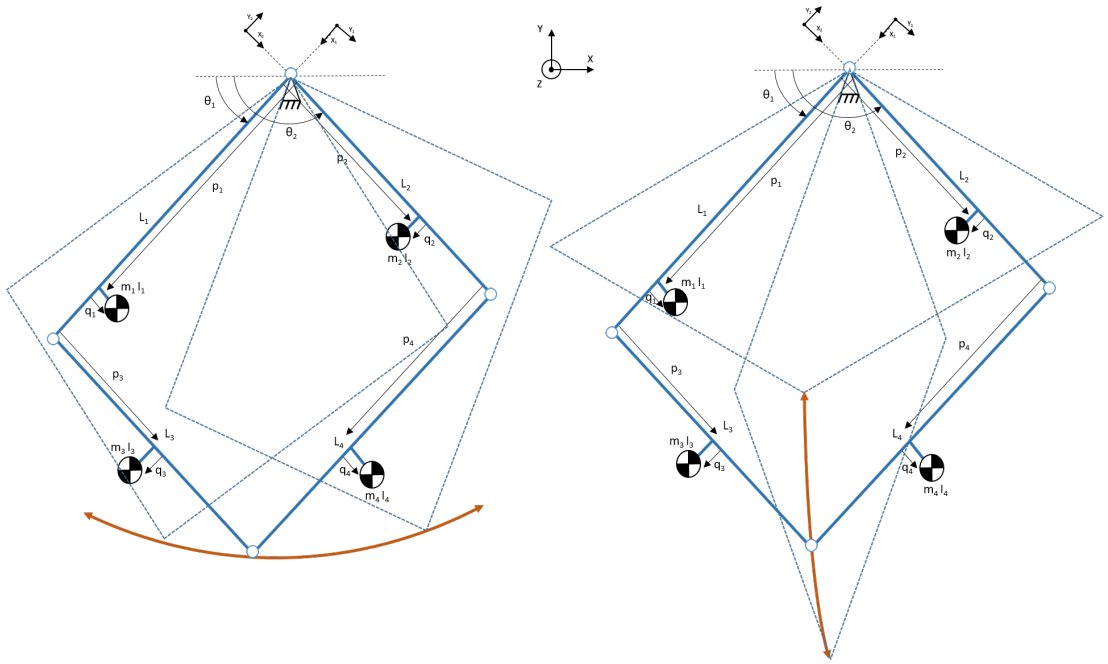

Figure 14. A visualisation of the two combined movements a parallelogram can make. First schematic is with positive $\dot{\theta}_1$ and $\dot{\theta}_2$ which creates a constant radii around the origin. The second is one of either being negative. This creates an eclipse from the origin to a point in space. This will be a straight line for equal-sided parallelograms. With a combination of these two movements, every trajectory in a plane can be made

B. Constant angular momentum for a expanding and collapsing parallelogram

Here is some more elaboration on why the second movement set of equation (8) will always be constant for a parallelogram. For an arbitrarily chosen parallelogram, the angular momentum is given by equations (4) till (7). As has been stated, beams 1 and 2 have no influence on the change of angular momentum. So $\bar{H}_3$ plus $\bar{H}_4$ must be constant while using the second movement set ($[-\dot{\theta}_1, \dot{\theta}_2]^T$). This will obtain the following

$$\bar{H}_{O3} = \begin{bmatrix} L_1 m_3(p_3 c(\theta_1 - \theta_2) + q_3 s(\theta_1 - \theta_2)) + m_3 L_1^2 \\ L_1 m_3(p_3 c(\theta_1 - \theta_2) + q_3 s(\theta_1 - \theta_2)) + I_3 + m_3(p_3^2 + q_3^2) \end{bmatrix} \cdot \begin{bmatrix} -\dot{\theta}_1 \\ \dot{\theta}_2 \end{bmatrix} \tag{21}$$

$$\bar{H}_{O4} = \begin{bmatrix} L_2 m_4(p_4 c(\theta_1 - \theta_2) - q_4 s(\theta_1 - \theta_2)) + I_4 + m_4(p_4^2 + q_4^2) \\ L_2 m_4(p_4 c(\theta_1 - \theta_2) - q_4 s(\theta_1 - \theta_2)) + m_4 L_2^2 \end{bmatrix} \cdot \begin{bmatrix} -\dot{\theta}_1 \\ \dot{\theta}_2 \end{bmatrix} \tag{22}$$

Filling these in will give the following

$$-\dot{\theta}_1(m_3 L_1^2 + I_4 + m_4(p_4^2 + q_4^2)) + \dot{\theta}_2(I_3 + m_3(p_3^2 + q_3^2) + m_4 L_2^2) \qquad = constant \tag{23}$$

This is true for every θ_1 and θ_2, and therefore an arbitrary parallelogram will always give a constant angular momentum for this movement set.

C. General solution to obtain constant angular momentum

In Fig. 15 a general solution to obtain constant angular momentum is visible. If the original parallelogram is copied and rotated around an angle (γ) and the perpendicular CoM position (q_i) of the links is equal to $-q_i^*$, and p_i is equal to p_i^*, then this will always obtain a solution to equations (11) till (14).

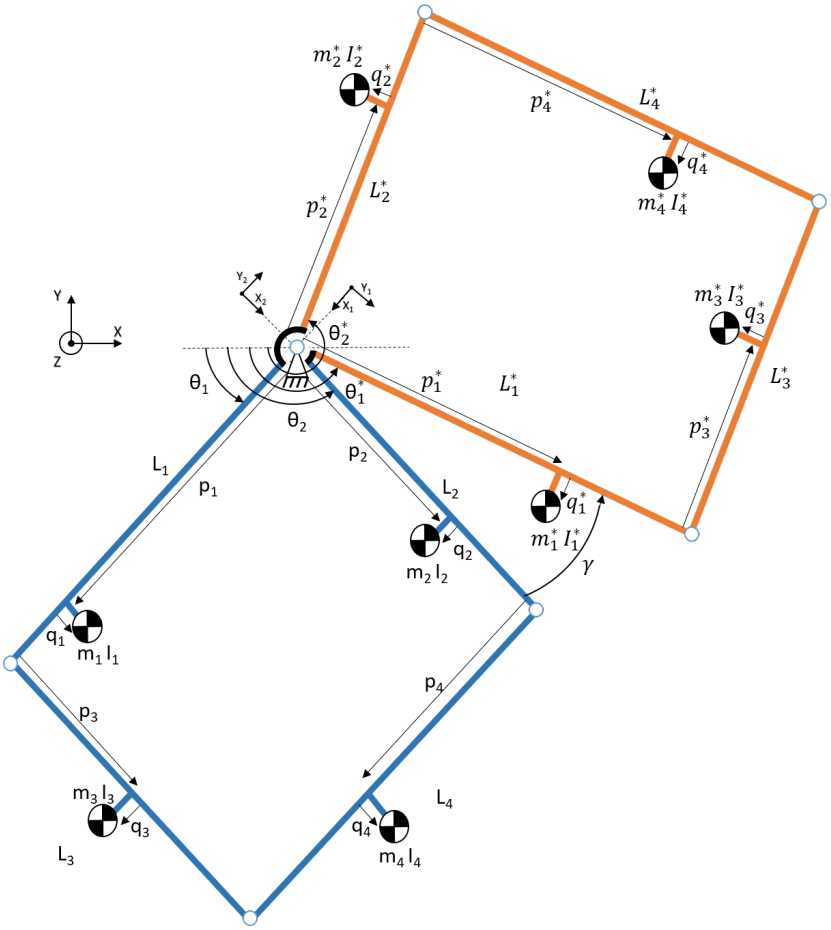

Figure 15. A second general solution to obtain constant inertia around the origin, is by adding a counter-parallelogram and rotating it around an angle (γ).

D. Reactionless four-bars

Here the three cases of Gosselin et al. [9] are further elaborated and their balancing conditions are given.

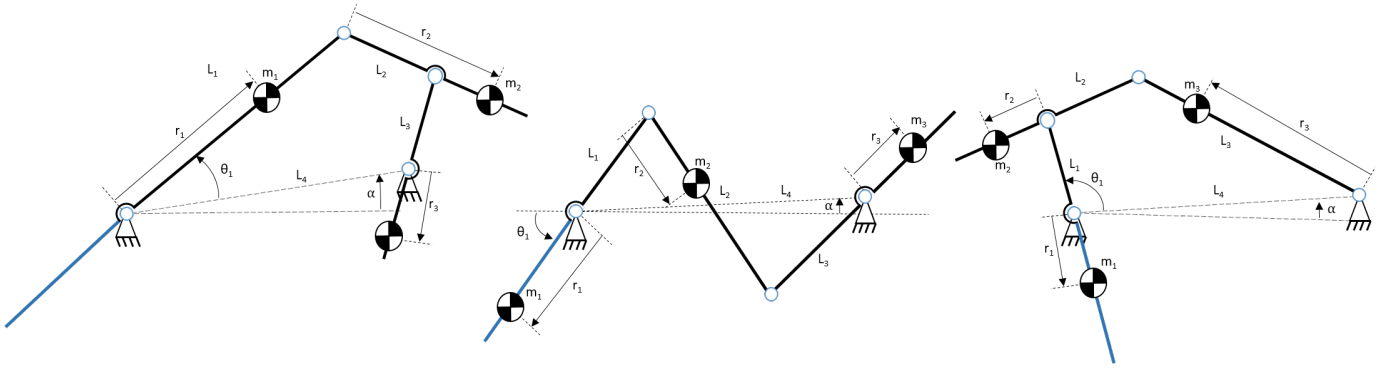

Figure 16. Case I till III of the reactionless four-bars, which are inherently dynamically balanced

$CaseI$	$CaseII$	$CaseIII$
$r_2 = L_2\dfrac{(1+m_1r_1)}{(m_2L_1)}$	$r_2 = L_2\dfrac{(1-m_1r_1)}{(m_2L_1)}$	$r_2 = -L_2 + \dfrac{m_1r_1}{m_2}$
$r_3 = \dfrac{(m_2r_2L_3)}{(m_3L_2)}$	$r_3 = \dfrac{(m_2r_2L_3)}{(m_3L_2)}$	$r_3 = \dfrac{(m_2r_2L_3)}{(m_3L_2)}$
$I_{2com} = m_2(L_2r_2 - r_2^2) - I_c$	$I_{2com} = m_2(L_2r_2 - r_2^2) - I_c$	$I_{2com} = -m_2(L_2r_2 + r_2^2) + I_c$
$I_{3com} = -m_3(L_3r_3 + r_3^2) - I_c$	$I_{3com} = -m_3(L_3r_3 + r_3^2) + I_c$	$I_{3com} = m_3(L_3r_3 - r_3^2) - I_c$
$I_c = I_{1com} + m_1r_1^2 - m_1r_1L_1$	$I_c = I_{1com} + m_1r_1^2 + m_1r_1L_1$	$I_c = I_{1com} + m_1r_1^2 + m_1r_1L_1$

E. 6-bar linkage constant angular momentum

In this appendix, the elaboration of obtaining constant angular momentum for a 6-bar linkage with a counter 6-bar is given. For a 6-bar, an extra link is added between the third and the fourth link. This fifth link should be kept horizontal to avoid adding an extra DoF. Mechanically, this can be done as has been done for the IRSBot-2 in Ref. [26]. The added links should also be the same length to maintain a parallel structure, so L_5=L_5^*=g. In figure (17), a schematic drawing of the mechanism is given. The angular momentum formulas for every beam for the two DoF's are obtained in equation (24) till (33).

$$\bar{H}_{a1} = \begin{bmatrix} m_1p_1^2 + m_1q_1^2 + I_1 \\ 0 \end{bmatrix} \cdot \begin{bmatrix} \dot{\theta}_1 \\ \dot{\theta}_2 \end{bmatrix} \tag{24}$$

$$\bar{H}_{a2} = \begin{bmatrix} 0 \\ m_2p_2^2 + m_2q_2^2 + I_2 \end{bmatrix} \cdot \begin{bmatrix} \dot{\theta}_1 \\ \dot{\theta}_2 \end{bmatrix} \tag{25}$$

$$\bar{H}_{a3} = \begin{bmatrix} L_1m_3(L_1 + p_3C(\theta_1 - \theta_2) - q_3S(\theta_1 - \theta_2)) \\ I_3 + m_3(p_3^2 + q_3^2 + gp_3C(\theta_2) + gq_3S(\theta_2) + L_1p_3C(\theta_1 - \theta_2) - L_1q_3S(\theta_1 - \theta_2)) \end{bmatrix} \cdot \begin{bmatrix} \dot{\theta}_1 \\ \dot{\theta}_2 \end{bmatrix} \tag{26}$$

$$\bar{H}_{a4} = \begin{bmatrix} I_4 + m_4(p_4^2 + q_4^2 - gp_4C(\theta_1) + gq_4S(\theta_1) + L_2p_4C(\theta_1 - \theta_2) - L_2q_4S(\theta_1 - \theta_2)) \\ L_2m_4(L_2 + p_4C(\theta_1 - \theta_2) - q_4S(\theta_1 - \theta_2)) \end{bmatrix} \cdot \begin{bmatrix} \dot{\theta}_1 \\ \dot{\theta}_2 \end{bmatrix} \tag{27}$$

$$\bar{H}_{a5} = \begin{bmatrix} L_1m_5(L_1 - p_{5\theta_1}C(\theta_1) + L_3C(\theta_1 - \theta_2) + q_5S(\theta_1)) \\ L_2m_5(L_2 + p_{5\theta_2}C(\theta_2) + L_4C(\theta_1 - \theta_2) + q_5S(\theta_2)) \end{bmatrix} \cdot \begin{bmatrix} \dot{\theta}_1 \\ \dot{\theta}_2 \end{bmatrix} \tag{28}$$

$$\bar{H}_{c1} = \begin{bmatrix} m_1^*p_1^{*2} + m_1^*q_1^{*2} + I_1^* \\ 0 \end{bmatrix} \cdot \begin{bmatrix} \dot{\theta}_1 \\ \dot{\theta}_2 \end{bmatrix} \tag{29}$$

$$\bar{H}_{c2} = \begin{bmatrix} 0 \\ m_2^*p_2^{*2} + m_2^*q_2^{*2} + I_2^* \end{bmatrix} \cdot \begin{bmatrix} \dot{\theta}_1 \\ \dot{\theta}_2 \end{bmatrix} \tag{30}$$

$$\bar{H}_{c3} = \begin{bmatrix} L_1^*m_3^*(L_1^* - p_3^*C(\theta_1 - \theta_2) + q_3^*S(\theta_1 - \theta_2)) \\ I_3^* + m_3^*p_3^{*2} + m_3^*q_3^{*2} + gm_3^*p_3^*C(\gamma + \theta_2) + gm_3^*q_3^*S(\gamma + \theta_2) - L_1^*m_3^*p_3^*C(\theta_1 - \theta_2) + L_1^*m_3^*q_3^*S(\theta_1 - \theta_2) \end{bmatrix} \cdot \begin{bmatrix} \dot{\theta}_1 \\ \dot{\theta}_2 \end{bmatrix} \tag{31}$$

$$\bar{H}_{c4} = \begin{bmatrix} I_4^* + m_4^*p_4^{*2} + m_4^*q_4^{*2} + gm_4^*p_4^*C(\gamma + \theta_1) - gm_4^*q_4^*S(\gamma + \theta_1) - L_2^*m_4^*p_4^*C(\theta_1 - \theta_2) + L_2^*m_4^*q_4^*S(\theta_1 - \theta_2) \\ L_2^*m_4^*(L_2^* - p_4^*C(\theta_1 - \theta_2) + q_4^*S(\theta_1 - \theta_2)) \end{bmatrix} \cdot \begin{bmatrix} \dot{\theta}_1 \\ \dot{\theta}_2 \end{bmatrix} \tag{32}$$

$$\bar{H}_{c5} = \begin{bmatrix} L_1^*m_5^*(L_1^* + p_{5\theta_1}^*C(\gamma + \theta_1) - q_5^*S(\gamma + \theta_1) - L_3^*C(\theta_1 - \theta_2)) \\ L_2^*m_5^*(L_2^* + p_{5\theta_2}^*C(\gamma + \theta_2) + q_5^*S(\gamma + \theta_2) - L_4^*C(\theta_1 - \theta_2)) \end{bmatrix} \cdot \begin{bmatrix} \dot{\theta}_1 \\ \dot{\theta}_2 \end{bmatrix} \tag{33}$$

To obtain constant angular momentum, every term should always be constant for a given input angle. The difference between a 6-bar and a 5-bar is the added link, which results in the angle (γ) that influences the angular momentum change. When all the constant terms are discarded and divided into the dependent angles, they can be written in the form of $\bar{E}q = \bar{A}\bar{x}$ with $\bar{x}$ being the variable angles and $\bar{A}$ being the terms that must be made zero. This will give the following equations for DoF θ_1.

$$\bar{E}q_1 = \begin{bmatrix} L_1L_3m_5 - L_1^*L_3^*m_5^* + L_1m_3p_3 + L_2m_4p_4 - L_1^*m_3^*p_3^* - L_2^*m_4^*p_4^* \\ L_1^*m_3^*q_3^* - L_2m_4q_4 - L_1m_3q_3 + L_2^*m_4^*q_4^* \\ -L_1m_5p_{5\theta_1} - gm_4p_4 \\ L_1m_5q_5 + gm_4q_4 \\ L_1^*m_5^*p_{5\theta_1}^* + gm_4^*p_4^* \\ -L_1^*m_5^*q_5^* - gm_4^*q_4^* \end{bmatrix} \cdot \begin{bmatrix} cos(\theta_1 - \theta_2) \\ sin(\theta_1 - \theta_2) \\ cos(\theta_1) \\ sin(\theta_1) \\ cos(\gamma + \theta_1) \\ sin(\gamma + \theta_1) \end{bmatrix} \tag{34}$$

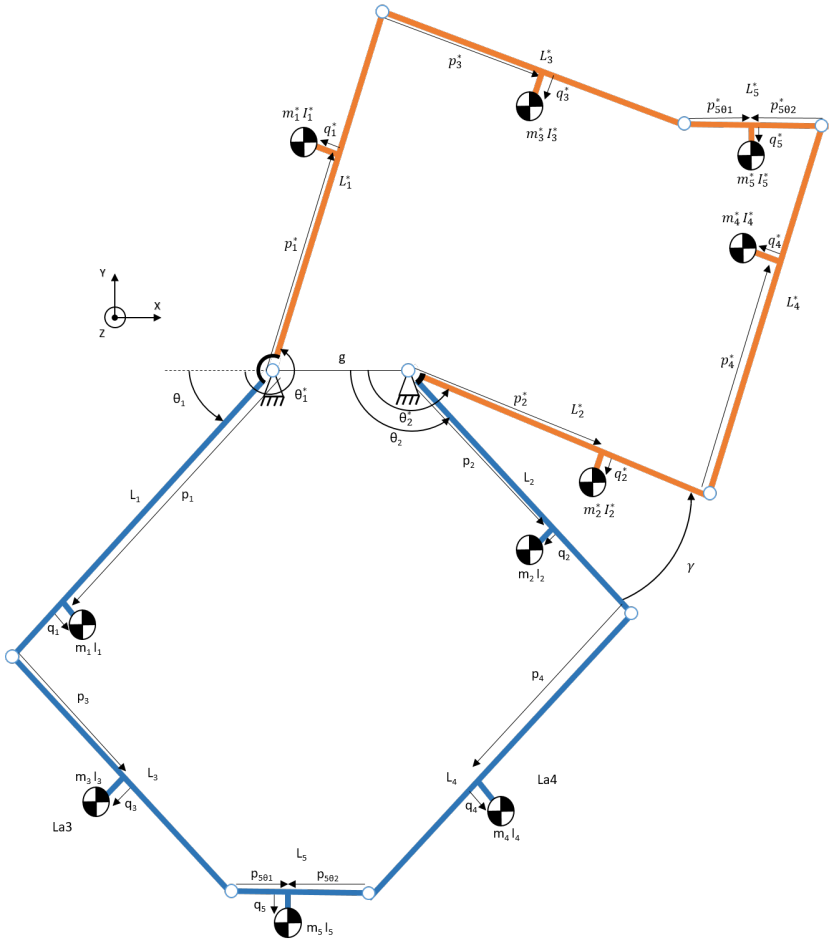

Figure 17. Schematic drawing of a 6-bar linkage with a counter-6-bar linkage to obtain constant angular momentum for every DoF

For the DoF θ_2 this will give the following equations.

$$\bar{E}q_2 = \begin{bmatrix} L_2L_4m_5 - L_2^*L_4^*m_5^* + L_1m_3p_3 + L_2m_4p_4 - L_1^*m_3^*p_3^* - L_2^*m_4^*p_4^* \\ L_1^*m_3^*q_3^* - L_2m_4q_4 - L_1m_3q_3 + L_2^*m_4^*q_4^* \\ L_2m_5p_{5\theta_2} + gm_3p_3 \\ L_2m_5q_5 + gm_3q_3 \\ L_2^*m_5^*p_{5\theta_2}^* + gm_3^*p_3^* \\ L_2^*m_5^*q_5^* + gm_3^*q_3^* \end{bmatrix} \cdot \begin{bmatrix} cos(\theta_1 - \theta_2) \\ sin(\theta_1 - \theta_2) \\ cos(\theta_2) \\ sin(\theta_2) \\ cos(\gamma + \theta_2) \\ sin(\gamma + \theta_2) \end{bmatrix} \tag{35}$$

These formulas are more tedious to solve then a five-bar linkage.

F. Design solution 2-DoF inherently balanced constant inertia tensor mechanism

In Fig. 18 a schematic drawing of a mechanism is visible that is a 2-DoF inherently balanced mechanism which has a constant inertia tensor, it is based on Ref: [9]. Here only one balanced DoF is drawn to make the figure clearer. Using two inverted four-bars for 1-DoF will heavily increase the complexity and crossings of the mechanism. Instead of an inverted four-bar, a Case I or III can also be used to obtain a 2-DoF inherently balanced constant inertia tensor mechanism.

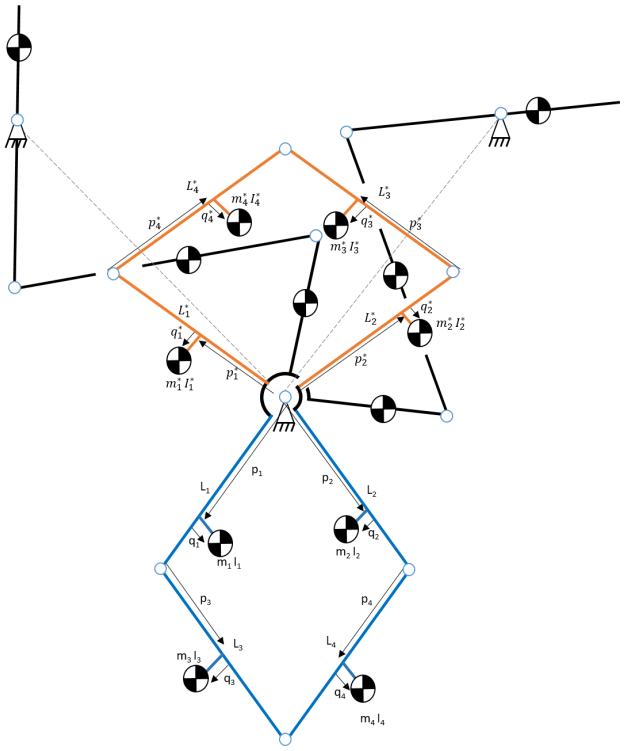

Figure 18. 2-DoF inherently balanced constant inertia tensor mechanism around its pivot point

4

Design, optimization and experimental evaluation of a high speed 2-DoF inherently dynamically balanced parallel manipulator with a constant inertia mechanism

Design, optimization and experimental evaluation of a high speed 2-DoF inherently dynamically balanced parallel manipulator with a constant inertia mechanism

D. Boere, V. van der Wijk

***Abstract*—It is desired to keep the settling time as low as possible for the pick-and-place industry. If the settling time is lower, more cycles can be made, increasing productivity. For high-speed parallel manipulators, a significant vibration cause that increases the settling time is the movable mass and inertia. By dynamic balancing the manipulator, these vibrations can be eliminated. However, balancing a structure relies on adding masses and inertia to movable links, which decreases controllability. In this paper, a 2-DoF, dynamically balanced parallel manipulator (Super-B) is designed and optimized for controllability. It is experimentally verified to be a structure suitable for high-acceleration applications. The lowest eigenfrequency of the Super-B is measured at 90 Hz. The robot obtained a 93.6% and 88.9% reduction in shaking force and shaking moment, respectively, for the first degree of freedom, compared to the unbalanced case and a 97.2% and 93.4%, for the second degree of freedom. The Super-B could reach up to 8 G of accelerations in a workspace of 20 by 20 cm. The results look promising for the high-speed industry and conclude that fully inherently dynamic balancing can be combined with high accelerations.**

I. Introduction

The use of parallel manipulators has become more popular in the industry. Especially with their appealing ability of high-speed, high stiffness to weight ratio, and therefore the increase of agility, accuracy and higher payload capacities [1]. The ability to move at high speed can reduce the cycle time of a pick-and-place operation, which increases the production rate. Although moving at high speed means high peak accelerations, it exerts high forces on the base, leading to fatigue, noise and vibrations. These vibrations themselves can increase the settling time (the time elapsed to stay within a certain boundary of the objective). A way to attenuate these vibrations is to balance the manipulator dynamically. Dynamically balancing means that the change of linear momentum (shaking force balanced) and the change of angular momentum (shaking moment balanced) is zero for every trajectory in the workspace [2]. Shaking moment balance also means that the centre of mass (CoM) stays in the same position for every movement. After it is designed, dynamic balancing of a manipulator will heavily increase the movable mass and inertia and therefore decrease the dynamic performance. If the balancing conditions are considered when designing a manipulator, it is more applicable for higher accelerations and will be more optimised.

Most examples of balanced manipulators only consider the force balancing and not the moment balance, as it is much harder to fulfil [3]. Few examples in the literature exist on dynamic balancing robots that are experimentally evaluated. Some manipulators that do include the moment balance are the Hummingbird, Besi robot, and the DUAL-V [4]–[6]. The Hummingbird and Besi robot both consist of the same balancing principles. Namely, using a parallelogram, using counter-masses to force balance the structure near the base, and using a flywheel that induces a counter-rotation to be dynamically balanced. This solution depends on active control of the flywheel, making it necessary to have optimal control. The Hummingbird had a workspace of 13 by 13 mm and could reach up to 50 G of accelerations. The reaction moments were only reduced by 90% because of the limited control. The Besi robot was designed for a much larger workspace (around 25 cm), but this came at the cost of accelerations being reduced to 10 G. No experimental values imply the reduced reaction forces. The DUAL-V balances itself because it relies on symmetric copying of a six-bar linkage. Structures that rely not on active balancing but on links that balance themself are called inherently balanced. The DUAL-V had a workspace of around 17 cm and could reach up to 20 G of accelerations. It had 97% lower shaking forces and up to a 96% lower shaking moment. In Ref. [7] some mechanisms for inherently dynamically balanced 2-DoF manipulators were proposed. Inverted four-bars are used to dynamically balance a parallelogram. The inherently dynamically balanced inverted four-bar is an appropriate building block for high dynamic performances. It obtains moment balance by distributing masses close to pivot points, and no additional counter-rotations are needed. This gives it the ability to obtain high controllability and an appropriate building block for high accelerations. In Ref. [8] it was concluded that the designs proposed were not fully balanced because of the variable inertia around the pivot point for the parallelogram in their workspace. A design with an added counter-parallelogram to obtain constant inertia was proposed. This counter-parallelogram does not add mass to distal links, which is terrible for the dynamic performance [9]. No experimental validation exists on this design. The goal of this paper is to evaluate the theory and to experimentally verify the proposed design of a 2-DoF inherently dynamically balanced manipulator.

In section II all the kinematics and balancing conditions of the Super-B are elaborated. Section III presents the mechanical design and design process of the Super-B. Section IV introduces the setup and the executed experiments. In section V the results are shown of the experiments. Section VI and VII give an elaborate discussion on the results and a conclusion, respectively.

II. Mechanism

In this chapter, all the kinematics of the Super-B are explained and investigated, why it is dynamically balanced

and what the balance conditions are. The Super-B is an inherently dynamic balanced parallel manipulator with two translating degrees of freedom. The architecture consists of a parallelogram, a counter-inertia with parallelogram characteristics (referred to as counter-parallelogram, that extracts when the parallelogram expands and vice versa), to obtain constant inertia around the origin and two inverted four-bars to inherently dynamically balance the two parallelograms. The complete mechanism is depicted in Fig. 4. Inverted-four bars are used because they are a closed-loop system with masses divided near pivot points, which gives it a high natural frequency compared to other balancing methods [7]. They also have a bigger workspace and become less rapidly singular compared to other inherently balanced four-bars [10].

A. Architecture

An inverted four-bar can dynamically balance a structure if the local CoM and angular momentum with constant input speed are both constant for the whole workspace. Alternatively said, it behaves like a rigid rotating beam. To obtain constant angular momentum, constant inertia around the origin is needed. A counter-parallelogram is used to obtain this, so balancing masses can be placed near the origin, and distal links do not need added mass, which is harmful to the natural frequency [11]. The parallelogram and counter-parallelogram (displayed in Fig. 1, in blue and orange, respectively), must comply with the balancing conditions in equations (1) and (2) to be able to be balanced by an inverted four-bar as they are obtained in Ref. [8].

$$L_1 m_3 p_3 + L_2 m_4 p_4 - L_1^* m_3^* p_3^* - L_2^* m_4^* p_4^* = 0 \tag{1}$$

$$\begin{aligned} \theta_1^* &= \theta_1 + \frac{3}{2}\pi \\ \theta_2^* &= \theta_2 + \frac{1}{2}\pi \end{aligned} \tag{2}$$

With $L_{i\theta_k}$, $p_{i\theta_k}$ and $m_{i\theta_k}$ the length, distance to the CoM and the mass, respectively. Because of the counter-parallelogram and its balancing conditions, the two parallelograms can be described as two beams with constant mass, distance to the CoM and constant inertia, as displayed in Fig. 1. The distance to the CoM of these imaginary beams can be obtained using vector calculations. All the beams' masses are in the middle of their width. With this in mind, the following equations can be made in $[x, y]^T$.

$$\bar{p}_{j_{\theta_1}} = \bar{R}_{j\theta_1} \begin{bmatrix} \frac{-(L_1 m_3 + p_1 m_1 + p_4 m_4)}{m_{j\theta_1}} \\ \frac{(L_1^* m_3^* + p_1^* m_1^* + p_4^* m_4^*)}{m_{j\theta_1}} \end{bmatrix} \tag{3}$$

$$\bar{p}_{j_{\theta_2}} = \bar{R}_{j\theta_2} \begin{bmatrix} \frac{(L_2 m_4 + p_2 m_2 + p_3 m_3)}{m_{j\theta_2}} \\ \frac{-(L_2^* m_4^* + p_2^* m_2^* + p_3^* m_3^*)}{m_{j\theta_2}} \end{bmatrix} \tag{4}$$

With $\bar{R}_{j\theta k}$ the rotation matrix of angle θ_1 and θ_2. $m_{j\theta_1}$ and $m_{j\theta_2}$ being the total mass of that DoF with the parallelogram and counter-parallelogram included as

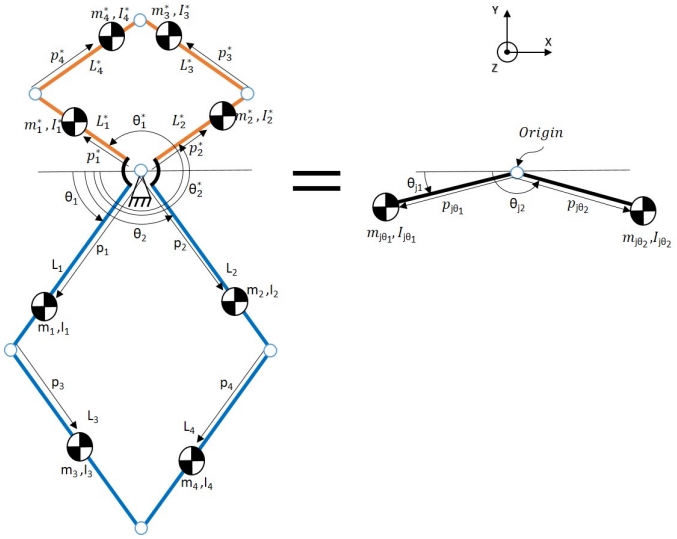

Figure 1: Transforming two parallelograms, that together are a constant inertia mechanism, to beams with the same properties for both DoF. With blue, the original parallelogram, and with orange, the counter-parallelogram

$$m_{j\theta_1} = mL_1 + mL_3 + mL_4 + mL_1^* + mL_3^* + mL_4^* \tag{5}$$

$$m_{j\theta_2} = mL_2 + mL_3 + mL_4 + mL_2^* + mL_3^* + mL_4^* \tag{6}$$

The angle that these imaginary beams make can be obtained by taking the arc-tangent of the coordinates (x,y) of equations (3) and (4). The following equations can obtain the moment of inertia of both DoF of the imaginary beams

$$\begin{aligned} I_{j\theta 1} = I_1 + m_1 p_1^2 + I_1^* + m_1^* p_1^{*2} + m_3 L_1^2 + m_3^* L_1^{*2} + \\ I_4 + m_4 p_4^2 + I_4^* + m_4^* p_4^{*2} - m_{j\theta_1} p_{j\theta_1}^2 \end{aligned} \tag{7}$$

$$\begin{aligned} I_{j\theta 2} = I_2 + m_2 p_2^2 + I_2^* + m_2^* p_2^{*2} + m_4 L_2^2 + m_4^* L_2^{*2} + \\ I_3 + m_3 p_3^2 + I_3^* + m_3^* p_3^{*2} - m_{j\theta_2} p_{j\theta_2}^2 \end{aligned} \tag{8}$$

B. Dynamic balancing

When the parallelogram and counter-parallelogram act as a beam together, it can be balanced by an inverted four-bar. Gosselin et al. established the balancing conditions in Ref. [10] can be applied to obtain a fully dynamic balanced structure. These conditions are given in the formulas (9-18) and the parameters are depicted in Fig. 1, and 2.

$$p_{2\theta_k} = L_{2\theta_k} \frac{(1 - m_{g\theta_k} p_{g\theta_k})}{(m_{2\theta_k} L_{1\theta_k})} \tag{9}$$

$$p_{3\theta_k} = \frac{(m_{2\theta_k} p_{2\theta_k} L_{3\theta_k})}{(m_{3\theta_k} L_{2\theta_k})} \tag{10}$$

$$I_{2\theta_k} = m_{2\theta_k} (L_{2\theta_k} p_{2\theta_k} - p_{2\theta_k}^2) - I_{c\theta_k} \tag{11}$$

$$I_{3\theta_k} = -m_{3\theta_k}(L_{3\theta_k}p_{3\theta_k} + p_{3\theta_k}^2) + I_{c\theta_k} \tag{12}$$

$$I_{c\theta_k} = I_{g\theta_k} + m_{g\theta_k}p_{g\theta_k}^2 + m_{g\theta_k}p_{g\theta_k}L_{1\theta_k} \tag{13}$$

With:

$$L_{1\theta_k} = L_{3\theta_k} \tag{14}$$

$$L_{2\theta_k} = L_{4\theta_k} \tag{15}$$

and

$$m_{g\theta_k} = m_{j\theta_k} + m_{1\theta_k} \tag{16}$$

$$p_{g\theta_k} = \frac{(p_{j\theta_k}m_{j\theta_k} + p_{1\theta_k}m_{1\theta_k})}{m_{g\theta_k}} \tag{17}$$

$$I_{g\theta_k} = I_{j\theta_k} + I_{1\theta_k} + m_{j\theta_k}p_{j\theta_k}^2 + m_{1\theta_k}p_{1\theta_k}^2 - m_{g\theta_k}p_{g\theta_k}^2 \tag{18}$$

With beam i for DoF k. Note that $I_{c\theta_k}$ is not the moment of inertia of a beam. Although it has the same units, it is more a conversion term [2]. The first two equations (9,10) are for force balance while the latter three (11-13) are for moment balance. $L_{1\theta_k}$ of the inverted-four bar must lay in collinear and opposite site with $p_{j\theta_k}$. Angle γ_{θ_k} can be varied to increase or decrease the workspace. If the angle becomes too small or too big, the links can become close to singular fast. For the biggest workspace clockwise and anti-clockwise, beam $L_{1\theta_k}$ and $L_{3\theta_k}$ must be parallel. This will give around 70 degrees of workspace in both directions, not including mechanical stops. Although this optimum will most likely collide with the other inverted four-bar in the same plane. The angle of this optimum can be calculated with the following equation

$$\gamma_{opt\theta_k} = tan^{-1}\left(\frac{L_{1\theta_k}cos(\theta_{kc}) - sin(\theta_{kc})(L_{4\theta_k}^2 - L_{1\theta_k}^2)^{1/2}}{L_{1\theta_k}sin(\theta_{kc}) + cos(\theta_{kc})(L_{4\theta_k}^2 - L_{1\theta_k}^2)^{1/2}}\right) + pi/2 \tag{19}$$

C. Inverse kinematics

Till this point on, the used coordinates as input were θ_1 and θ_2, as those angles are used to balance the manipulator and the primary balancing technique is to balance from the parallelogram to the counter-parallelogram, as last the inverted four-bar. For the inverse kinematics angle, $\psi_{3\theta_1}$ and $\psi_{3\theta_2}$ are taken as generalised coordinates because this is the place where the actuators are placed for the Super-B. These are the actuators' output angles and, therefore, the system's input. The generalised coordinates are

$$\begin{aligned} q_1 &= \psi_{3\theta_1} \\ q_2 &= \psi_{3\theta_2} \end{aligned} \tag{20}$$

First, all the angles of the inverted four-bar will be described as is done in Ref. [12].

$$\begin{aligned} \psi_{2\theta_k} &= g_k + \gamma_{\theta_k} + 2\pi - acos(D_k/(2\sqrt{B_k}L_{1\theta_k})) - \\ &\quad atan(A_k/(L_{2\theta_k} - L_{1\theta_k}cos(g_k))) \\ \psi_{1\theta_k} &= \psi_{2\theta_k} - g_k - \pi \end{aligned} \tag{21}$$

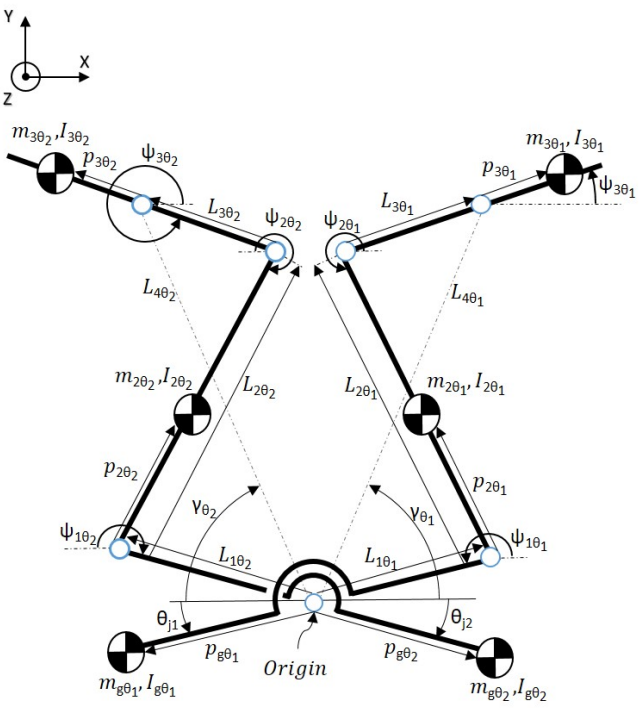

Figure 2: Adding inverted four-bars to the imaginary beams made in Fig. 1 to inherently balance the whole workspace.

With

$$\begin{aligned} g_1 &= q_1 - \gamma_{\theta 1} \\ g_2 &= \pi - q_2 - \gamma_{\theta 2} \\ K_k &= 2L_{1\theta_k}^2 \\ A_k &= L_{1\theta_k}sin(g_k) \\ B_k &= L_{1\theta_k}^2 - 2cos(g_k)L_{1\theta_k}L_{2\theta_k} + L_{2\theta_k}^2 \\ D_k &= K_k - 2L_{2\theta_k}cos(g_k)L_{1\theta_k} \end{aligned} \tag{22}$$

and

$$\begin{aligned} \theta_1 &= \theta_{m1} + \psi_{1\theta_1} - \pi \\ \theta_2 &= \theta_{m2} - \psi_{1\theta_2} + 2\pi \end{aligned} \tag{23}$$

Where θ_m is the angle between the imaginary beam in Fig. 2, and the link of the original parallelogram (L_1 or L_2) that it is corresponding with.

$$\begin{aligned} \theta_{m1} &= tan^{-1}\left(\frac{(L_1^*m_3^* + p_1^*m_1^* + p_4^*m_4^*)}{(L_1m_3 + p_1m_1 + p_4m_4)}\right) \\ \theta_{m2} &= -tan^{-1}\left(\frac{(L_2^*m_4^* + p_2^*m_2^* + p_3^*m_3^*)}{(L_2m_4 + p_2m_2 + p_3m_3)}\right) \end{aligned} \tag{24}$$

When the conversion is known from $\psi_{3\theta_k}$ to θ_k, the end-effector can be described with the following equation

$$\begin{bmatrix} X_e \\ Y_e \end{bmatrix} = \begin{bmatrix} -cos(\theta_1)L_1 - cos(\theta_2)L_2 \\ -sin(\theta_1)L_1 - sin(\theta_2)L_2 \end{bmatrix} \tag{25}$$

Writing this in the full length to obtain the coordinates described in the generalised coordinates and constants will give

$$\begin{aligned} X_e = {} & L_2 c(\theta_{m2} - \gamma_{\theta_2} + t^{-1}((L_{1\theta_2} s(q_2 + \gamma_{\theta_2}))/ \\ & (L_{2\theta_2} + L_{1\theta_2} c(q_2 + \gamma_{\theta_2})))+ \\ & c^{-1}((L_{1\theta_2} + L_{2\theta_2} c(q_2 + \gamma_{\theta_2}))/ \\ & (L_{1\theta_2}^2 + 2c(q_2 + \gamma_{\theta_2}) L_{1\theta_2} L_{2\theta_2} + L_{2\theta_2}^2)^{1/2}))- \\ & L_1 c(\theta_{m1} + \gamma_{\theta_1} - c^{-1}((L_{1\theta_1} - L_{2\theta_1} c(q_1 - \gamma_{\theta_1}))/ \\ & (L_{1\theta_1}^2 - 2c(q_1 - \gamma_{\theta_1}) L_{1\theta_1} L_{2\theta_1} + L_{2\theta_1}^2)^{1/2})- \\ & t^{-1}((L_{1\theta_1} s(q_1 - \gamma_{\theta_1}))/(L_{2\theta_1} - L_{1\theta_1} c(q_1 - \gamma_{\theta_1})))) \end{aligned} \tag{26}$$

$$\begin{aligned} Y_e = {} & L_2 s(\theta_{m2} - \gamma_{\theta_2} + t^{-1}((L_{1\theta_2} s(q_2 + \gamma_{\theta_2}))/ \\ & (L_{2\theta_2} + L_{1\theta_2} c(q_2 + \gamma_{\theta_2})))+ \\ & c^{-1}((L_{1\theta_2} + L_{2\theta_2} c(q_2 + \gamma_{\theta_2}))/ \\ & (L_{1\theta_2}^2 + 2c(q_2 + \gamma_{\theta_2}) L_{1\theta_2} L_{2\theta_2} + L_{2\theta_2}^2)^{1/2}))- \\ & L_1 s(\theta_{m1} + \gamma_{\theta_1} - c^{-1}((L_{1\theta_1} - L_{2\theta_1} c(q_1 - \gamma_{\theta_1}))/ \\ & (L_{1\theta_1}^2 - 2c(q_1 - \gamma_{\theta_1}) L_{1\theta_1} L_{2\theta_1} + L_{2\theta_1}^2)^{1/2})- \\ & t^{-1}((L_{1\theta_1} s(q_1 - \gamma_{\theta_1}))/(L_{2\theta_1} - L_{1\theta_1} c(q_1 - \gamma_{\theta_1})))) \end{aligned} \tag{27}$$

With t(), s() and c() as shorthand for tan(), sin() and cos(), respectively. With the inverse kinematics the velocity matrix of the end-effector can be obtained as is done in equation (34) and (35) in appendix -D.

The inertia of an inverted four-bar at the actuator can be calculated by using the velocity transformations as in Ref. [13], as the input and output are related by a conversion formula as can be seen in the following equations

$$\dot{\psi}_{2\theta_k} = \dot{\psi}_{1\theta_k} k_{12_k} \tag{28}$$

$$\dot{\psi}_{3\theta_k} = \dot{\psi}_{1\theta_k} k_{13_k} \tag{29}$$

With the transformations being

$$k_{12\theta_k} - \frac{(L_{1\theta_k} sin(-\psi_{1\theta_k} + g_k + \gamma_{\theta_k}))}{(L_{2\theta_k} sin(\psi_{1\theta_k} - \gamma_{\theta_k}))} \tag{30}$$

$$k_{13\theta_k} = \frac{(L_{1\theta_k} sin(g_k))}{(L_{3\theta_k} sin(\psi_{1\theta_k} - \gamma_{\theta_k}))} \tag{31}$$

Using the system's total kinetic energy, the inertia of a DoF can be calculated, so the torque needed to accelerate an actuator by an angle $\psi_{3\theta_k}$ can be obtained. Berkof formulated the total kinetic energy for a four-bar linkage in Ref. [14]. By using equations (30) and (31) to transform the angular velocities from beam 2 and 3 to an angular velocity of beam 1 will give the following equation

$$\begin{aligned} & I_{O\theta_k} = (2L_{1\theta_k} r_{2\theta_k} m_{2\theta_k} cos(g_k)) k_{12\theta_k} + L_{1\theta_k}^2 m_{2\theta_k} + \\ & (I_{g\theta_k} + m_{1\theta_k} r_{1\theta_k}^2) + (I_{2\theta_k} + m_{2\theta_k} r_{2\theta_k}^2) k_{12\theta_k}^2 + \\ & (I_{3\theta_k} + m_{3\theta_k} r_{3\theta_k}^2) k_{13\theta_k}^2 \end{aligned} \tag{32}$$

To obtain the inertia at the place of the actuator, formula (33) has to be multiplied by the inverse of equation (31), this will give

$$I_{\psi_{3\theta_k}} = I_{O\theta_k} k_{13\theta_k}^{-2} \tag{33}$$

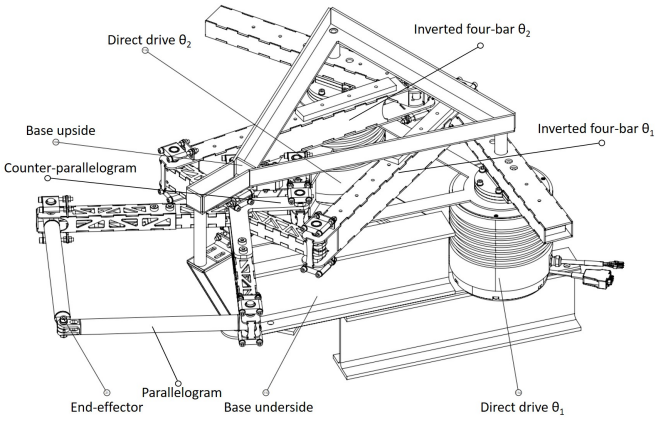

Figure 3: A 3D view of the CAD of the Super-B (patented). With the constant inertia mechanism consisting of the Parallelogram and counter-parallelogram. The two inverted four-bars obtain moment balance that are driven by direct drives.

III. Design

In this chapter, the design of the Super-B (patented) will be discussed. The whole design is visible in Fig. 3.

A. Mechanism design

For the Super-B, most beams are laser-cut stainless steel (AISI 304) plates, and TIG welded to each other. This will keep the cost low and an option to create holes to reduce the mass. Laser-cutting also has a viable precision suitable for its cost. Stainless steel does not need filler material to be TIG welded, so the mass will be kept the same when welded. The beams that will be welded have overhanging structures near their shafts, so other beams connected via an axis inside of them will not collide. Some stiffeners are added to increase the stiffness near the axis of the overhanging beams. These can be seen in Fig. 5. The holes in L_1 and L_2 (see fig 4) reduce the eigenfrequencies by 5%. Although the lowered mass far away from the origin makes the 5% up by rearranging the place of $m_{g\theta_k}$. This ensures θ_{mk} to be in a more optimal position in the workspace as in equation (24). Beams L_3 and L_4 are made of carbon tubes. This will greatly reduce the mass while still keeping high stiffness. Because of the reduced mass, the total inertia of a DoF will be reduced by around 30%. Masses placed far away from a fixed point greatly reduce the eigenfrequency, so these have to be made with the least amount of possible mass [11]. All the connection pieces for the carbon tubes are made of aluminium and are glued together with Araldite 2015. All the shafts, except the shaft between L_3^* and L_4^*, are made of aluminium also to reduce the mass. The shaft between link L_3^* and L_4^* is made of stainless steel, as there has to be added mass on these links anyway. All bearings and bearing tensioners are made of high-end polymers. The bearing tensioners are used to remove play in the bearings. A trade-off must be made between friction and the play of the mechanism. On the end-effector, a mass is added near the mass of a small solenoid.

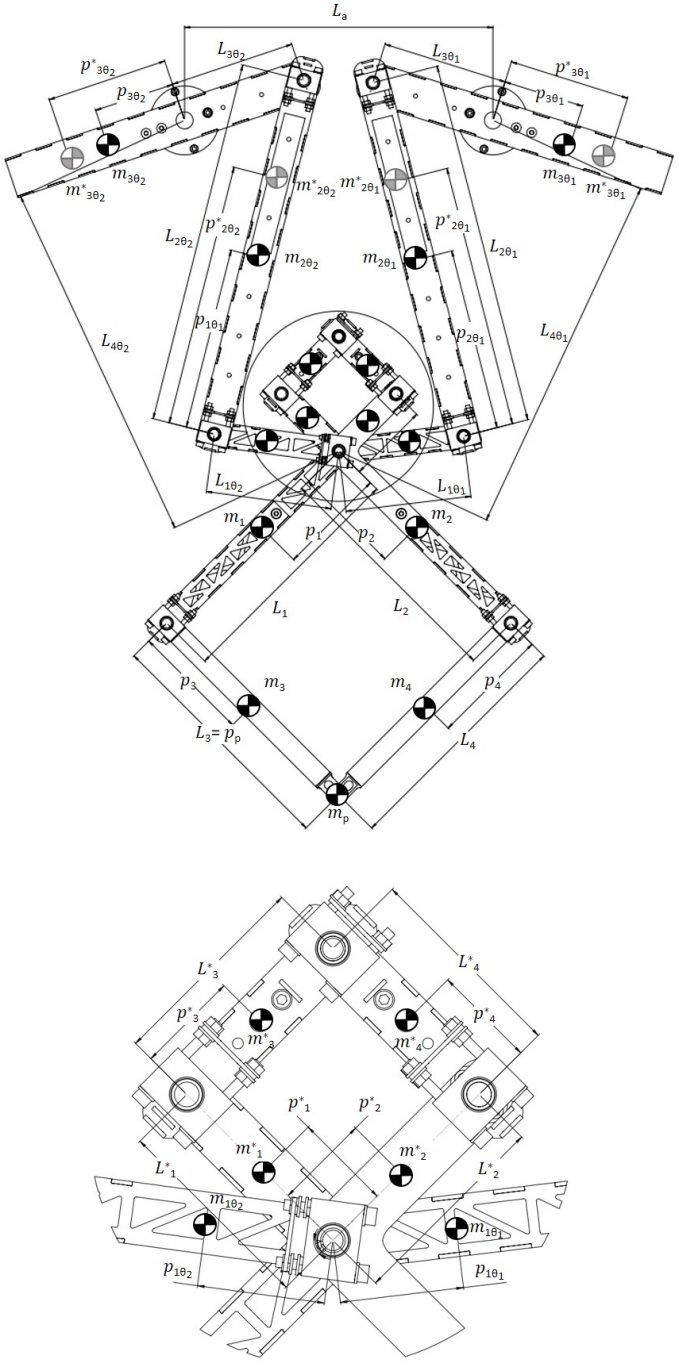

Figure 4: Top view of the Super-B, and all its parameters. With the bottom sketch, a close-up of the circle in the upper sketch depicting the counter-parallelogram

Table I: Parameters of the Super-B

(mm)	(mm)	(g)	(kgm^2)
	$p_p = 300$	$m_p = 12.44$	$I_p = 0.0000001503$
$L_1 = 300$	$p_1 = 153.76$	$m_1 = 695.94$	$I_1 = 0.0057666176$
$L_2 = 300$	$p_2 = 144.69$	$m_2 = 781.04$	$I_2 = 0.0064139761$
$L_3 = 300$	$p_3 = 88.88$	$m_3 = 102.18$	$I_3 = 0.0012285762$
$L_4 = 300$	$p_4 = 110.93$	$m_4 = 107.31$	$I_4 = 0.0020132935$
$L^*_1 = 100$	$p^*_1 = 63.19$	$m^*_1 = 358.44$	$I^*_1 = 0.0003699159$
$L^*_2 = 100$	$p^*_2 = 63.08$	$m^*_2 = 323.16$	$I^*_2 = 0.0003437013$
$L^*_3 = 100$	$p^*_3 = 55.31$	$m^*_3 = 546.13$	$I^*_3 = 0.0006775521$
$L^*_4 = 100$	$p^*_4 = 62.53$	$m^*_4 = 702.81$	$I^*_4 = 0.0009680726$
$L_{1\theta_1} = 155$	$p_{1\theta_1} = 72.81$	$m_{1\theta_1} = 561.49$	$I_{1\theta_1} = 0.0021473852$
$L_{2\theta_1} = 450$	$p_{2\theta_1} = 223.86$	$m_{2\theta_1} = 1575.66$	$I_{2\theta_1} = 0.0319837846$
$L_{3\theta_1} = 155$	$p_{3\theta_1} = 16.26$	$m_{3\theta_1} = 2286.42$	$I_{3\theta_1} = 0.0184049301$
$L_{4\theta_1} = 450$			
$L_{1\theta_2} = 155$	$p_{1\theta_2} = 84.59$	$m_{1\theta_2} = 494.12$	$I_{1\theta_2} = 0.0016473731$
$L_{2\theta_2} = 450$	$p_{2\theta_2} = 223.88$	$m_{2\theta_2} = 1586.20$	$I_{2\theta_2} = 0.0319564449$
$L_{3\theta_2} = 155$	$p_{3\theta_2} = 16.29$	$m_{3\theta_2} = 2290.83$	$I_{3\theta_2} = 0.0185019230$
$L_{4\theta_2} = 450$			
	$p^*_{2\theta_1} = 319$	$m^*_{2\theta_1} = 705.04$	$I^*_{2\theta_1} = 0.0017802812$
	$p^*_{3\theta_1} = 109$	$m^*_{3\theta_1} = 725.14$	$I^*_{3\theta_1} = 0.0029795983$
	$p^*_{2\theta_2} = 312$	$m^*_{2\theta_2} = 1484.27$	$I^*_{2\theta_2} = 0.0046212003$
	$p^*_{3\theta_2} = 110$	$m^*_{3\theta_2} = 1481.17$	$I^*_{3\theta_2} = 0.0051546398$
$L_a = 380$			$I_{actuator} = 0.00336$

The origin of the Super-B is a tedious point to manufacture. Six beams come together at this point and have to cross each other. To solve this, one can stack the beams onto each other, creating a height difference, as is also done for the Besi robot [5]. If the CoM of all the beams does not lay in the same coordinates of the z-axis, it is challenging to obtain the inverted four-bars in the same plane. The Super-B lets the beams run through each other like the Hummingbird [4]. This way, the stiffness will be compromised by having the CoM of every beam on the same z-coordinate, making it easier for manufacturing. For the first bit of the first beams of the parallelogram and counter-parallelogram (L_2 and L^*_2), this will create overhanging flat beams which cannot be connected in the middle, resulting in a loss in out-of-plane stiffness. A close-up can be seen in Fig. 5. The rigidity of the base of a manipulator is essential to keep in mind while designing. Having a base that is not rigid enough can induce a frequency drop on the manipulator. In Ref. [15], it was reviewed that the elasticity of the base lowered the frequency, making the base more rigid, which increased it by 55%. For this reason, a connection on the upside is made between the actuators and the origin (see Fig. 3). Making the structure a closed loop and, therefore, more rigid. The base is made of laser-cut steel plates to fix the actuators in good positions relative to the middle point. Steel I-profiles are welded, so it makes the base rigid for a relatively low cost.

All the parameters are obtained by iterating the optimization process of the Super-B on eigenfrequency. Together with a MSA model [16] in Matlab [17] and a Spacar model [18], link lengths, masses and the CoM for the parallelogram and counter-parallelogram are obtained. With this information, a sufficient CAD model is acquired, so the inverted four-bars could be optimized and confirmed with Comsol [19] a finite element analysis. All the main parameters of every beam are visible in table I and II. Every part is weighted on a hundredth of a gram and assembled in Solidworks [20] to obtain the moment of inertia.

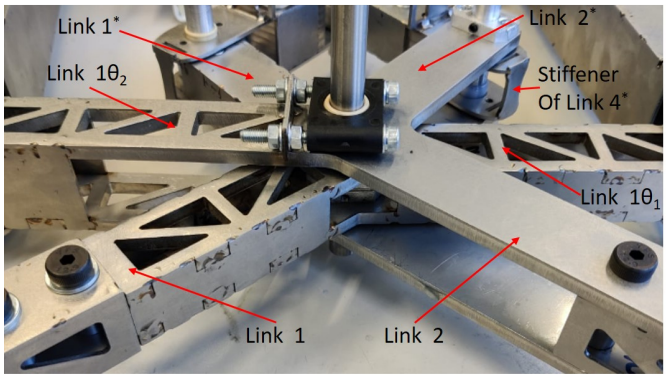

Figure 5: The middle point of the Super-B where six links come together

Table II: Dimensions of the links, with Th as thickness. Note that the first part of beam L_1 and L_2 are the same as L_1^* and L_2^*, respectively.

Link	Height (mm)	Width (mm)	Th height (mm)	Th width (mm)
1	30	30	2	2
2	30	30	2	2
3	25 ∅	-	1	-
4	25 ∅	-	1	-
1*	26	30	6	2
2*	42	30	6	-
3*	32	28	2	2
4*	26	28	2	2
$1\theta_1$	26	30	6	2
$2\theta_1$	50	40	3	2
$3\theta_1$	30	50	3	2
$1\theta_2$	42	30	6	-
$2\theta_2$	50	40	3	2
$3\theta_2$	30	50	3	2

The length of 0.3 m is chosen for the parallelogram links, as the workspace will be able to make a standard Adept cycle. Before the design process, estimated guesses of the Super-B were made to obtain sufficient workspace. Material choices, link width, and height are optimized to increase the in and out-of-plane frequency of the parallelogram.

The counter-parallelogram is made smaller, so it will less likely have a collision with the inverted four-bars. Making the length smaller will increase the needed mass of these links to obtain constant inertia (see formula (1)). Making the length smaller also increases the eigenfrequencies compared to making them longer. As was also reviewed in Ref. [7] and in appendix -C.

Changing the thickness of $L_{1\theta_k}$, $L_{2\theta_k}$ and $L_{3\theta_k}$ will conclude in changing the maximum limit of the length for both as the mass per unit length changes. The mass can not transcend a specific value as the balancing conditions become unsolvable. Making $L_{1\theta_k}$, and therefore $L_{3\theta_k}$ too short, will result in a smaller workspace or even collision between the inverted four-bars and the counter-parallelogram. Having the counter-masses of the two beams of L_3^* and L_4^* in places where it is positive for the stiffness instead of dead weight will have positive effects on the eigenfrequencies.

For the inverted four-bars, the initial lengths of $L_{2\theta_k}$ and $L_{3\theta_k}$ were 160 mm and 465 mm, respectively. For this configuration, 2 mm thickness of $L_{2\theta_k}$ and $L_{3\theta_k}$ was used. For those link lengths, the out-of-plane frequency was lower than the lowest frequency of the parallelogram. So the thickness of the height was changed to 3 mm, resulting in a non-existent solution. The lengths were altered to 155 mm and 450 mm, so the solution was sufficient, resulting in a reduction in the workspace, so the Super-B could not make a full Adept cycle. Link 1_{θ_k} is a weak link for the out-of-plane frequency of the inverted four-bar as it is overhanging and has no sides. To increase the eigenfrequency, side panels are welded to the sides, which increases it by 63%. This also increased the mass too much for a feasible solution, so triangular cut-outs were made to reduce the mass again, resulting in a frequency drop of 29%.

The counter-masses of the inverted four-bars have to be placed on the links themselves. $p^*_{2\theta_k}$ and $p^*_{3\theta_k}$ heavily influence the counter-masses' mass and inertia. The place of $p^*_{3\theta_k}$ is chosen, so the counter-masses fit inside Link 3_{θ_k}, so it will increase the stiffness. For Link 2_{θ_k}, it is impossible to place the masses on the inside as it would collide with Link 3_{θ_k}. The total mass will increase by a factor of 9.9 times the original parallelogram. The inertia will increase roughly 4 times for both DoF. This means that the torques that the actuators need to deliver also increase.

B. Finite Element Analysis

The eigenfrequencies are one of the essential properties of a high-speed manipulator. Briot et al. warned the community that when high dynamic performance is wanted, the lowest eigenfrequency in any direction can be the threshold for that manipulator [1]. So to get a good insight into the system, the in-plane and out-of-plane frequencies must be obtained with a more complex vibration model.

To obtain better knowledge of the Super-B, a Finite Element Analysis is done in Comsol [19] to obtain the out-of-plane eigenfrequencies. Beams are modelled as rigid beams instead of point welded plates, and the bolts and bearing tensioners are modelled as point masses to obtain a simplified model with a lower computational time. The mounting points at the origin and the actuators are modelled as clamped. The frequencies are calculated for $\theta_1 = 45°$ and $\theta_2 = 135°$ as this will be around the middle of the workspace. In Fig.6, the first three out-of-plane mode shapes are visualized. With frequencies being 117 Hz, 157 Hz and 203 Hz. The lowest out-of-plane frequency will be located at the parallelogram as this structure is the furthest away from a clamped support. The mass placed on the end-effector has much influence on the out-of-plane frequency. Inducing a frequency drop of an estimated 0.8 Hz per gram added on the end-effector, see Appendix -A.

The in-plane eigenfrequencies are modelled with a multi-body simulation in Spacar [18], with assumed infinite actuator stiffness. For any point in the workspace, the eigenfrequencies will change, with lower in-plane frequencies near the border of the workspace due to coming closer to singularity positions. However, mechanical stops will prevent the Super-B from becoming singular in the workspace. The first two frequencies in Fig.7, are close to each other. The first will be the in-plane frequency of θ_1, and the second will be the same for θ_2 as this

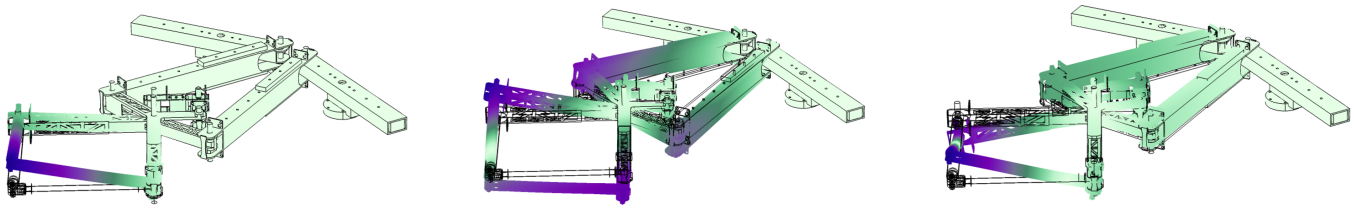

((a)) First frequency at 117Hz ((b)) Second frequency at 157Hz ((c)) Third frequency at 203Hz

Figure 6: Out-of-plane eigenfrequencies of the Super-B at θ_1=45°and θ_2=135°, with the purple colour being the place where that frequency is the most exerted

has a slightly different mass distribution. This phenomenon that the following frequencies are close to each other for both DoF will carry through to at least the 10th eigenfrequency, as long as the structure is symmetrical. The lowest in-plane eigenfrequency will be 195 Hz, slightly higher than the lowest out-of-plane frequency.

IV. Experimental setup

The Super-B is placed in an experimental setup to obtain the measured reaction forces on the base. The robot is suspended vertically from four wires to a rigid welded steel base, see Fig. 8. These wires are suspended with a length of approximately two meters. The length of these wires influences the eigenfrequency of the system; therefore, the wires are longer, so they intervene less with the measurements. Three Futek load cells, with a max force of 44.5 N and a precision of ±0.1%, are attached to the Super-B and the base via threaded rods. The load cells are sampled at a rate of 10 kHz. The rods are pretensioned, so the system has no play. They have high stiffness in the axial direction and can move in the transverse direction, so the Super-B is perfectly constrained in its plane. One load cell is used to measure the forces in the y-direction, and two load cells are used to measure the forces in the x-direction. Multiplying the measured forces of the two sensors in the x-direction with the distance placed of the CoM will obtain the moment around the z-axis. These two load cells are placed at equal distances from the CoM by 13 cm. Attention must be paid to the vibrations off the suspension of the sensors, as these can intervene with the force analysis of the system, as has been encountered in Ref. [15]. The rod's length is 100 mm and has a thickness of 3 mm.

To obtain the reduced reaction forces and moments, a motion profile visible in Fig. 9 is imposed on the actuator to compare the balanced and unbalanced reaction forces. If one actuator moves, the other actuator is mechanically locked. Otherwise, the PID of the locked actuator would intervene with the measurements. In this figure the movement of ψ_2 is visible that starts at θ_1 is 45°and θ_2 is 150°. For ψ_1 the same motion profile is used but anti-clockwise. The starting position is θ_1 is 30°and θ_2 is 135°. For both motions, the end-effector will move through the middle of its workspace, obtaining a valid value of the reduced reaction forces and moments. The unbalanced case is the Super-B without the added counter-masses, and inertia's off $m^*_{2\theta_k}$ and $m^*_{3\theta_k}$, and without links L^*_3 and L^*_4. The reaction forces will be calculated by obtaining the maximum of $\sqrt{(F_x^2 + F_y^2)}$. The moment balance is calculated with the maximum moment measured (M_z).

The theoretical tip accelerations will be calculated with forward kinematics, with the theoretical displacements of the actuator as input. The actuators are two ETEL RTMBi140-100 direct drive motors, which both can deliver a maximum torque of 131 Nm. These actuators are controlled by an ETEL motion controller with PID. A frequency sweep for one DoF obtains the in-plane eigenfrequencies. This is done in the middle of the workspace at θ_1 is 45°, and θ_2 is 135°.

V. Experimental results

In this chapter, the experimental results are presented. First, the reaction forces induced on the base are plotted for different maximum tip accelerations. Secondly, the frequency sweep and its results are given.

A. Balance quality when comparing the balanced and unbalanced manipulator

The measured values of the force sensors are plotted in a time-related graph for the balanced and unbalanced cases. The motion profile in Fig. 9 is used for both DoF. In Fig. 10, the reaction forces and moments are visible for the balanced and unbalanced cases, as are the simulated values. The shaking force and shaking moment reduction is 93.6% and 88.9%, respectively, for θ_1 and 97.2% and 93.4% for θ_2, both compared to the unbalanced case.

B. Reaction forces when dynamically balanced

For higher accelerations, the unbalanced case exceeds the force sensors' values and is inappropriate to use. The maximum value of acceleration that is still measurable is near 3.1 G for the unbalanced case. This is plotted in Fig. 11 for both actuations and both the balanced and unbalanced cases, as well as the simulated values in Spacar. For 8 G, only the balanced case is presented in Fig. 12.

C. Eigenfrequency analyse

The values of the frequency sweep for both actuators can be seen in table III and are compared to the FEA. The bode plot of both sweeps is visible in appendix -F. The measured results are lower compared to the FEA. An explanation can be that all the beams are point welded, and in the FEA, these

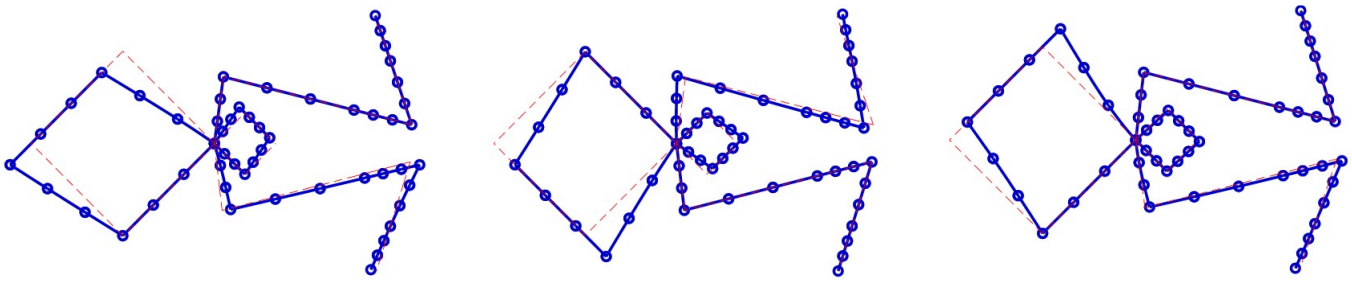

((a)) First frequency at 195Hz ((b)) Second frequency at 197Hz ((c)) Third frequency at 390Hz

Figure 7: The first three in-plane eigenfrequencies of the Super-B at location θ_1=45°and θ_2=135°

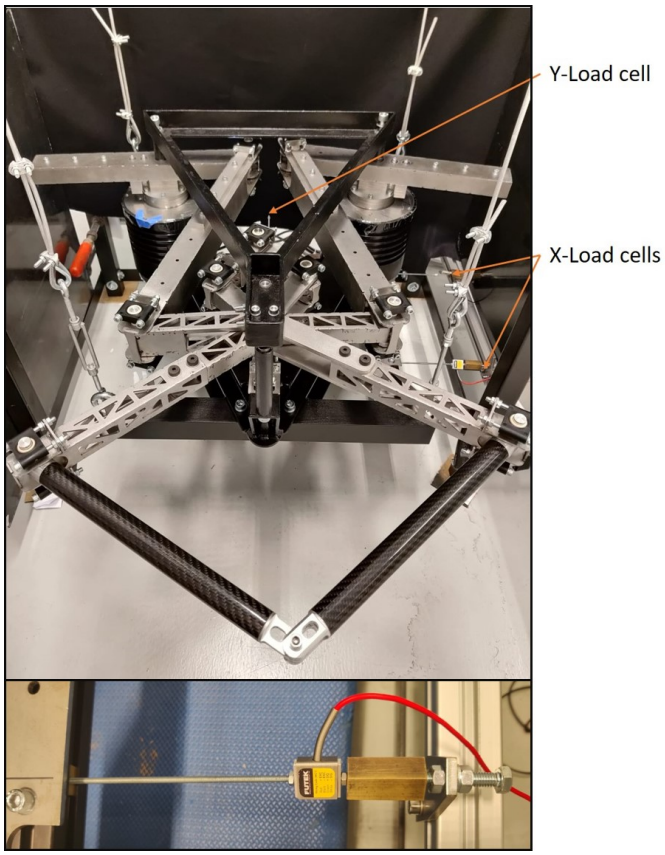

Figure 8: The Super-B suspended from four wires. The load cells are pointed out with arrows. A close up can be seen in the bottom picture of a load cell

Table III: Eigenfrequencies compared with the FEA

	Eigenfreq 1	**Eigenfreq 2**	**Eigenfreq 3**
FEA θ_1	195 Hz	392 Hz	466 Hz
FEA θ_2	197 Hz	395 Hz	482 Hz
Frequency sweep θ_1	108 Hz	146 Hz	159 Hz
Frequency sweep θ_2	91 Hz	122 Hz	154 Hz

beams are modelled as rigid beams gaining some stiffness. In the experimental setup, it is not known what effects the stiffness has on the elasticity. While the actuator is modelled as infinite stiff, it has a finite stiffness in reality. As long as the actuator's stiffness is high enough, it will have minor effects on the in-plane frequencies; see appendix -B for calculations.

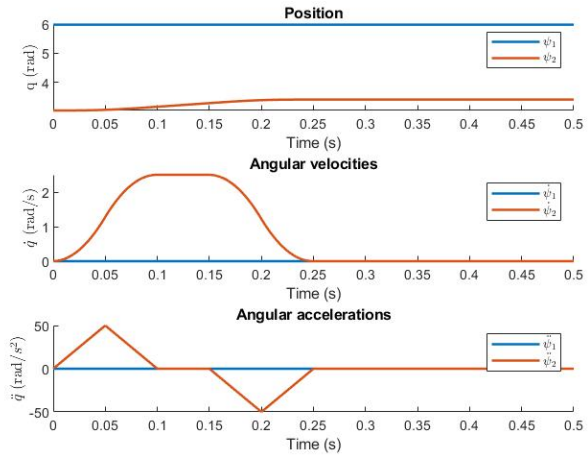

Figure 9: The motion profile used to obtain the reduced reaction forces with 1.5 G of tip acceleration for ψ_2

VI. Discussion

This paper presents a way to dynamically balance a 2-DoF parallelogram and the design and experimental verification of the fabricated prototype. The main focus was to obtain a feasible design sufficient for high acceleration applications while still holding a reasonable workspace. Experimentally, the shaking force and shaking moment are reduced by around 90% for θ_1 and 95% for θ_2, compared to the unbalanced case. In the plots of Fig 10 till 12 it can be seen that the reaction forces of θ_1 are higher than θ_2 for the measured and simulated values because the counter-masses added to this DoF were too light. Recalculating the balancing conditions and adding extra counter-masses can reduce the reaction forces even further. The reaction moment values are comparable to the simulated cases. However, a small distance from the sensors to the CoM is used to calculate the reaction moments. Increasing this distance can lead to less error in the measurements. The measured values are higher for the reaction forces than the simulated ones. For the simulated values, the theoretical accelerations are used to calculate the forces. The poor PID resulted in a vibrating displacement development, concluding in not-so-accurate comparability of the simulated and measured values. Slowed videos also reviewed that the rise time was accomplished in one-third of the simulated value (for

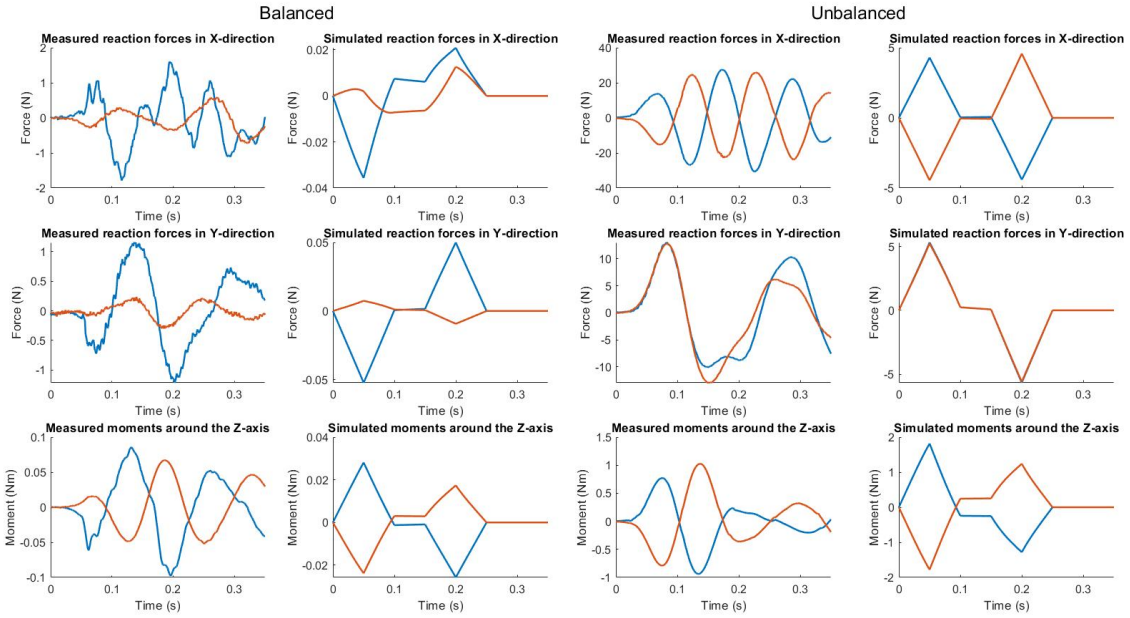

Figure 10: The shaking force and shaking moment of the balanced and unbalanced case with the motion profile in Fig. 9 obtaining 1.6 G tip acceleration. With the blue line representing θ_1 and the red line representing θ_2

8 G), concluding that the peak accelerations are higher than estimated, resulting in higher measured forces. Sensors were close to the ground, and the base was minimally damped. So vibrations from the surroundings were also measured, which gave an estimated error of 0.4 N.

The poor PID also results in an overshoot at the desired destination. Creating vibrations that are measured and visible. The base does not dampen these vibrations well, so the whole Super-B will vibrate after the movement is succeeded. This can conclude the sinusoidal waves at the end of every measurement plot, which depletes slowly over time. For future measurements, more damping is strongly advised. The poor PID also resulted in a theoretical maximum of 8 G as of higher accelerations the overshoot resulted in a mechanical stop being hit. Feedforward can be an excellent solution to obtain higher accelerations as all the parts are designed to be strong enough to withstand the forces induced by moving at 21 G. In appendix -E more information is given on the theoretical max accelerations.

The measured values for the unbalanced case follow the simulated values for the direction they first move in. For the balanced case, the measured values are often mirrored or do not follow simulated values. Concluding that the mass deviation is different for the balanced case than the simulated one. This mass deviation also concludes in a force reduction of less than 100%. A few possible can cause these to differ could be the following. Both θ_j are slightly off by 0.2° because of manufacturing errors. However, this could be compensated for by adding masses to L_1^* and L_2^*, which do not influence having constant inertia. However, this will alter the counter-masses and inertia needed on the inverted four-bars, which can more easily be added than making the middle again where this manufacturing error occurred (see Link $1\theta_k$ in Fig. 5). All the individual parts were weighted and imported into Solidworks. Although after assembling, the links were sanded, altering their mass by a small percentage. While this mass loss was accounted for, the place where this mass was altered, was chosen to be equally distributed on the outside. So a different mass deviation is plausible, and therefore, the mass moment of inertia can be off by an estimated maximum of 0.6%. The mass moment of inertia can also be obtained on different experimental methods, but if this is better than the estimated value in Solidworks is discussable [21]. The supplier's given inertia value of the actuators can also be off, as it is not tested. The most influence on the moment balancing is, in the end, the kinematic errors [15].

The measured eigenfrequencies of the Super-B are lower than the FEA model. However, if this will be the threshold for this manipulator must still be investigated as the first peaks in the gain plots are not high, concluding that the system is well damped for these frequencies. A reason for lower eigenfrequencies can be that the cut-outs of beams $L_{1\theta_k}$ are not considered reducing the stiffness. Also, the beams are TIG welded on spots and do not consist of one rigid part. This can lower the stiffness. Although the welded beams can also increase internal stresses, increasing the frequency [22]. Welding induces heat; therefore, warping can occur as has happened for L_2^*, which curved a little outwards. This warping can make the axis have a little slope to a side, inducing tension in the closed system. A little tension on the axis can be good because it increases the in-plane frequency, but too much and the friction becomes too high, and the system cannot move correctly. A way to make the beams and not use welding is to laser cut squared tubes, so the axle holes are in a fixed

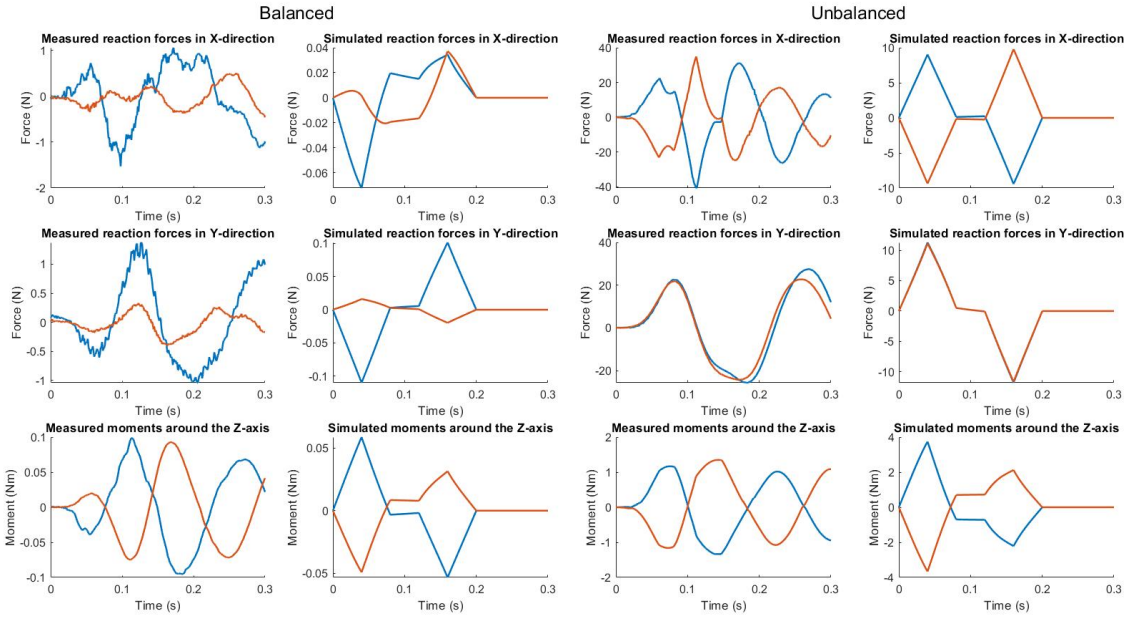

Figure 11: Measured and simulated values of the balanced and unbalanced cases shaking force and shaking moment, obtaining 3.1 G of tip acceleration. The blue line represents θ_1 and the red line represents θ_2. Note that at around 0.07 and 0.13 s at the 'Measured forces in the x-direction for the unbalanced case, the graph has little dents, not running smooth. This is because the maximum value of the load cell is being exceeded

location with low error, and for this technique, cut-outs can still be made. However, no different-sized wall thicknesses can be used for different beams to increase the stiffness in that direction. A less cost-efficient way is to design and use milling operations to fabricate beams. Alternatively, use topology optimization to increase the eigenfrequency further, as has been done in Ref. [23], [24]. Changing the material of beam L_1 and L_2 to carbon can significantly reduce the total mass and inertia of the system, roughly estimated at 25% and 65%, respectively. However, the origin will be even more tedious to design and manufacture. Reducing the mass too much of the parallelogram can make the balancing conditions unsolvable, as $L_{1\theta_k}$ becomes too heavy. So reducing the mass or changing the material to carbon is required for this link if the same kinematics have to hold. Carbon can also be used for the inverted four-bars and not for the parallelogram so that the mass will reduce, and the lengths of these beams can be made longer, so the workspace can increase as there is less collision between the counter-parallelogram and the inverted four-bars. If this will be positive for the controllability must still be investigated. Instead of placing the actuators at links 3_{θ_k}, they can also be placed at the origin. This will increase the difficulty of manufacturing the origin. However, it can alter the in-plane frequencies. For the Super-B, the origin is a revolute joint that is not fixed. The closest fixed point for the mode-shape at the parallelogram is the rigid point at 3_{θ_k}. Using the actuators in the origin will "split" the structure in half so it will be decoupled. This will heavily increase the in-plane frequency at the parallelogram, with an estimated value of 50%. For the inverted four-bar, placing the actuators at the origin will decrease their in-plane frequency heavily as beams $L_{2\theta_k}$ and $L_{3\theta_k}$ have notably higher inertia than other beams. A quick calculation was made, and the frequency dropped below the lowest out-of-plane frequency that can be seen in (a) in Fig. 7. For the Super-B, the inverse kinematics will be easier to solve if the actuators are placed at the origin. However, the drop in eigenfrequency makes it not advisable to change the location. Actuation redundancy can also be added, so less torque is needed per actuator, and higher accelerations can be obtained. This will also increase the in-plane frequencies. However, the system's control will become more difficult [25]. How beneficial it is to add extra actuators must still be researched.

In this study, multiple programs are used to deter the eigenfrequencies. The out-of-plane frequencies were obtained with another program than the in-plane frequencies. This lead to inconsistency. For future work, it is advised to use a program for later stages in the design process that can calculate the in and out-of-plane frequencies simultaneously, be close to the real manipulator's shapes and properties, and have a reasonable computation time for fast adaptation.

Out-of-plane frequencies will become smaller for the parallelogram as it reaches further away from the origin (see Appendix -A). So pick-and-place trajectories should be as close to the origin to obtain a higher controllable path. No measurements were done to obtain the out-of-plane frequencies, but the simulations pointed out that the lowest will be in this direction. For high-speed manipulators, this can be the threshold of its controllability [1]. Increasing the out-of-plane frequency at the parallelogram will be challenging. Multiple links connected to the end-effector can increase its stiffness

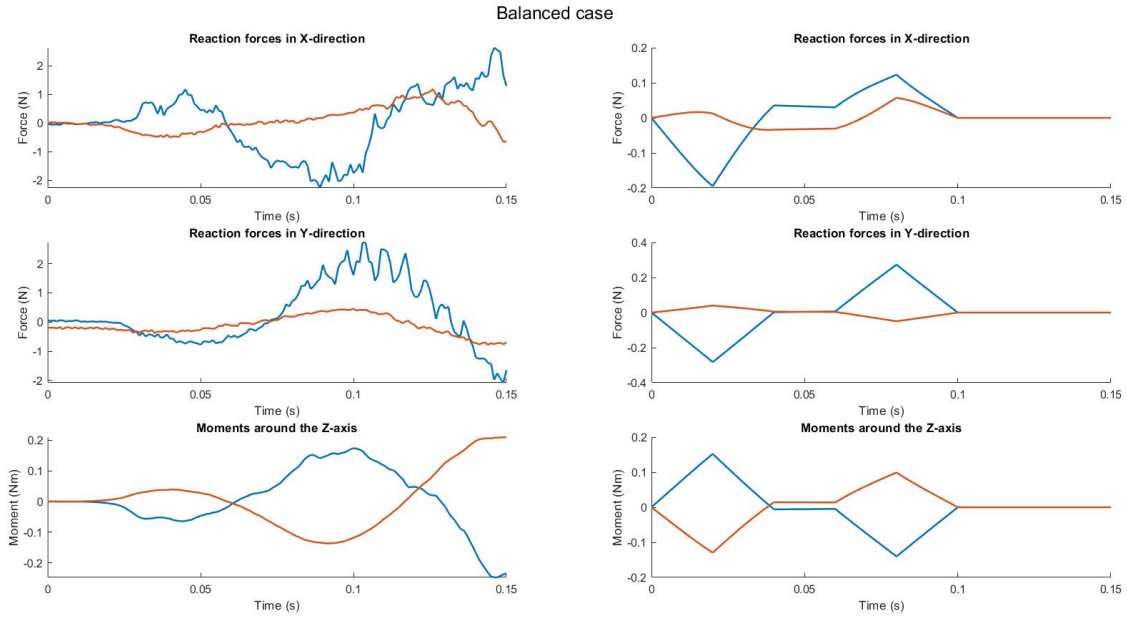

Figure 12: Shaking force and shaking moment of the balanced and unbalanced case obtaining 8 G of tip acceleration. With the blue line representing θ_1 and the red line representing θ_2

[26]. Multiple solutions can be done to accomplish this, adding an extra arm that is stiff in the out-of-plane direction but can move in the other directions. The problem is that the extra arm must also be dynamically balanced, which in itself can be hard to accomplish as spatial terms are harder to balance. The whole Super-B can also be copied around the end-effector, creating a DUAL-V-like manipulator [6], which doubles the links connected to the end-effector and increases the stiffness.

The Super-B is a planar manipulator, while standard pick-and-place manipulators have mainly three or more DoF. The Super-B can be used as a building block to be extended to three dimensions. Although balancing in three dimensions is much more complicated than in a plane, as three angular velocities must be made constant instead of one. More investigation is needed if the structure of the Super-B can be used to obtain dynamic balancing in three-dimensional space and to be sufficient for high acceleration purposes.

VII. Conclusion

In this paper, the Super-B, an inherently dynamically balanced parallel manipulator, is designed, optimized and tested to prove that this design can be made in reality as well, as it is suitable for high accelerations. The added counter-parallelogram ensures that, together with the original parallelogram, they act together as a beam. Meaning that the distance to the CoM, the mass and inertia all stay the same in its local frame. Adding inverted four bars creates a fully balanced 2-DoF manipulator.Adding all the balancing structures will increase the mass and inertia, with around a 9.9 and 4 times increase, respectively, compared to the original parallelogram. The balancing quality of the Super-B were experimentally obtained. Gaining a 93.6% and 88.9% reduction in shaking force and shaking moment, respectively for θ_1, and a 97.2% and 93.4% respectively, for θ_2. Tip accelerations of over 8 G are achieved for both DoF. The lowest in-plane eigenfrequency is measured with a frequency sweep at 91 Hz. The Super-B is manufactured with relative low-cost productions and an appropriate design for the high-speed industry. So fully inherently dynamic balancing can be combined with high accelerations.

References

[1] S. Briot, A. Pashkevich, and D. Chablat, "On the optimal design of parallel robots taking into account their deformations and natural frequencies," *Proceedings of the ASME Design Engineering Technical Conference*, vol. 7, no. PARTS A AND B, pp. 367–376, 2009.

[2] S. Briot and V. Arakelian, "Complete Shaking Force and Shaking Moment Balancing of In-line Four-bar Linkages by adding a Class-two RRR or RRP Assur Group," Tech. Rep. [Online]. Available: https://hal.archives-ouvertes.fr/hal-00683213

[3] B. Wei and D. Zhang, "A Review of Dynamic Balancing for Robotic Mechanisms," pp. 55–71, jan 2021.

[4] J. P. Karidis, G. Mcvicker, J. P. Pawletko, L. C. Zai, M. Goldowsky, R. E. Brown, and R. R. Comulada, "The Hummingbird Minipositioner-Providing Three-Axis Motion At 50 G's With Low Reactions," Tech. Rep.

[5] B. van der Zon, "Besi zoekt snelheidslimiet pakken en plaatsen op," *Besi zoekt snelheidslimiet pakken en plaatsen op – Mechatronicaamp;Machinebouw*, Sep 2007. [Online]. Available: https://mechatronicamachinebouw.nl/artikel/besi-zoekt-snelheidslimiet-pakken-en-plaatsen-op/

[6] V. van der Wijk, S. Krut, F. Pierrot, and J. L. Herder, "Design and experimental evaluation of a dynamically balanced redundant planar 4-RRR parallel manipulator," *The International Journal of Robotics Research*, vol. 32, no. 6, pp. 744–759, may 2013.

[7] M. V. d. W. Zomerdijk, "Reducing settling time in high acceleration applications of macro scale robotic manipulators with dynamic balancing," Dec 2020. [Online]. Available: http://resolver.tudelft.nl/uuid:5cadc48b-098a-4a82-adfa-c68500d8764f

[8] D. Boere and V. van der Wijk, "Design solutions to inherently dynamically balance a 2-DoF parallelogram with a constant inertia mechanism," *TU Delft Repositories*, 2022.

[9] A. Klimchik, "Enhanced stiffness modeling of serial and parallel manipulators for robotic-based processing of high performance materials To cite this version : HAL Id : tel-00711978," 2012.

[10] C. Gosselin, R. Ricard, and C. M. Gosselin, "On the development of reactionless parallel manipulators Cable-driven robotics, dynamic trajectory planning View project Master in Robotics View project ON THE DEVELOPMENT OF REACTIONLESS PARALLEL MANIPULATORS," Tech. Rep. [Online]. Available: https://www.researchgate.net/publication/247035201

[11] J. J. De Jong, B. E. Schaars, and D. M. Brouwer, "The influence of flexibility on the force balance quality: A frequency domain approach," in *European Society for Precision Engineering and Nanotechnology, Conference Proceedings - 19th International Conference and Exhibition, EUSPEN 2019*, 2019.

[12] H. Vallery and A. L. Schwab, *Advanced Dynamics*. Delft University of Technology, 2017.

[13] W.-T. Chang and D.-Y. Yang, "A note on equivalent linkages of direct-contact mechanisms," *Robotics*, vol. 9, no. 2, p. 38, 2020.

[14] R. S. Berkof, "The input torque in linkages," *Mechanism and Machine Theory*, vol. 14, no. 1, pp. 61–73, 1979.

[15] M. J. J. Zomerdijk and V. van der Wijk, "Structural design and experiments of a dynamically balanced inverted four-bar linkage as manipulator arm for high acceleration applications," *Actuators*, vol. 11, no. 5, 2022. [Online]. Available: https://www.mdpi.com/2076-0825/11/5/131

[16] A. Klimchik, A. Pashkevich, and D. Chablat, "Fundamentals of manipulator stiffness modeling using matrix structural analysis," *Mechanism and Machine Theory*, vol. 133, pp. 365–394, 2019. [Online]. Available: https://doi.org/10.1016/j.mechmachtheory.2018.11.023

[17] MATLAB, "version 7.10.0 (r2020b)," 2020.

[18] J. B. Jonker and J. P. Meijaard, *SPACAR — Computer Program for Dynamic Analysis of Flexible Spatial Mechanisms and Manipulators*. Berlin, Heidelberg: Springer Berlin Heidelberg, 1990, pp. 123–143.

[19] "Comsol multiphysics®."

[20] "Solidworks®," 2021.

[21] G. Genta and C. Delprete, "Some considerations on the experimental determination of moments of inertia," *Meccanica*, vol. 29, no. 2, pp. 125–141, 1994.

[22] M. A. ADLI, K. NAGAI, K. MIYATA, and H. HANAFUSA, "Analysis of Internal Force Effect in Parallel Manipulators," *Transactions of the Society of Instrument and Control Engineers*, vol. 27, no. 11, pp. 1266–1273, 1991.

[23] S. Briot, A. Goldsztejn, S. Briot, A. Goldsztejn, T. Optimization, and R. Application, "Topology Optimization of Industrial Robots : Application to a Five-bar Mechanism To cite this version : HAL Id : hal-01587979 Topology Optimization of Industrial Robots : Application to a Five-bar Mechanism," 2019.

[24] E. Ayala, J. Cervantes-Sanchez *et al.*, "Structural topology optimization of reactionless four-bar linkages," 2022.

[25] K. Nagai and Z. Liu, "Re-design of force redundant parallel mechanisms by introducing kinematical redundancy," *2009 IEEE/RSJ International Conference on Intelligent Robots and Systems, IROS 2009*, pp. 5898–5904, 2009.

[26] J. Wu, T. Li, J. Wang, and L. Wang, "Stiffness and natural frequency of a 3-DOF parallel manipulator with consideration of additional leg candidates," *Robotics and Autonomous Systems*, vol. 61, no. 8, pp. 868–875, 2013. [Online]. Available: http://dx.doi.org/10.1016/j.robot.2013.03.001

VIII. Appendices

A. *Out-of-plane eigenfrequency for in the workspace*

In Fig. 13(a), the out-of-plane eigenfrequencies are visible in the estimated workspace. This is calculated with a MSA. The minimum angle is estimated at 20°and the maximum at 70°.

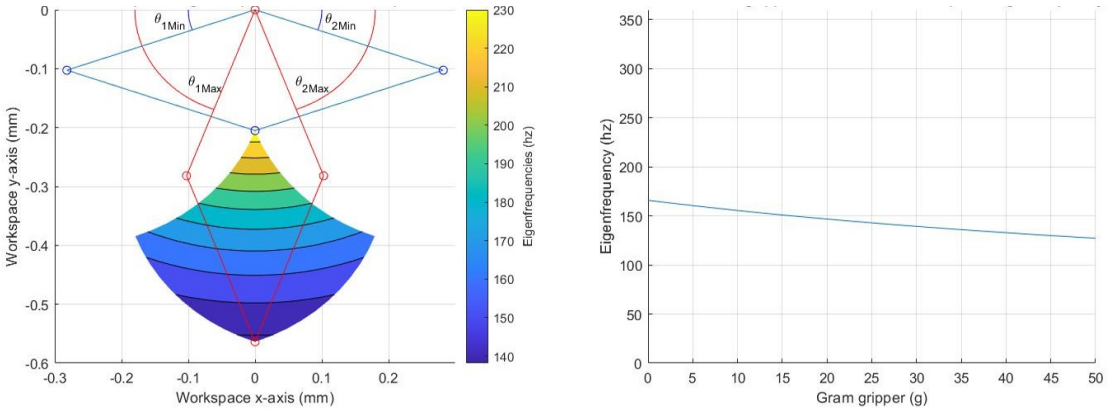

((a)) ((b))

Figure 13: (a) The out-of-plane eigenfrequency of the parallelogram in its workspace. (b) The effects of the mass of the end-effector on the out-of-plane eigenfrequencies of the parallelogram

The mass of the end-effector has a huge impact on the out-of-plane eigenfrequencies. Because it is a point far from a fixed point, creating a moment with every gram of mass added. In Fig. 13(b), this effect is plotted. θ_1 and θ_2 are taken at 45°and 135°respectively. The lengths and masses are taken from table I. With the slightest mass increase, the out-of-plane eigenfrequency shows a fast decay. This can be estimated at around 0.8 Hz per gram. It is advised to keep the mass off the end-effector as low as possible.

B. *Eigenfrequency of a beam that depends on actuator stiffness*

It is important that the stiffness of an actuator is high enough so that the lowest eigenfrequency, or rigid body mode, will not be reduced by it. In Fig. 14, the dependency on the eigenfrequency of the actuator stiffness is plotted. A steel beam of 30x30x2 mm with a length of 600 mm and an actuator at the base is used. The yellow line will be representing a clamped beam (infinite actuator stiffness). The blue line is the same beam, but with a torsion spring with variable stiffness, instead of it being clamped. This line will neglect the beam frequency. The red line will be the situation that is obtained from Spacar, so both frequencies are included. It can be seen that at low actuator stiffness the first eigenfrequency will be heavily dependent on the stiffness of the actuator. At high actuator stiffness, the lowest eigenfrequency will be the same as that of a clamped beam (blue). This example is not representative of the Super-B, although it gives an insight into the importance of the actuator stiffness, that it can have huge effects on the eigenfrequency. Note that this examples does not take into account the coupling or decoupling of a beam or mass that continuous behind the described beam. which is the case for the Super-B.

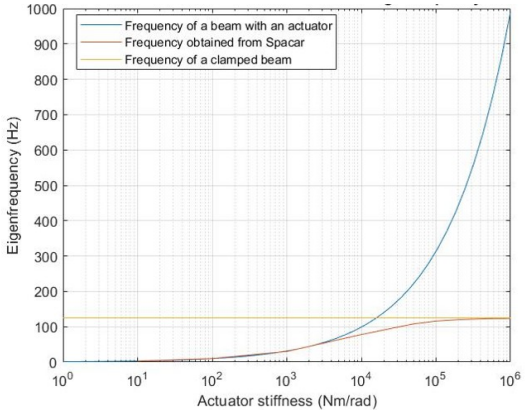

Figure 14: The effects on eigenfrequency with variable actuator stiffness compared to a clamped beam

C. Influence of the counter-masses that are placed on the counter-parallelogram on the out-of-plane eigenfrequency

In the Super-B, counter-masses on the counter-parallelogram are used to obtain constant inertia. The place of the counter-masses affects the out-of-plane frequency of the counter-parallelogram. If the mass of L_3^* or L_4^* is further away from the origin, it needs less mass to obtain constant inertia, as is stated in formula (1). Oversimplified situations are used to simulate what the place of the counter-masses can have on the out-of-plane eigenfrequency. In Fig. 15, the effects on the place of the counter-mass and its weight are visible. The mass is calculated by using the parameters of the parallelogram and counter-parallelogram, without the counter-masses, that are displayed in table I. If the counter-mass is further away, it creates a more significant moment and, thus, needs less mass to balance. Two simple examples are worked out to see the effects of relocating the counter-mass. Example1 uses squared tubes for L_{12} and L_{34} to obtain a parallelogram. Example2, instead of using squared tubes for L_{12}, it uses two solid flat beams parallel to each other, creating a more realistic model compared to the Super-B. Both parameters are listed in table IV. In Fig. 16, both the eigenfrequencies of the examples are plotted. Both have a different optimum, and both also show decay in eigenfrequency in the increased distance. So placing the counter-masses at the proper distance can have fewer negative effects on the out-of-plane eigenfrequency. The Super-B will likely look like Example2 as it also has two flat parallel beams. Checking the place in an FEA is advised because the models only clarify that the optimum can differ.

Table IV

Example1 (mm)	$h_{12}=6$	$b_{12}=30$		$h_{34}=15$	$b_{34}=15$	$t_{34}=2$
Example2 (mm)	$h_{12}=20$	$b_{12}=20$	$t_{12}=2$	$h_{34}=15$	$b_{34}=15$	$t_{34}=2$

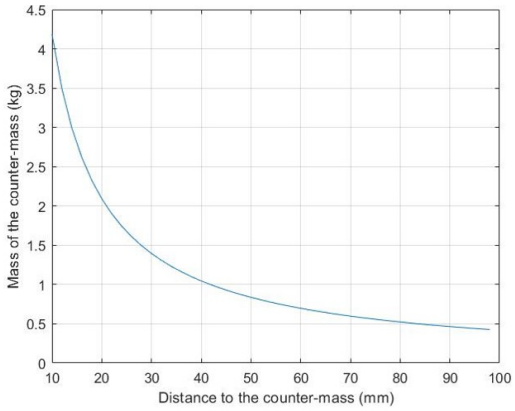

Figure 15: The distance of the counter-mass and the effects on its mass

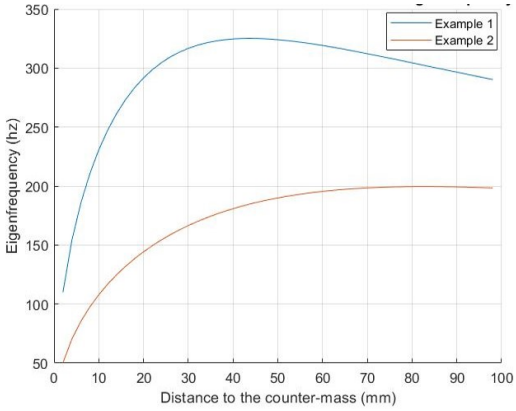

Figure 16: The distance of the counter-mass and the effects on the out-of-plane eigenfrequency

D. Kinematics elaboration of the Super-B

The velocity of the end-effector in ([X,Y]) coordinates with the actuator angle and speed as input can be obtained by taking the Jacobian with respect to the generalized coordinates of equations (26) and (27), and multiplying it with the derivative of the generalized coordinate. This will give

$$
\begin{aligned}
\dot{X}_e = {} & L_1\dot{q_1}s(\theta_{m1}+\gamma_{\theta_1}-ac((L_{1\theta_1}-L_{2\theta_1}c(\gamma_{\theta_2}-\gamma_{\theta_1}))/(L_{1\theta_1}^2-2c(\gamma_{\theta_2}-\gamma_{\theta_1})L_{1\theta_1}L_{2\theta_1}+L_{2\theta_1}^2)^{1/2})- \\
& at((L_{1\theta_1}s(\gamma_{\theta_2}-\gamma_{\theta_1}))/(L_{2\theta_1}-L_{1\theta_1}c(\gamma_{\theta_2}-\gamma_{\theta_1})))) \\
& ((s(\gamma_{\theta_2}-\gamma_{\theta_1})L_{2\theta_1}^3-(L_{1\theta_1}s(2\gamma_{\theta_2}-2\gamma_{\theta_1})L_{2\theta_1}^2)/2)/((L_{1\theta_1}^2-2c(\gamma_{\theta_2}-\gamma_{\theta_1})L_{1\theta_1}L_{2\theta_1}+L_{2\theta_1}^2)^{3/2} \\
& (-(L_{2\theta_1}^2(c(\gamma_{\theta_2}-\gamma_{\theta_1})^2-1))/(L_{1\theta_1}^2-2c(\gamma_{\theta_2}-\gamma_{\theta_1})L_{1\theta_1}L_{2\theta_1}+L_{2\theta_1}^2))^{1/2})+ \\
& (L_{1\theta_1}(L_{1\theta_1}-L_{2\theta_1}c(\gamma_{\theta_2}-\gamma_{\theta_1})))/(L_{1\theta_1}^2-2c(\gamma_{\theta_2}-\gamma_{\theta_1})L_{1\theta_1}L_{2\theta_1}+L_{2\theta_1}^2))- \\
& L_2\dot{q_2}s(\theta_{m2}-\gamma_{\theta_2}+at((L_{1\theta_2}s(q_2+\gamma_{\theta_2}))/(L_{2\theta_2}+L_{1\theta_2}c(q_2+\gamma_{\theta_2})))+ \\
& ac((L_{1\theta_2}+L_{2\theta_2}c(q_2+\gamma_{\theta_2}))/(L_{1\theta_2}^2+2c(q_2+\gamma_{\theta_2})L_{1\theta_2}L_{2\theta_2}+L_{2\theta_2}^2)^{1/2})) \\
& ((L_{1\theta_2}(L_{1\theta_2}+L_{2\theta_2}c(q_2+\gamma_{\theta_2})))/(L_{1\theta_2}^2+2c(q_2+\gamma_{\theta_2})L_{1\theta_2}L_{2\theta_2}+L_{2\theta_2}^2)+ \\
& (L_{2\theta_2}^2(L_{1\theta_2}s(2q_2+2\gamma_{\theta_2})+2L_{2\theta_2}s(q_2+\gamma_{\theta_2})))/ \\
& (2(-(L_{2\theta_2}^2(c(q_2+\gamma_{\theta_2})^2-1))/(L_{1\theta_2}^2+2c(q_2+\gamma_{\theta_2})L_{1\theta_2}L_{2\theta_2}+L_{2\theta_2}^2))^{1/2} \\
& (L_{1\theta_2}^2+2c(q_2+\gamma_{\theta_2})L_{1\theta_2}L_{2\theta_2}+L_{2\theta_2}^2)^{3/2}))
\end{aligned}
\tag{34}
$$

$$
\begin{aligned}
\dot{Y_e} = {} & L_2\dot{q_2}c(\theta_{m2} - \gamma_{\theta_2} + at((L_{1\theta_2}s(q_2 + \gamma_{\theta_2}))/(L_{2\theta_2} + L_{1\theta_2}c(q_2 + \gamma_{\theta_2})))+ \\
& ac((L_{1\theta_2} + L_{2\theta_2}c(q_2 + \gamma_{\theta_2}))/(L_{1\theta_2}^2 + 2c(q_2 + \gamma_{\theta_2})L_{1\theta_2}L_{2\theta_2} + L_{2\theta_2}^2)^{1/2})) \\
& ((L_{1\theta_2}(L_{1\theta_2} + L_{2\theta_2}c(q_2 + \gamma_{\theta_2})))/(L_{1\theta_2}^2 + 2c(q_2 + \gamma_{\theta_2})L_{1\theta_2}L_{2\theta_2} + L_{2\theta_2}^2)+ \\
& (L_{2\theta_2}^2(L_{1\theta_2}s(2q_2 + 2\gamma_{\theta_2}) + 2L_{2\theta_2}s(q_2 + \gamma_{\theta_2})))/(2(-(L_{2\theta_2}^2(c(q_2 + \gamma_{\theta_2})^2 - 1))/ \\
& (L_{1\theta_2}^2 + 2c(q_2 + \gamma_{\theta_2})L_{1\theta_2}L_{2\theta_2} + L_{2\theta_2}^2))^{1/2}(L_{1\theta_2}^2 + 2c(q_2 + \gamma_{\theta_2})L_{1\theta_2}L_{2\theta_2} + L_{2\theta_2}^2)^{3/2}))- \\
& L_1\dot{q_1}c(\theta_{m1} + \gamma_{\theta_1} - ac((L_{1\theta_1} - L_{2\theta_1}c(\gamma_{\theta_2} - \gamma_{\theta_1}))/ \\
& (L_{1\theta_1}^2 - 2c(\gamma_{\theta_2} - \gamma_{\theta_1})L_{1\theta_1}L_{2\theta_1} + L_{2\theta_1}^2)^{1/2})- \\
& at((L_{1\theta_1}s(\gamma_{\theta_2} - \gamma_{\theta_1}))/(L_{2\theta_1} - L_{1\theta_1}c(\gamma_{\theta_2} - \gamma_{\theta_1})))) \\
& ((s(\gamma_{\theta_2} - \gamma_{\theta_1})L_{2\theta_1}^3 - (L_{1\theta_1}s(2\gamma_{\theta_2} - 2\gamma_{\theta_1})L_{2\theta_1}^2)/2)/ \\
& ((L_{1\theta_1}^2 - 2c(\gamma_{\theta_2} - \gamma_{\theta_1})L_{1\theta_1}L_{2\theta_1} + L_{2\theta_1}^2)^{3/2} \\
& (-(L_{2\theta_1}^2(c(\gamma_{\theta_2} - \gamma_{\theta_1})^2 - 1))/(L_{1\theta_1}^2 - 2c(\gamma_{\theta_2} - \gamma_{\theta_1})L_{1\theta_1}L_{2\theta_1} + L_{2\theta_1}^2))^{1/2})+ \\
& (L_{1\theta_1}(L_{1\theta_1} - L_{2\theta_1}c(\gamma_{\theta_2} - \gamma_{\theta_1})))/(L_{1\theta_1}^2 - 2c(\gamma_{\theta_2} - \gamma_{\theta_1})L_{1\theta_1}L_{2\theta_1} + L_{2\theta_1}^2))L_{2\theta_1}^2))
\end{aligned}
\tag{35}
$$

E. Theoretical maximum acceleration and its reaction force reduction

In this appendix, the Super-B is evaluated on the theoretical accelerations it can obtain if the PID controller is not the limiting factor. Also, the simulated reaction forces and moments compared to its unbalanced variations are plotted. The Super-B is highly non-linear, so its inertia will differ in its workspace. In Fig. 17(a) and 17(b) the inertia's are plotted for the theoretical workspace for both DoF.

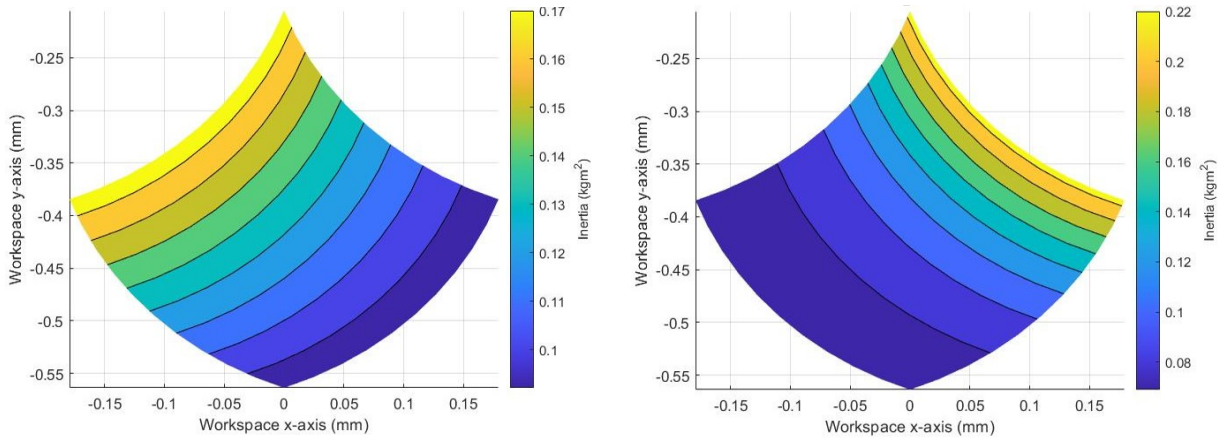

((a)) ((b))

Figure 17: The inertia differences of the Super-B of both DoF in the workspace. With DoF θ_1 in (a) and with DoF θ_2 in (b)

For the movement, an s-curves is implemented on the actuator ψ_1. The starting position is in the middle for both DoF at the corner of the workspace at θ_1 = 30 and θ_2 = 135. In this trajectory, the max inertia will be estimated at 0.13 kgm^2. The motion profile that is used is visible in the leftmost plots in Fig. 18. In this situation the peak torque will not exceed the maximum given value of 131 Nm with an estimated friction factor of 30%. It could reach up to 21 G of acceleration with this motion profile. All the critical parts are used in a FEM analyse and can withstand the forces that will be released at 21 G. If both actuators are used in a bigger piece of the workspace, even higher peak acceleration can be obtained. However, if the parts can withstand the forces must first be investigated. Comparing the balanced and unbalanced cases will give a theoretical reduction of 99.1% reaction forces and a reduction of 98.4% reaction moments at high accelerations. The simulated forces can be seen in the middle and the right of Fig. 18.

F. Bode plots of both actuators

In this appendix, the bode plots of the frequency sweeps are visible for both DoF. In Fig. 19 the frequency sweep of actuator ψ_1 is depicted. In Fig. 20 the frequency sweep of actuator ψ_2 is visible.

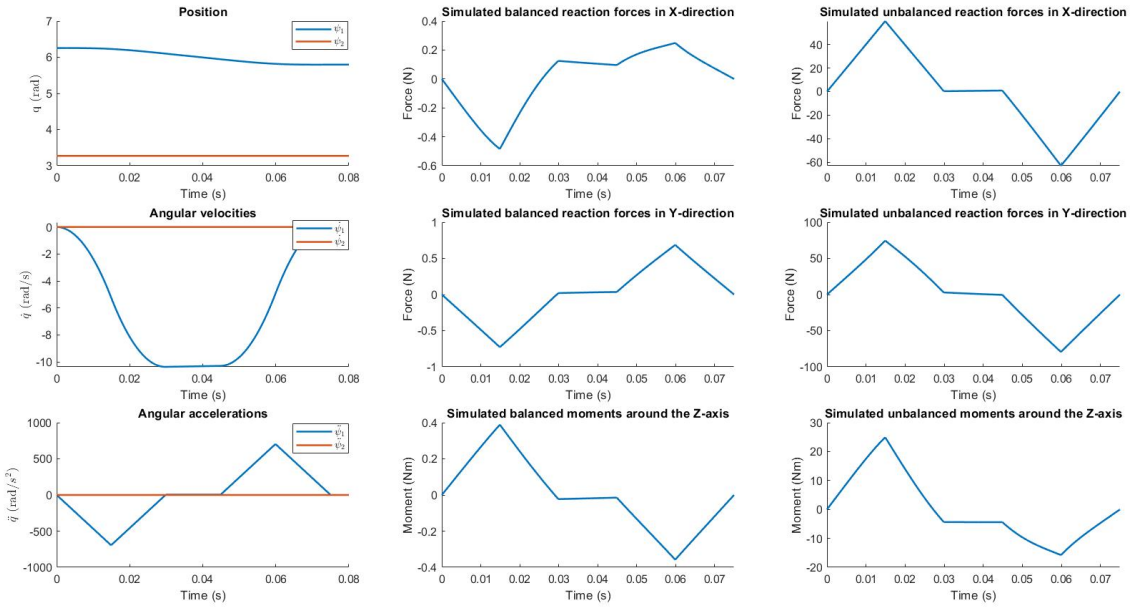

Figure 18: Simulated motion, reaction forces, and moments for a movement with peak tip accelerations of over 21 G

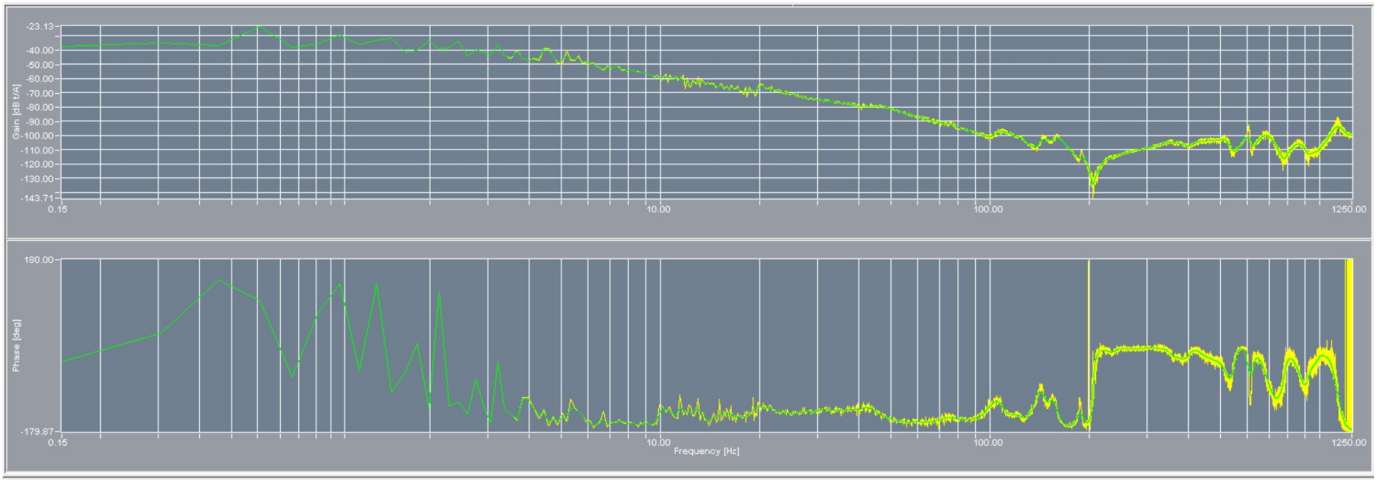

Figure 19: Bode plot of the frequency sweep of actuator ψ_1

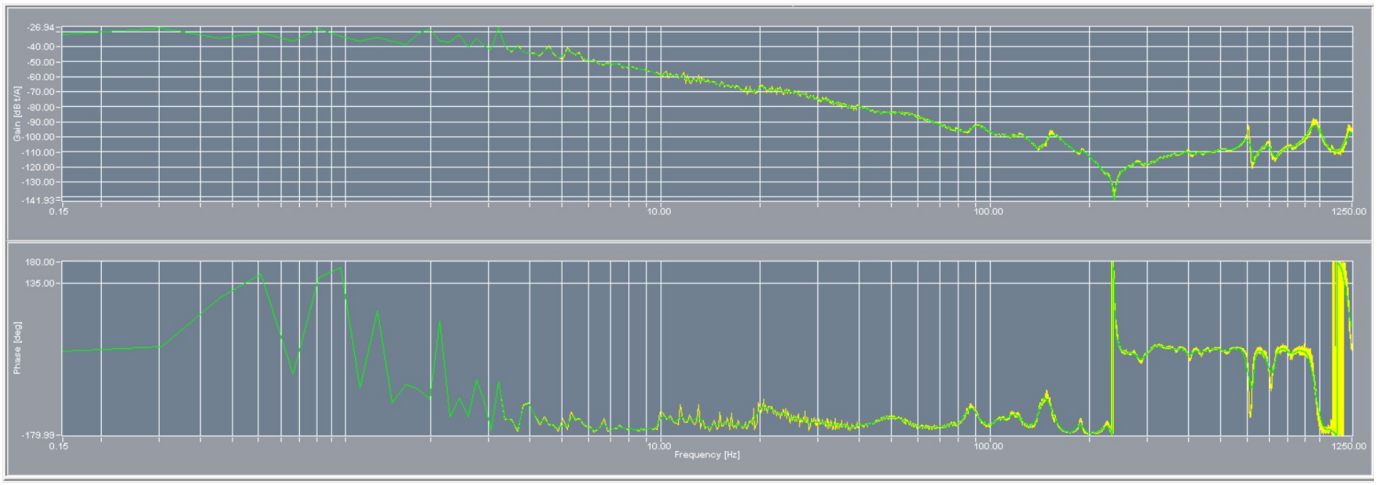

Figure 20: Bode plot of the frequency sweep of actuator ψ_2

5

Discussion

This thesis aimed to build a dynamically balanced manipulator sufficient for higher acceleration purposes, with a constant inertia mechanism. In this discussion, some notable points, as well as future research possibilities, are discussed.

5.1. Model improvements

Chapter 2 focused on the design choices made for high-speed manipulators and their effects on stiffness. The design guidelines were used in the design process of Chapter 3 and 4. Almost every design choice influences stiffness. So it is essential to obtain a sufficient model, so every design choice can be evaluated. For this project, multiple tools and programs were used to obtain the eigenfrequency. Spacar [20] in Matlab to obtain the in-plane eigenfrequencies. A self-written MSA program [21] to obtain the out-of-plane eigenfrequencies in the early stages, with low computation time, and Comsol [22] to obtain the eigenfrequencies for the final design. For future projects, it is advised to use a program with low computation time that can simultaneously identify the in-plane and out-of-plane frequencies while still being fateful to the design so the error will not be too big. This will give the option to optimise the manipulator better and faster and obtain the effects of every design choice. While simultaneously having the objective function be the in- and out-of-plane frequencies.

The actuator stiffness is assumed as infinite, creating decoupling between the counter-masses of the third link of the inverted four-bars and the rest of the mechanism. For further research, it is advised to obtain the actuator's stiffness experimentally and use this value in the simulations. Gaining a more realistic value of the in-plane eigenfrequencies.

5.2. Increase of controllability

To achieve 20 G or even 50 G with good dynamic characteristics, the eigenfrequencies must become higher. As seen in chapter 4, the out-of-plane frequencies are the lowest. In chapter 2, multiple suggestions are given that can help to increase the stiffness. A promising solution can be adding one or multiple redundant chains to the end-effector, which can also be actuated to add extra torque to the system, leading to very high accelerations. An example of active redundant chains is the NINJA robot which can reach 100 G of acceleration [23]. An easy way is to add a structure that moves in the same plane and is connected to the end-effector, as no spatial balancing must be done. The kinematics of the Super-B can be copied around the end-effector with an angle (α), creating a structure as is depicted in Fig.5.1. Although such a structure is very complicated, and when it is completely mirrored (α is 180°), it can better be depicted as a 4-RRR manipulator [17]. This will be dynamically balanced in a perpendicular path through the middle and have a lower mass and inertia ratio compared to the doubled Super-B structure. Adding a structure in the same plane to the end-effector will increase the stiffness but can also negatively affect the out-of-plane frequencies because of the added mass [24]. So attention must be paid to the controllability of the added links.

To achieve higher out-of-plane frequencies, stiffness needs to be added spatially. So ideally, adding a redundant spatial chain. However, this will increase the difficulty of balancing. What can be done is

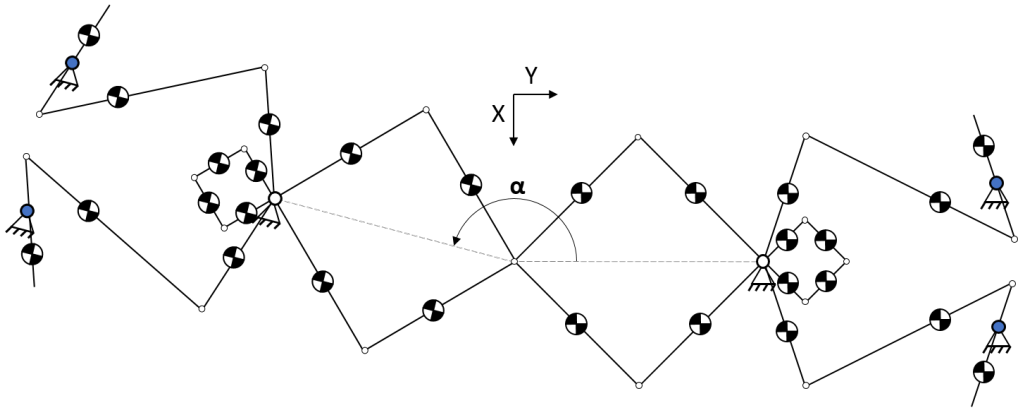

Figure 5.1: The Super-B and a copied version around the end-effector, to increase stiffness at the end-effector

doing the link-by-link balancing and adding an already balanced link. A suggestion can be seen in Fig. 5.2. This extra link is on a rotatable platform (which can also be an inverted four-bar), increasing the movable mass and inertia significantly. Using an extra redundant chain to the end-effector to increase out-of-plane stiffness is a good topic for further research.

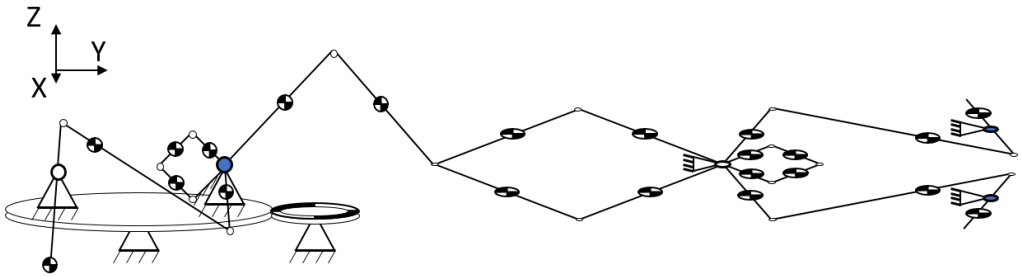

Figure 5.2: The Super-B with an added active balanced redundant chain to the end-effector

5.3. Dynamic balancing toward spatial structures

For the pick-and-place industry, mostly three or more DoF are wanted. Obtaining a spatial DoF can be done in multiple ways. A way is to use the Super-B as a building block and add a third spatial DoF on the origin. This is drawn in grey in Fig. 5.3. This way, the spatial actuator can be placed at the base. To obtain constant inertia for this spatial DoF, it will need a counter-structure that moves in the opposite direction. Although doing this will create a structure that messes up the original balancing conditions of the Super-B because of the spatial movement, making it unbalanced. This needs more investigation on how to use a counter-parallelogram structure to obtain constant inertia for spatial terms. As the spatial terms are much harder to balance and if it is even possible to obtain constant inertia in spatial is even questionable. Doing research on constant inertia mechanisms with, e.g. (compliant) mechanisms or foldable mechanism, can be an exciting topic. As in the end, it is just the correct mass placement on the right location.

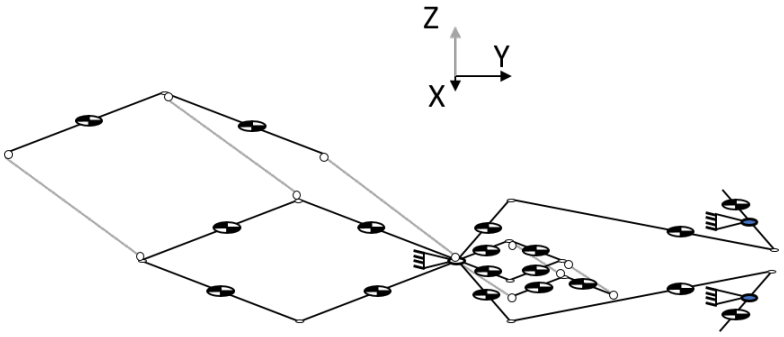

Figure 5.3: A proposed spatial mechanism that might be dynamically balanceable. The grey links depict the spatial beams. Note that a spatial reactionless four-bar still has to be added in the origin. This structure can not yet be balanced as the spatial inertias are not constant around the origin.

Another way to insert a spatial DoF is to imitate the R4 manipulator [25]. Suppose the 6-Bar linkage is possible to be dynamically balanced easily by a counter-6-bar as is explained in chapter (see Fig. 5.4a). In that case, it might be possible to add two of them perpendicular together (see Fig. 5.4b), creating a manipulator that looks like the R4 or even the Delta-robot [26]. The distal links of the six-bar should be doubled to obtain an extra DoF spatially, as is explained in Ref. [27]. The reactionless four-bars that should dynamically balance the entire structure are not drawn as it would make the figure unclear. If it is even possible to obtain a balanced spatial structure that is feasible for high-acceleration purposes should be further researched. So for spatial balancing, firstly, a structure must be found that can be balanced spatially. Suppose the structure does not balance distal links, and the actuators can be placed at the base. In that case, it has a good chance of being a proper structure for the high-speed industry if the controllability and balancing equations are included in the optimisation steps.

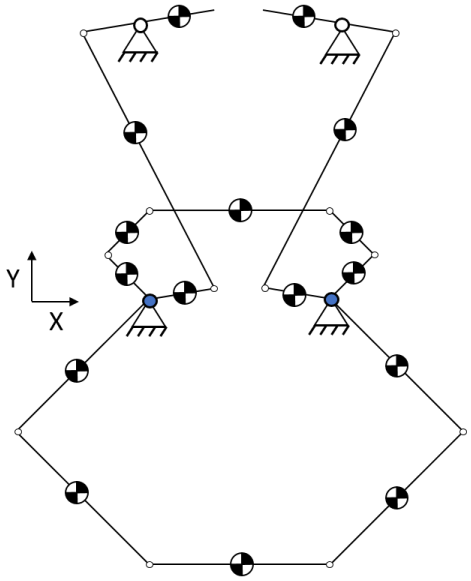

(a) A six-bar linkage uses a counter-six-bar linkage to obtain constant angular momentum for both DoF around their actuation point. The platform should be constrained horizontally as can be done as in Ref. [28]

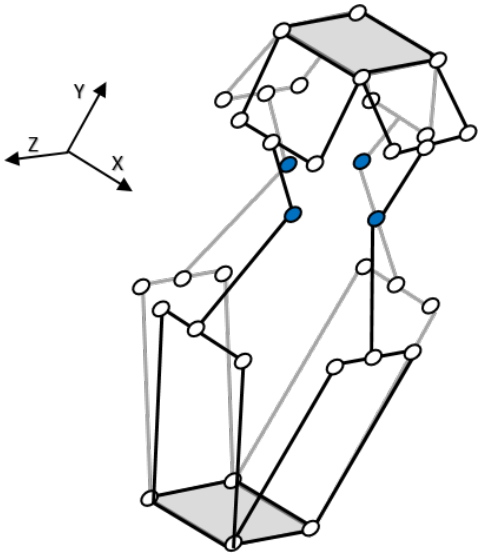

(b) A spatial mechanism that might be balanceable by four reactionless four-bars. The reactionless four-bars are not drawn to make the structure clearer.

Figure 5.4: The use of a six-bar linkage with a counter-six-bar linkage and its balancing possibilities

6

Conclusion

The objective of this thesis is to combine controllability and dynamic balancing to develop a 2-DoF inherently dynamically balanced manipulator, applicable for high accelerations. In the literature study design guidelines for obtaining sufficient stiffness are presented. Stiffness in any direction is important to obtain high controllabillety and almost all design choices influence the stiffness.

A 2-DoF constant inertia mechanism (CIM) with the aim of controllabillety is developed. It consists of two coupled parallelograms that obtain constant inertia around their pivot point in their workspace. Variations of this mechanism are presented by changing the coupled angle, either-or the properties of the links. Using the CIM, seven design solutions are given that are inherently dynamically balanced in their full workspace.

A design solution, consisting of a CIM and two inverted four-bars, optimal for controllability, was designed and optimized in a demonstrating prototype (Super-B). The kinematics and optimization process is elaborated. The Super-B consists mainly of laser-cut RVS plates that are TIG welded together. This showed that the manipulator could be manufactured with low-cost production methods. Experimentally a reduction of 93.6% and 88.9% in shaking force and shaking moment compared to the unbalanced case, respectively, is obtained for the first DoF and a 97.2% and 93.4% reduction, respectively, for the second DoF. The manipulator had a measured lowest eigenfrequency of 91 Hz and a workspace of around 20 cm. Up to 8 G of tip acceleration was achieved. So fully inherently dynamic balancing can be combined with high accelerations.

Structures that use the theory introduced, are speculated for obtaining spatial dynamic balancing. The research in this thesis gives a good step toward dynamically balancing multi-DoF with the aim of controllability, eventually obtaining a high-speed, inherently dynamically balanced multi-DoF manipulator.

Bibliography

[1] S. Briot, A. Pashkevich, and D. Chablat, “On the optimal design of parallel robots taking into account their deformations and natural frequencies,” *Proceedings of the ASME Design Engineering Technical Conference*, vol. 7, no. PARTS A AND B, pp. 367–376, 2009.

[2] V. Van der Wijk, B. Demeulenaere, C. Gosselin, and J. L. Herder, “Comparative analysis for low-mass and low-inertia dynamic balancing of mechanisms,” 2012.

[3] J. J. De Jong, B. E. Schaars, and D. M. Brouwer, “The influence of flexibility on the force balance quality: A frequency domain approach,” in *European Society for Precision Engineering and Nanotechnology, Conference Proceedings - 19th International Conference and Exhibition, EUSPEN 2019*, 2019.

[4] B. Wei and D. Zhang, “A Review of Dynamic Balancing for Robotic Mechanisms,” pp. 55–71, jan 2021.

[5] E. Uzunoğlu, M. Özkahya, E. Paksoy, B. Taner, M. I. Can Dede, and G. Kiper, “Conceptual Design of a 2-DoF Planar High-Speed Industrial Parallel Manipulator,” *Mechanisms and Machine Science*, vol. 79, pp. 344–353, 2020.

[6] C. Gosselin, R. Ricard, and C. M. Gosselin, “On the development of reactionless parallel manipulators Cable-driven robotics, dynamic trajectory planning View project Master in Robotics View project ON THE DEVELOPMENT OF REACTIONLESS PARALLEL MANIPULATORS,” Tech. Rep. [Online]. Available: https://www.researchgate.net/publication/247035201

[7] V. van der Wijk and J. L. Herder, “Active dynamic balancing unit for controlled shaking force and shaking moment balancing,” in *International Design Engineering Technical Conferences and Computers and Information in Engineering Conference*, vol. 44106, 2010, pp. 1515–1522.

[8] J. Herder, A. Ariens, B. Bakker, and H. Menschaar, “Wo2006080846 - five-bar mechanism with dynamic balancing means and method for dynamically balancing a five-bar mechanism,” Patent, 2006.

[9] V. Van Der Wijk and J. L. Herder, “Synthesis of dynamically balanced mechanisms by using counter-rotary countermass balanced double pendula,” *Journal of Mechanical Design, Transactions of the ASME*, vol. 131, no. 11, pp. 1 110 031–1 110 038, 2009.

[10] T. Laliberté and C. Gosselin, “Synthesis, optimization and experimental validation of reactionless two-DOF parallel mechanisms using counter-mechanisms,” *Meccanica*, vol. 51, no. 12, pp. 3211–3225, dec 2016.

[11] J. J. de Jong, J. van Dijk, and J. L. Herder, “A screw based methodology for instantaneous dynamic balance,” *Mechanism and Machine Theory*, vol. 141, pp. 267–282, nov 2019.

[12] Y. Wu and C. M. Gosselin, “Synthesis of reactionless spatial 3-DoF and 6-DoF mechanisms without separate counter-rotations,” *International Journal of Robotics Research*, vol. 23, no. 6, pp. 625–642, jun 2004.

[13] J.-F. Collard and C. Gosselin, “OPTIMAL SYNTHESIS OF A PLANAR REACTIONLESS THREE-DEGREE-OF-FREEDOM PARALLEL MECHANISm,” 2010.

[14] V. H. Arakelian and M. R. Smith, “Design of planar 3-DOF 3-RRR reactionless parallel manipulators,” *Mechatronics*, vol. 18, no. 10, pp. 601–606, 2008. [Online]. Available: http://dx.doi.org/10.1016/j.mechatronics.2008.05.002

[15] J. P. Karidis, G. Mcvicker, J. P. Pawletko, L. C. Zai, M. Goldowsky, R. E. Brown, and R. R. Comulada, “The Hummingbird Minipositioner-Providing Three-Axis Motion At 50 G’s With Low Reactions,” Tech. Rep.

[16] B. van der Zon, “Besi zoekt snelheidslimiet pakken en plaatsen op,” Sep 2007. [Online]. Available: https://mechatronicamachinebouw.nl/artikel/besi-zoekt-snelheidslimiet-pakken-en-plaatsen-op/

[17] V. van der Wijk, S. Krut, F. Pierrot, and J. L. Herder, “Design and experimental evaluation of a dynamically balanced redundant planar 4-RRR parallel manipulator,” *The International Journal of Robotics Research*, vol. 32, no. 6, pp. 744–759, may 2013.

[18] M. V. d. W. Zomerdijk, “Reducing settling time in high acceleration applications of macro scale robotic manipulators with dynamic balancing,” Dec 2020. [Online]. Available: http://resolver.tudelft.nl/uuid:5cadc48b-098a-4a82-adfa-c68500d8764f

[19] M. J. J. Zomerdijk and V. van der Wijk, “Structural design and experiments of a dynamically balanced inverted four-bar linkage as manipulator arm for high acceleration applications,” *Actuators*, vol. 11, no. 5, 2022. [Online]. Available: https://www.mdpi.com/2076-0825/11/5/131

[20] J. B. Jonker and J. P. Meijaard, “Spacar — computer program for dynamic analysis of flexible spatial mechanisms and manipulators,” Berlin, Heidelberg, pp. 123–143, 1990.

[21] A. Klimchik, A. Pashkevich, and D. Chablat, “Fundamentals of manipulator stiffness modeling using matrix structural analysis,” *Mechanism and Machine Theory*, vol. 133, pp. 365–394, 2019. [Online]. Available: https://doi.org/10.1016/j.mechmachtheory.2018.11.023

[22] “Comsol multiphysics®.”

[23] K. Nagait, “Development of Parallel Manipulator “ NINJA ” with Ult ra-High- Accelerat ion 1 Introduction Trade-off in mechanism design and,” pp. 3678–3685, 2003.

[24] J. Wu, T. Li, J. Wang, and L. Wang, “Stiffness and natural frequency of a 3-DOF parallel manipulator with consideration of additional leg candidates,” *Robotics and Autonomous Systems*, vol. 61, no. 8, pp. 868–875, 2013. [Online]. Available: http://dx.doi.org/10.1016/j.robot.2013.03.001

[25] G. S. Natal, A. Chemori, and F. Pierrot, “Dual-space control of extremely fast parallel manipulators: Payload changes and the 100G experiment,” *IEEE Transactions on Control Systems Technology*, vol. 23, no. 4, pp. 1520–1535, 2015.

[26] F. Pierrot, C. Reynaud, and A. Fournier, “Delta: A simple and efficient parallel robot,” *Robotica*, vol. 8, no. 2, pp. 105–109, 1990.

[27] X. J. Liu and J. Wang, “Some new parallel mechanisms containing the planar four-bar parallelogram,” *International Journal of Robotics Research*, vol. 22, no. 9, pp. 717–732, 2003.

[28] C. Germain, S. Briot, V. Glazunov, S. Caro, C. Germain, S. Briot, V. Glazunov, S. Caro, and P. W. I. A, “IRSBOT-2 : A Novel Two-Dof Parallel Robot for High-Speed Operations To cite this version : HAL Id : hal-00590082,” 2019.